

# HUMAN NME6 PROTEIN: SUBCELLULAR LOCALIZATION, STRUCTURE AND FUNCTION

---

**Proust, Bastien Lucien Jean**

**Doctoral thesis / Disertacija**

**2022**

*Degree Grantor / Ustanova koja je dodijelila akademski / stručni stupanj:* **University of Zagreb, Faculty of Science / Sveučilište u Zagrebu, Prirodoslovno-matematički fakultet**

*Permanent link / Trajna poveznica:* <https://um.nsk.hr/um:nbn:hr:217:788932>

*Rights / Prava:* [In copyright](#) / [Zaštićeno autorskim pravom.](#)

*Download date / Datum preuzimanja:* **2024-07-15**



*Repository / Repozitorij:*

[Repository of the Faculty of Science - University of Zagreb](#)





University of Zagreb

FACULTY OF SCIENCE  
DEPARTMENT OF BIOLOGY

Bastien Lucien Jean Proust

**HUMAN NME6 PROTEIN:  
SUBCELLULAR LOCALIZATION,  
STRUCTURE AND FUNCTION**

DOCTORAL THESIS

Supervisor:

Dr. Maja Herak Bosnar

Zagreb, 2022.



Sveučilište u Zagrebu

PRIRODOSLOVNO-MATEMATIČKI FAKULTET  
BIOLOŠKI ODSJEK

Bastien Lucien Jean Proust

**UNUTARSTANIČNI SMJEŠTAJ,  
STRUKTURA I FUNKCIJA PROTEINA  
NME6 U ČOVJEKA**

DOKTORSKI RAD

Mentor:

Dr. sc. Maja Herak Bosnar

Zagreb, 2022.

This doctoral thesis was prepared in the Laboratory for Protein Dynamics of the Division of Molecular Medicine, Ruđer Bošković Institute in Zagreb, under the supervision of Dr. Maja Herak Bosnar, within the University Postgraduate Doctoral Study of Biology at the Department of Biology, Faculty of Science, University of Zagreb.

The dissertation was prepared within the project of the Croatian Science Foundation entitled “Nemo6 - Structure, Function and Evolution of Nme6/Nm23-H6 Protein” (IP-2016-06-4021).

## **SUPERVISOR BIOGRAPHY**

Maja Herak Bosnar, PhD, obtained her Bachelor, Master degree and PhD from the Faculty of Science, University of Zagreb. She is currently a senior scientist and a group leader at the Laboratory for Protein Dynamics, at Ruđer Bošković Institute, Zagreb. Her main field of interest is the structure, function and evolution of NME/NDPK/Nm23 family of proteins and their involvement in tumor progression. She published 38 scientific papers mostly linked to this and related topics. She was a principal investigator of a scientific project financed by the Croatian Ministry for Science and Education and the Croatian Science Foundation, as well as two French-Croatian bilateral projects. She was also a work package leader of the FP7/Regpot-Innomol project (2013-2016). She organized several scientific conferences and was the main organizer of the International Conference on Nm23/NME/NDPK in Dubrovnik in 2016. She is currently a vice president of the Croatian Microscopy Society and a member of the Oversight Committee of the Croatian Branch of the European Association of Cancer Research. MHB was also a member of the Scientific Council of the Ruđer Bošković Institute (2016-2022) and its vice president (2019-2022). MHB is associate professor at University J.J. Strossmeyer in Osijek and a course leader at the Faculty of Science, University of Zagreb. To this date, she mentored five doctoral and four master theses. She gave several invited lectures at international and domestic conferences. For almost 10 years she was involved as a course leader in Courses in Biology and Medicine organized by Ruđer Bošković Institute and reviewed a number of high school textbooks published by Neodidacta d.o.o. Maja Herak Bosnar is one of the editors and authors of the university textbook “Metode u molekularnoj biologiji” published by Ruđer Bošković Institute, awarded by the Croatian Academy of Sciences and Arts and Zagreb Fair for the best scientific publishing achievement in 2007. Maja Herak Bosnar is active in promotion of science, she is the editor-in-chief of the scientific journal *Periodicum biologorum* and is a member of the National Council for Cancer Therapy Guided by Comprehensive Gene Profiling.

## ACKNOWLEDGMENTS

*First, I would like to express my gratitude to my supervisor dr. sc. Maja Herak Bosnar, for giving me the opportunity to learn and work at her side. Thank you for putting your trust in me and for offering this nice, human working atmosphere, where everything is discussable on equal terms, without the burden of ranks or titles. Our team is the best!*

*Thanks to dr. sc. Neda Slade, the head of the Laboratory for Protein Dynamics, for accepting me in the Lab as a Master student during my first visit to Croatia, for her time, patience and kindness over those years. Thanks to all Lab members, Ana Tadijan and Anđela Horvat for helping me with flow cytometry, Ignacija Vlašić and Maja Jazvinščak Jembrek, and to the members of Laboratory for Hereditary Cancer, Maja Sabol for our very appreciable morning coffees, Sonja Levanat, Petar Ozretić, Vesna Musani, Tina Petrić, Josipa Čonkaš, Nikolina Piteša and Matea Kurtović for the fun gathering moments we spent together and for your endless tips and tricks regarding experiments. An immense thanks to Martina Pehar, who watches over the smooth running of the laboratory, and without whom our work would be terribly difficult. The validation of a doctoral dissertation is an individual reward that would be impossible without an intense teamwork.*

*Special thanks to my best teammates Nikolina Škrobot Vidaček and Martina Radić. Nikolina, you did teach me so much during those years, and still are. Thanks for all those fun moments we had in the lab. Tina, we went together through the craziness of the doctorate, and survived! Thank you for your help, your patience, and your unlimited kindness.*

*Thanks to dr. sc. Helena Četković, for the help, tips and tricks she gave us, that were essential for a successful cloning, protein production and many other experiments.*

*To all colleagues from the Division of Molecular Medicine and the Division of Molecular Biology, thanks for the support, experiment counselling and help.*

*Special thanks to Prof. Uwe Schlattner for enabling my venue in his laboratory. Thanks to all the members of the Laboratory of Fundamental and Applied Bioenergetics, for the warm welcome, the intense brainstorming and working sessions and the successful collaboration. Thanks to dr. Malgorzata Tokarska-Schlattner for teaching me the delicate subfractionation of mitochondria.*

*I want to thank my family, who contributed in making who I am today. Thanks to my parents Marie-Claire and Philippe for their love, for supporting my education and my choices, even the crazy idea of quitting everything to live on the other side of Europe. Thanks to Dana and Slavko for welcoming me with open heart in their home. Without your help none of this would have been possible.*

*Finally, an immense thanks to the loves of my life. Maja you are the origin of this story, the solution of most problems and the sunshine in my life. Thank you for sharing this journey with me, for the support you bring in every aspect of my life, I love you. To Gabriel and Ema, you are the most precious treasures in this world... Papa vous aime.*

## **ABSTRACT**

### **HUMAN NME6 PROTEIN: SUBCELLULAR LOCALIZATION, STRUCTURE AND FUNCTION**

**BASTIEN LUCIEN JEAN PROUST**

Ruđer Bošković Institute

Nucleoside diphosphate kinase (NDPK/NME/NM23) family of enzymes catalyze the transfer of gamma phosphate group from nucleoside triphosphates to nucleoside diphosphates. The family sparked interest after the discovery of metastasis suppressor activity of NME1, leading to a comprehensive characterization of Group I members (NME1-NME4). In contrast, the evolutionary ancient Group II members (NME5-NME9) are to date barely explored. We aimed to produce an extensive description of the human NME6 protein, by revealing its expression pattern, enzymatic activity, subcellular localization, quaternary structure and cellular function. Our results show the ubiquitous expression of NME6. We demonstrated a lack of enzymatic activity linked to oligomerization deficiency. We confirmed the mitochondrial localization and refined it to a matrix-facing protein, partially bound to the mitochondrial inner membrane, where NME6 interacts with RCC1L protein. Finally, we unraveled a negative impact of NME6 on mitochondrial respiration, possibly linked to the regulation of mitochondria-encoded protein expression.

(137 pages, 50 figures, 24 tables, 149 references, original in English)

Keywords: NME, NM23, NDPK, NME6, RCC1L, WBSCR16, Mitochondria

Supervisor: Dr. Maja Herak Bosnar, senior scientist

Reviewers:

1. Assoc. prof. dr. Maja Matulić
2. Prof. dr. Biljana Balen
3. Prof. dr. Uwe Schlattner

## SAŽETAK

### UNUTARSTANIČNI SMJEŠTAJ, STRUKTURA I FUNKCIJA PROTEINA NME6 U ČOVJEKA

BASTIEN LUCIEN JEAN PROUST

Institute Ruđer Bošković

Nukleozid difosfatske kinaze, (NDPK/NME/NM23), kataliziraju prijenos gama fosfata s nukleozid trifosfata na nukleozid difosfate. Ova obitelj enzima privukla je veliku pozornost nakon otkrića da je jedan od njenih članova, NME1, uključen u sprječavanje nastanka metastaza. To je dovelo do sveobuhvatnih istraživanja članova NME iz skupine I (od NME1 do NME4). Nasuprot tome, evolucijski „stariji“ članovi Grupe II (od NME5 do NME9) do danas su vrlo malo istraženi. Cilj ovog rada bio je detaljnije istražiti ljudski protein NME6, utvrditi njegovu ekspresiju, enzimsku aktivnosti, unutarstanični smještaj, kvarternu strukturu i stanične funkcije. Naši rezultati pokazuju sveprisutnu ekspresiju proteina NME6. Pokazali smo da NME6 ne stvara oligomere te da, u vezi s time, ne pokazuje ni enzimatsku aktivnost. Pokazali smo da je protein smješten u matriksu mitohondrija, vjerojatno djelomično vezan na unutarnju membranu, gdje stupa u interakciju s proteinom RCC1L. Konačno, otkrili smo negativan utjecaj pojačane ekspresije NME6 na stanično disanje, što je vjerojatno povezano s regulacijom ekspresije proteina kodiranih mitohondrijskom DNA.

(137 stranica, 50 slika, 24 tablica, 149 literaturnih navoda, jezik izvornika: Engleski)

Ključne riječi: NME, NM23, NDPK, NME6, RCC1L, WBSCR16, Mitohondrij

Mentor: Dr. sc. Maja Herak Bosnar, zn. savj.

Ocjenjivači:

1. Izv. prof. dr. sc. Maja Matulić
2. Prof. dr. sc. Biljana Balen
3. Prof. dr. Uwe Schlattner



## PROŠIRENI SAŽETAK DOKTORSKE DISERTACIJE

Nukleozid difosfatske kinaze (NDPK/NME/NM23) čine obitelj proteina koji sadrže jednu, nekoliko ili čak djelomične domene nukleozid difosfatske kinaze (NDPK). NDP kinaze su prvi put opisane prije gotovo 70 godina u prsnim mišićima golubova i kvascu, u kojima su autori opisali njihovu glavnu enzimsku aktivnost: prijenos terminalne  $\gamma$ -fosfatne skupine s nukleozid trifosfata na nukleozid difosfat. Kako se ova skupina proteina stalno iznova otkrivala u različitim znanstvenim poljima i modelnim organizmima, koristila se i neobična i zbudjujuća nomenklatura. Osim NDPK, članovi obitelji se također nazivaju i NM23 ili NME (nemetastatski klon 23) zbog antimetastatskih svojstava nekih članova, ili čak AWD (prema engl. *abnormal wing discs*) prema razvojnom poremećaju u vrsti *Drosophila melanogaster* koji je izazvan mutacijom. Radi jasnoće ovog doktorskog rada, proteini NDPK/NME/NM23 će se označavati isključivo kao NME, dok će se glavna enzimska aktivnost i domena označavati kao aktivnost NDPK, odnosno, domena NDPK.

Na temelju filogenetskih analiza i strukture introna i eksona obitelj NDPK/NME u ljudi podijeljena je u dvije skupine: članovi skupine I (NME1-NME4) posjeduju značajan stupanj međusobne homologije nukleotidnog slijeda i svi pokazuju aktivnost NDPK. Članovi skupine II (NME5-NME9) posjeduju znatno manji stupanj homologije te nemaju aktivnost NDPK, uz moguću iznimku proteina NME6.

Iako su proteini NME opisani prije nekoliko desetljeća, ranih devedesetih godina privukli su pozornost istraživača nakon što je otkriveno da NME1 posjeduje svojstva supresora metastaziranja. Godine istraživanja, posebno članova Grupe I, pokazala su da protein NME mora oligomerizirati kako bi posjedovao enzimsku aktivnost. Nadalje, mutacije u petlji Kpn (engl. Kpn loop - *killer of prune*) i modifikacije na C-kraju proteina uzrokuju nestabilnost oligomera i smanjenu aktivnost NDPK. Proteini NME posjeduju i druge biokemijske uloge: aktivnost histidinske kinaze, sudjeluju u transkripciji gena pokazuju aktivnost 3'-5' egzonukleaze.

Biološke uloge proteina NME su raznolike i ovise o specifičnosti tkiva i stanica, unutarstaničnom smještaju i enzimskoj aktivnosti. Proteini NME eksprimiraju se ili tkivno specifično (NME5 u testisima) ili su prisutni u svim tkivima. Uglavnom su smješteni u citosolu i jezgri (NME1 i NME2), mitohondriju (NME3 i NME4) ili vezani uz citoskelet (NME7).

Obitelj NME drevna je skupina gena/proteina, prisutna u sve tri domene života: bakterijama, arhejama i eukariotima, što ukazuje na njihovu važnost u ključnim funkcijama i fiziologiji

stanice. Evolucijski gledano, članovi skupine II nastali su ranije od većine članova skupine I, tj. evolucijski su „stariji“. Istraživanja na jednostavnijim životinjama kao što su spužve, koje predstavljaju model zajedničkog pretka svih životinja, pokazala su da drevni spužvin protein NMEGp1Sd pokazuje strukturu, smještaj i funkciju vrlo sličnu ljudskom homologu NME1/2. S druge strane, istraživanje provedeno na spužvinom homologu NME6, NME6Sd, pokazalo je da se stanična funkcija ovog proteina vjerojatno promijenila tijekom evolucije.

Za razliku od proteina NME iz skupine I koje se desetljećima opsežno istraživalo, članovi skupine II do danas su vrlo slabo istraženi. Dostupne informacije o ljudskom proteinu NME6 uglavnom se temelje na tri publikacije s kraja devedesetih godina prošlog stoljeća. Godine 1999. dvije nezavisne skupine prvi su put opisale gen *NME6*, međutim opisali su dvije proteinske izoforme koje se međusobno razlikuju u prvih nekoliko aminokiselina. Pitanje postojećih izoformi koje se zaista eksprimiraju u ljudskim stanicama do danas nije riješeno. Slično, iako su aminokiseline koje smatramo važnim za enzimsku strukturu i katalitičku aktivnost proteina NME očuvane u NME6, potencijalna aktivnost NDPK ljudskog NME6 ostala je predmetom rasprave. Čini se da je NME6 smješten u mitohondrijima, iako mu nedostaje uobičajeni slijed koji odvodi proteine u mitohondrij (od engl. *mitochondrial targeting sequence*, MTS).

**Cilj:** Cilj ovog doktorskog rada bio je provesti opsežno istraživanje ljudskog proteina NME6, s naglaskom na stanični i unutarstanični smještaj, aktivnost NDPK, status oligomerizacije, partnere u interakciji, ali i njegov utjecaj na osnovne stanične funkcije kao što su apoptoza, stanični ciklus i mitohondrijsko disanje. **Metode:** Kako bi se otkrila dominantna izoforma(e) proteina NME6 i njezin/njihov profil ekspresije, ljudski protein NME6 analizirao sam metodom Western blotting na velikom panelu ljudskih staničnih linija, a koristio sam i spektrometriju masa. Detaljniji opis staničnog smještaja proteina NME6 utvrdio sam konfokalnom mikroskopijom živih i fiksiranih stanica te metodama staničnog frakcioniranja i metodom Western blotting. Enzimska svojstva rekombinantnog proteina NME6 ispitao sam testom za mjerenje aktivnosti NDP kinaze *in vitro*. Status oligomerizacije provjerio sam umrežavanjem proteina uz pomoć glutaraldehida, gel filtracijom i ko-imunoprecipitacijom. Kandidate za interakcijske partnere proteina NME6 analizirao sam ko-imunoprecipitacijom. Ulogu NME6 u osnovnim staničnim funkcijama kao što su apoptoza i stanični ciklus ispitao sam metodama protočne citometrije dok sam stanično disanje proučavao uz pomoć oksimetrije. **Hipoteza:** Endogeni ljudski protein NME6 eksprimira se u svim staničnim linijama čovjeka različitog podrijetla, u obliku jedne ili obje izoforme opisane u literaturi (194 i/ili 186

aminokiselina). Protein je smješten u mitohondrijima i vjerojatno stupa u interakciju s drugim mitohondrijskim proteinima iz obitelji NME i/ili s proteinima koji su navedeni u opsežnim analizama proteomskih podataka. NME6 ne posjeduje aktivnost NDPK, ali je uključen u jednu ili nekoliko osnovnih staničnih funkcija. **Rezultati:** NME6 se eksprimira u svim staničnim linijama čovjeka koje sam ispitivao i to pretežno kao izoforma od 186 aminokiselina. Utvrdio sam da histidin u NME6 nije fosforiliran te da protein NME6 ne tvori oligomere i ne pokazuje aktivnost NDPK. NME6 je smješten u matriksu mitohondrija i vjerojatno je djelomično u interakciji s MIM-om (od engl. *mitochondrial inner membrane*, MIM) što sam dodatno utvrdio otkrićem interakcije NME6 s RCC1L, proteinom koji je smješten u matriksu, a za kojeg je pokazano da je vezan s mitoribosomima. Promjene u razini NME6 nisu utjecale na apoptozu i stanični ciklus, ali sam utvrdio značajno smanjenje mitohondrijskog disanja uz dodatak ATP-a nakon prekomjerne ekspresije NME6. Istodobno, uočio sam smanjenje razine ekspresije nekih komponenata proteinskih kompleksa oksidativne fosforilacije. Ukratko, pokazao sam da se NME6 u stanici uglavnom nalazi u obliku monomera, nema aktivnost NDP kinaze, smješten je u matriksu mitohondrija te utječe na stanično disanje.

## **TABLE OF CONTENTS**

1	INTRODUCTION .....	1
2	LITERATURE OVERVIEW .....	4
2.1	Mitochondria and respiration .....	4
2.1.1	Mitochondrial origin .....	4
2.1.2	Mitochondrial organization.....	4
2.1.3	Mitochondrial dynamic .....	6
2.1.4	Mitochondrial genome/proteome .....	7
2.1.5	Mitochondrial protein import.....	8
2.1.6	Mitochondrial functions .....	9
2.1.6.1	Apoptosis .....	10
2.1.6.2	Aerobic respiration.....	11
2.2	NDPK activity.....	13
2.3	Human NME family .....	18
2.4	Human NME6 protein.....	21
2.5	RCC1L protein.....	26
3	MATERIALS AND METHODS.....	28
3.1	Materials .....	28
3.1.1	Chemicals and buffers.....	28
3.1.2	Instruments and material .....	32
3.1.3	Commercial products .....	33
3.1.4	Cell culture.....	37
3.1.5	Plasmids, primers and silencers .....	40
3.1.6	Software .....	42
3.2	Methods.....	43
3.2.1	Preparation .....	43
3.2.1.1	Cloning of specific plasmids.....	43
3.2.1.2	Transformation of bacteria by electroporation.....	46
3.2.1.3	Production of recombinant proteins .....	47
3.2.2	Cell culture.....	49
3.2.2.1	Culture of cells in sterile conditions.....	49
3.2.2.2	Maintenance/collection of cells.....	49
3.2.2.3	Freezing and thawing cells.....	50
3.2.2.4	Counting cells .....	50
3.2.2.5	Transfection .....	50
3.2.2.6	Silencing .....	51
3.2.2.7	Production of NME6-KI (Knock-In) and NME6-KO (Knockout) clones .....	51

3.2.3	Protein analysis .....	54
3.2.3.1	Cell lysate preparation for Western blot analysis .....	54
3.2.3.2	Protein concentration measurement .....	54
3.2.3.3	Standard immunoblotting.....	55
3.2.3.4	Phospho-Histidine immunoblotting .....	56
3.2.3.5	Immunoprecipitation.....	57
3.2.3.6	NME6 expression in human cell lines .....	58
3.2.3.7	NDPK activity.....	58
3.2.3.8	His-Tag removal by thrombin cleavage of NME recombinant proteins .....	60
3.2.3.9	Homo-oligomerization status of NME6 recombinant proteins .....	61
3.2.3.10	Multiple reaction monitoring mass spectrometry (MRM-MS) .....	61
3.2.3.11	Isolation and purification of mitochondria.....	62
3.2.3.12	Mitochondrial subfractionation.....	62
3.2.3.13	Cell fractionation using a commercial kit .....	63
3.2.4	Confocal microscopy .....	63
3.2.4.1	Live cell imaging .....	64
3.2.4.2	Fluorescent immunocytochemistry .....	64
3.2.5	Cellular functions.....	64
3.2.5.1	Apoptosis .....	64
3.2.5.2	Cell cycle .....	65
3.2.5.3	Cellular respiration.....	65
3.2.6	Statistical analysis .....	66
4	RESULTS .....	67
4.1	Preparation .....	67
4.1.1	Production of NME6-KI stable clones.....	67
4.1.2	Production of NME6-KO stable clones .....	70
4.1.3	NME6 silencing .....	72
4.1.4	Production of recombinant proteins.....	74
4.2	NME6 expression and characterization .....	77
4.2.1	NME6 expression in human cell lines .....	77
4.2.2	Detection of NME6 isoforms by Western blot .....	78
4.2.3	NME6-186 isoform predominates in human cells .....	78
4.2.4	Detection of endogenous NME6 isoforms by mass spectrometry .....	79
4.3	NME6 subcellular localization.....	80
4.3.1	Immunofluorescent labeling of endogenous NME6 .....	81
4.3.2	Live cell imaging of exogenous GFP-tagged NME6 isoforms .....	81
4.3.3	Cellular fractionation .....	83

4.3.4	Mitochondrial sub-fractionation.....	85
4.4	NME6 enzymatic properties .....	88
4.4.1	NDPK activity.....	88
4.4.2	Histidine phosphorylation status of endogenous NME6.....	89
4.4.3	Homo-oligomerization status .....	90
4.4.4	Hetero-oligomerization status .....	93
4.5	NME6 interacting partners.....	95
4.5.1	Interactions with other proteins.....	95
4.6	NME6 impact on cellular functions .....	97
4.6.1	Apoptosis .....	97
4.6.2	Cell cycle .....	99
4.6.3	Mitochondrial respiration.....	100
4.6.4	Respiratory chain complexes abundance .....	104
5	DISCUSSION.....	107
6	CONCLUSION.....	117
7	ABBREVIATION.....	118
8	LITERATURE.....	121
9	CURRICULUM VITAE.....	137

# **1 INTRODUCTION**

The nucleoside diphosphate kinases (NDPK/NME/NM23) compose a family of proteins that display one, several or even partial nucleoside diphosphate kinase (NDPK) domains [1]. NDPKs were first described nearly 70 years ago in pigeon breast muscle [2] and yeast [3], where authors described the main enzymatic activity corresponding to the transfer of a terminal  $\gamma$ -phosphate group from a nucleoside triphosphate (NTP) to a nucleoside diphosphate (NDP). As this group of proteins kept on being rediscovered in unrelated fields and model organisms, a peculiar and confusing nomenclature was used to describe the family. Apart to NDPK, the family's members were also named after the anti-metastatic properties of some members, as NME (non-metastatic) or NM23 (non-metastatic clone 23), or even denominated as AWD (abnormal wing discs) after the developmental phenotype defect observed in *Drosophila melanogaster* upon mutation [4]. For the clarity of this dissertation, NDPK/NME/NM23 proteins will be referred exclusively as NME, while the main enzymatic activity and domain will be referred as NDPK activity and NDPK domain.

The human NME family is divided in two groups based on phylogenetic analyses [1]. Group I members (NME1-NME4) share high sequence homology and all display NDPK activity [5,6]. Group II (NME5-NME9) members are more divergent and all lack NDPK activity, with a possible exception for NME6 [6–8].

Although NME proteins have been described decades ago, they sparked considerable interest in the early nineties after the discovery of metastasis suppressor activity of NME1 [9]. The resulting rapid accumulation of knowledge, especially for Group I members, pinpointed that NME protein must oligomerize [10] in order to display NDPK activity. Furthermore, mutations of the *Kpn* (Killer of prune) loop and C-terminal modifications of the proteins were associated with oligomer instability and reduced NDPK activity [11–13]. Other biochemical roles have been associated with NME proteins, including histidine kinase activity [14], transcriptional regulatory functions [15] and 3'-5' exonuclease activity [16].

The biological roles of NME proteins are diverse and dependent on tissue and cell specificity, subcellular localization and enzymatic activity. NME proteins can be either tissues specific (NME5 in testis) [11] or ubiquitously expressed [17,18]. They localize among others, within the cytosol and nucleus (NME1-NME2) [17], mitochondria (NME3 and NME4) [19–21], or cytoskeleton (NME7 in microtubules) [22]. They are associated with a large range of biological effects and diseases, as extensively described in the section (2.3).

The NME family is an ancient group of genes/proteins, found throughout all three domains of life: Bacteria, Archaea and Eukaryota [23], thus emphasizing their necessity in key cellular functions and physiology of cells [24,25]. Group II members arose earlier than most of the members of Group I during the course of evolution, i.e. they are evolutionary “older” [1]. Studies on simple metazoan models like sponges, representing common ancestor of animals, showed that the ancestral sponge NMEGp1Sd displayed similar structure, localization and function as the human NME1/2 homolog [26]. On the other hand, a study conducted on the sponge NME6Sd, a homolog of human NME6, concluded that the cellular function of this protein possibly changed from sponge to human [27].

Unlike NME proteins of the Group I that underwent decades of intensive research, the Group II members are to date barely explored. Available information on the human NME6 is mostly based on three publications from the early 2000s. In 1999, two independent groups first described the *NME6* gene, but disagreed on the length of the resulting protein, describing isoforms of 186 amino acid (aa) or 194 aa long [8,28]. The question about the actual isoform(s) expressed in human cells remained unsolved until now. Similarly, the potential NDPK activity of human NME6 remained debatable [6,8,28], even though the few amino acids deemed essential for enzymatic structure and catalytic activity of the protein are conserved [1]. NME6 seems to localize with mitochondria, although the protein lacks a conventional mitochondrial targeting sequence (MTS) [8,28].

**Aim:** The aim of this doctoral thesis was to produce an extensive description of the human NME6 protein, regarding the cellular and subcellular localization, NDPK activity, oligomerization status, interacting partners, but also the impact on basic cellular functions such as apoptosis, cell cycle and mitochondrial respiration. **Methods:** The human NME6 protein was analyzed by Western blotting and mass spectrometry to unravel the dominant NME6 isoform(s) and its related expression profile in a large panel of human cell lines. The fine cellular localization of NME6 protein was addressed by both confocal microscopy of live and fixed cells, and by cellular fractionation methods followed by Western blotting. The enzymatic properties of the recombinant protein were tested *in vitro* using the standard pyruvate kinase-lactate dehydrogenase coupled assay to measure NDPK activity, while the phosphorylated-histidine status of the endogenous NME6 was tested by Western blotting. The NME6 oligomerization status was tested by crosslinking, size exclusion chromatography and co-immunoprecipitation. Candidate interacting partners were assayed by co-immunoprecipitation. The role of NME6 in basic cellular functions was unrevealed by studying apoptosis and cell



cycle by flow cytometry methods, and mitochondrial respiration using oximetry methods. **Hypothesis:** The endogenous human NME6 protein is expressed in all human cell lines of different tissues of origin, as one or both isoforms described in the literature (194 aa and/or 186 aa). The protein localizes in the mitochondria and potentially interacts with other mitochondrial NME proteins, and/or with proteins suggested by large-scale proteomic data analysis. NME6 is devoid of NDPK activity, but is involved in the regulation of one or several basic cellular functions. **Results:** The NME6 protein is ubiquitously expressed in human cell lines, predominantly as the 186 aa isoform. NME6 failed to display phosphorylated histidine (pHis) and was unable to oligomerize, and accordingly did not display the NDPK activity. NME6 was localized to the mitochondria, facing the matrix space and partially interacting with the mitochondrial inner membrane (MIM). The results were reinforced by NME6 interaction with RCC1L, a protein interacting with mitoribosomes and localized in the mitochondrial matrix compartment. Changes in the NME6 levels did not affect apoptosis or cell cycle, but strongly reduced ADP stimulated respiration upon overexpression, associated with downregulation of respiratory complexes abundance.

To summarize, the NME6 protein is a monomeric, enzymatically inactive NME member, localized in the mitochondrial matrix and impacting mitochondrial respiration.

## **2 LITERATURE OVERVIEW**

### **2.1 Mitochondria and respiration**

#### **2.1.1 Mitochondrial origin**

Mitochondria arose only once in evolution, from the endosymbiosis of an  $\alpha$ -proteobacterium into a proto-eukaryotic cell, early after the emergence of eukaryotes, as widely accepted in the endosymbiotic hypothesis [29,30]. Accordingly, mitochondria possess their own DNA and transcription/translation machinery. The symbiosis event conferred advantages to the eukaryotic cell, among which the key improvement is the generation of ATP through aerobic respiration [31].

#### **2.1.2 Mitochondrial organization**

Mitochondria are tube-shaped, double-membrane organelles, with a diameter ranging from 0.5 to 1  $\mu\text{m}$ , and a variable length from 1 to 10  $\mu\text{m}$ . The mitochondrial outer membrane (MOM, also shortened as OMM and OM in literature), similar to eukaryotic membranes in lipids composition, is surrounding the cardiolipin-rich mitochondrial inner membrane (MIM, also shortened as IMM and IM in literature), similar to cardiolipin-containing bacterial membranes [31]. The aqueous compartment between the two membranes is called the intermembrane space (IMS), while the aqueous compartment surrounded by the MIM is called the matrix (Figure 1).

The MOM forms the first barrier and controls the diffusion of molecules inside and outside the mitochondria (ions, nucleotides, metabolites, proteins) via specific channels, carriers and translocase complexes. The MOM is relatively permeable to ions and small molecules due to porin protein complexes (typically VDAC: voltage dependent anion channel) that allow the passage of molecules smaller than 6000 Daltons, leading to an IMS chemical composition comparable to cytosol in this respect [32].

The MIM, in contrast, shows strong impermeability, even to the smallest of ions ( $\text{H}^+$ ) [33]. It can be divided into several compartments. Large MIM invaginations within the mitochondria, called cristae, are apically closed by cristae junctions (CJ) that represent a diffusion barrier for  $\text{Ca}^{2+}$  and  $\text{H}^+$  between the cristae lumen and the IMS [34]. Cristae are essential for oxidative phosphorylation (OXPHOS), based on the creation of a proton gradient between cristae lumen and matrix, as described in section (2.1.6.2). The rest of the MIM, directly facing the MOM is called inner boundary membrane (IBM), where MIM and MOM are parallel and form contact

sites [35]. It is believed that IBM host numerous carriers important for efficient exchanges between cytosol and mitochondria, including, among others, protein translocase supercomplexes (translocase of the inner membrane / translocase of the outer membrane, (TIM/TOM)), metabolite carriers (adenine nucleotide translocator (ANT), mitochondrial creatine kinase (mtCK)) and ions channels [35,36].

The matrix compartment hosts the entire mitochondrial genetic system. The mitochondrial DNA (mtDNA) and transcription machinery forms the nucleoid. The transcribed polycistronic RNA is processed in the RNA granule, where mitoribosomes are also assembled [37,38]. The protein translation occurs in the vicinity of the MIM, where mature mitoribosomes are localized [39]. Matrix is the site for numerous metabolic processes, including the Krebs cycle and the  $\beta$ -oxidation of fatty acids. The aerobic respiration leads to the massive production of ATP, within the matrix, as described in the section (2.1.6.2).

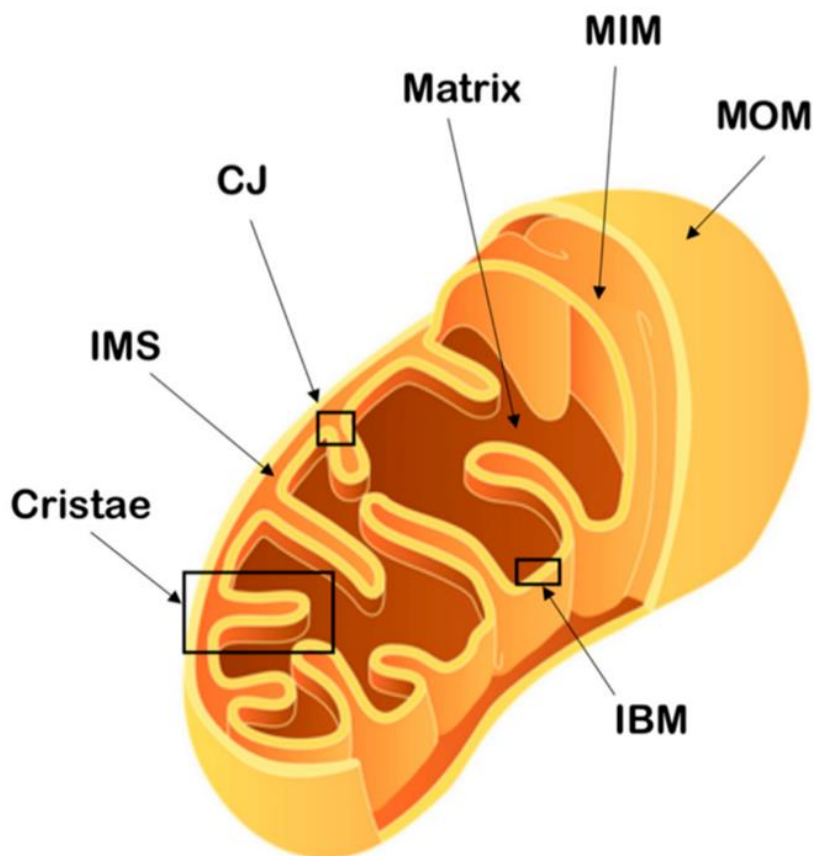


*Figure 1 : The mitochondrial structure. The mitochondrial outer membrane (MOM), mitochondrial inner membrane (MIM), inner boundary membrane (IBM), cristae junctions (CJ), intermembrane space (IMS), cristae and mitochondrial matrix are indicated. (adapted from Protasoni et al., 2021) [40]*

### **2.1.3 Mitochondrial dynamic**

Mitochondria are dynamic organelles, and adjust their shape, distribution and size through coordinated fusion/fission events [41]. The fusion results in a long network of branched mitochondria, while fission leads to round and isolated mitochondria. The fusion/fission balance is dynamically tuned to meet the cellular needs [42]. The rapid morphological changes of mitochondria are important for several cellular processes, including cell cycle and apoptosis [41]. Fusion and fission are mainly controlled by GTPases of the dynamin family [43].

The mitochondrial fission (Figure 2) results in the division of one mitochondrial filament into two or more daughter mitochondria. The main actor of fission is Drp1 (dynamin-related protein 1), a cytosolic protein recruited at the MOM surface and driving membrane constriction via GTP hydrolysis. Fission takes place at the endoplasmic reticulum (ER)/mitochondria contact sites. The ER plays an important role in mitochondria pre-constriction [41,42].

The mitochondrial fusion (Figure 2) allows the sharing and exchange of mtDNA, proteins, lipids and metabolites and lead to filamentous mitochondria network. The fusion is driven by GTPases of the dynamin family: mitofusins MFN1 and MFN2 mediate the fusion of the MOM by forming oligomers, while OPA1 (optic atrophy 1) mediates the fusion of the MIM [41,42].

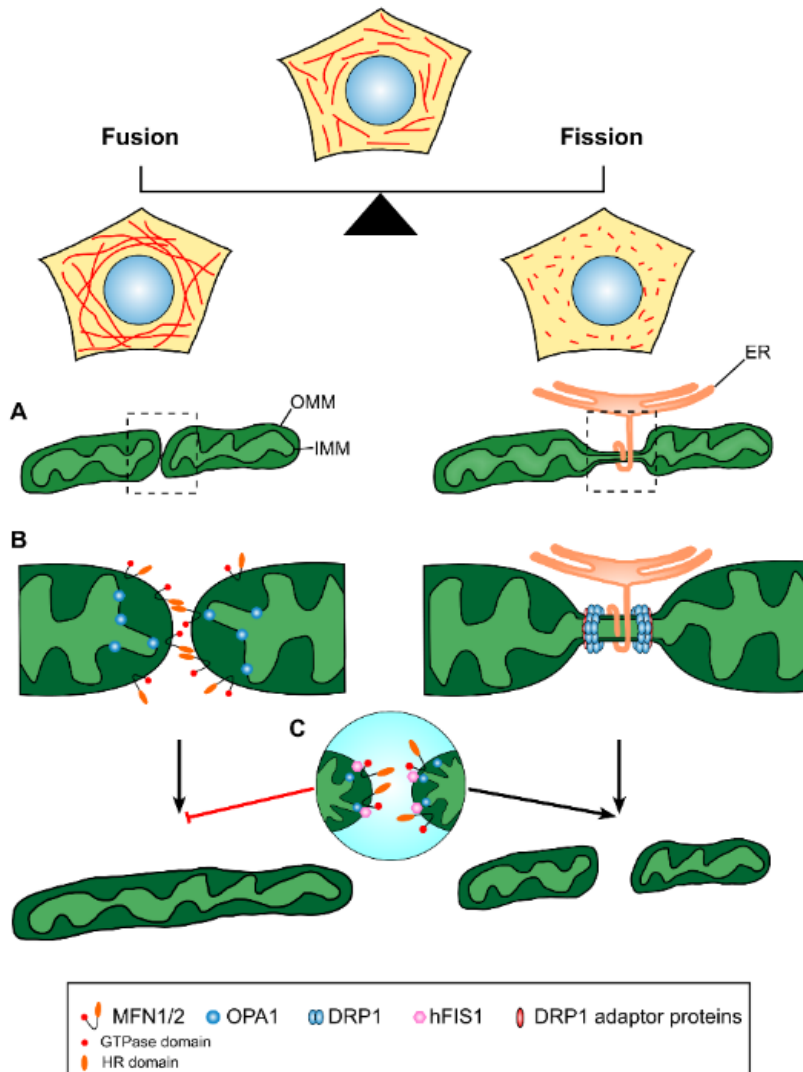


*Figure 2 : Mitochondrial fusion and fission mechanisms. (A) Mitochondrial fusion (left) results in the merging of two distinct mitochondria, while mitochondrial fission (right) results in the division of a mitochondria involving endoplasmic reticulum (ER) at the prestriction site. (B) OMM fusion are promoted by MFN1/MFN2, while IMM fusion is mediated by OPA1. Mitochondrial fission is regulated by the DRP1 and adaptor proteins. (C) The mitochondrial fission 1 (hFIS1) help the fission by blocking MFN1, MFN2 and OPA1 GTPase function. OMM, outer mitochondrial membrane; IMM, inner mitochondrial membrane; HR, heptad repeat. (Taken from Kyriakoudi et al., 2021) [42]*

#### **2.1.4 Mitochondrial genome/proteome**

Mitochondria possess their own DNA, inherited from the ancestral bacteria during the endosymbiosis event [29,30]. However, the mitochondrial genome is highly reduced compared to existing proteobacteria, due to a loss of non-essential genes and a massive endosymbiotic

transfer of essential genes from mitochondrial to nuclear DNA during evolution [44]. Nowadays, the human mtDNA encodes only 37 genes: 11 mRNAs translated in 13 proteins, all components of the OXPHOS complexes, 2 rRNAs (16S and 12S), and 22 tRNAs (Figure 3). The mtDNA is transcribed in two long polycistronic RNAs (light and heavy strand), that are further cleaved and processed to release mature RNAs used by the mitochondria [40,45]. The remaining 1100 to 1400 mitochondrial proteins (99% of the mitochondrial proteome) are encoded in the nucleus, translated in the cytosol and imported to the mitochondria through several mechanisms [46]. This organization implies a constant cross-talk between mitochondria and the nucleus to ensure cellular homeostasis, called mitonuclear communication [47].

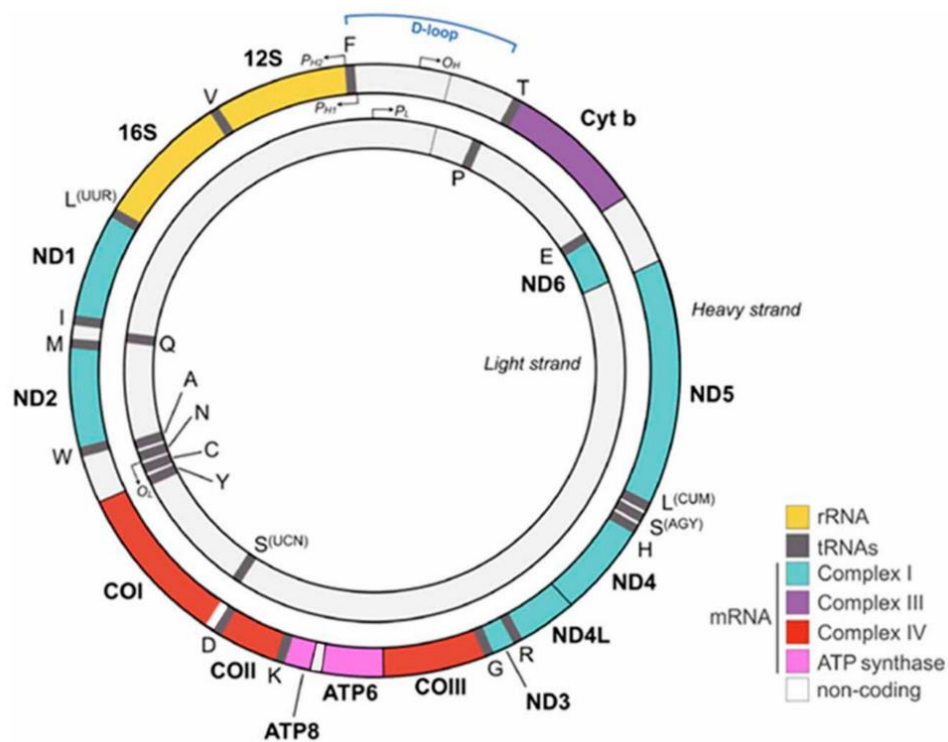


*Figure 3 : Organization of the human mitochondrial DNA (mtDNA). Each gene is indicated with a colored bar and all the genes encoding protein subunits of the same complex are represented by the same color. rRNAs are indicated in yellow and tRNAs in gray. (Taken from Protasoni et al., 2021) [40]*

### **2.1.5 Mitochondrial protein import**

Protein import to the mitochondria is a mechanism of major importance, since proteins produced in the cytosol cannot freely pass through the mitochondrial membranes. Several pathways have been described, as presented in Figure 4 [48]. The presequence pathway relies

on a specific N-terminal amino acid sequence, called mitochondrial targeting sequence (MTS), recognized by the TOM/TIM machinery to import proteins directly into the matrix. The MTS is often cleaved after import and allows the shortened protein to fold in a mature and active conformation. About two thirds of mitochondria-imported proteins display the MTS and use the presequence pathway [49]. Other mechanisms are specific for the incorporation of proteins within the MOM (SAM and MIM pathways), or within the IMM (MIA and carrier pathways), and rely on specific motifs and/or chaperones to help the import (Figure 4) [48]. It is to note that some well characterized proteins of the mitoribosome are imported into the matrix without displaying the classical MTS sequence [50]. Lately, novel mechanisms based on internal MTS sequences (iMTS) were proposed to help the import of proteins within the matrix [50,51].

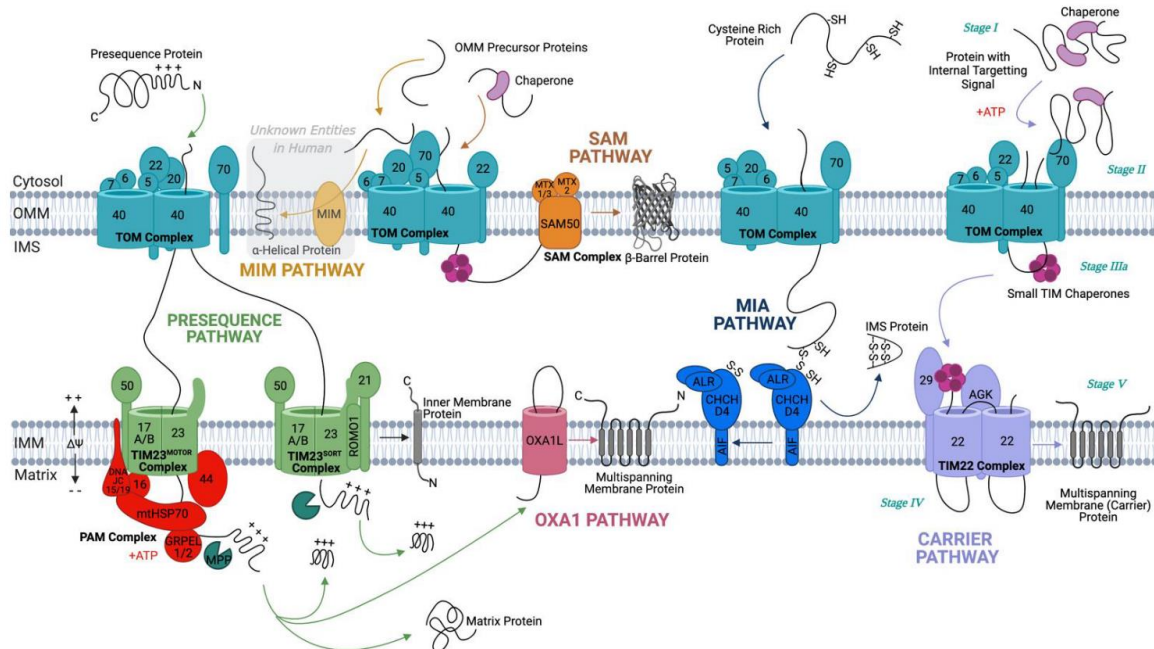


Figure 4 : The human mitochondrial protein import pathways. (Taken from Needs et al., 2021) [48]

### 2.1.6 Mitochondrial functions

Mitochondria are involved in numerous and diverse cellular functions (Figure 5), including apoptosis, cell differentiation, stem cell maintenance, inflammation, and others (reviewed in [52]).

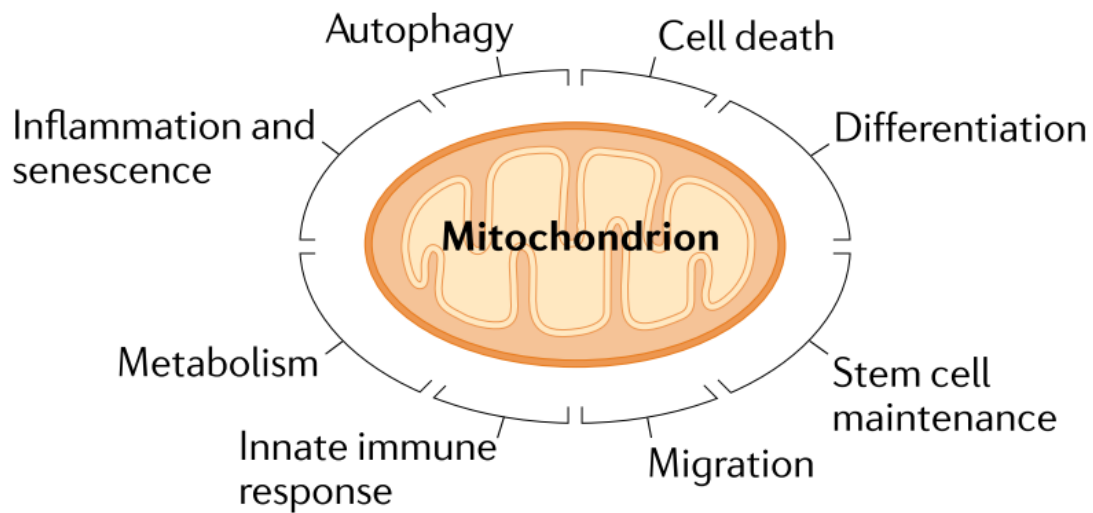


Figure 5 : Mitochondrial impacts on cellular functions. (Taken from Giacomello et al., 2020) [52]

### 2.1.6.1 Apoptosis

Ironically, the fine regulation of cell death is essential for health and life of multicellular organisms [53]. Cancers and auto-immune diseases are promoted by inhibition of cell death, while neurodegenerative diseases are triggered by an excess of cell death [54]. Apoptosis is the major form of regulated cell death, and was shown to be crucial for multicellular organisms, from embryonic development to immune homeostasis [55]. Apoptosis is triggered via two major pathways (Figure 6): the extrinsic pathway is the result of a ligand's fixation on death receptors at the surface of the plasma membrane, while the intrinsic pathway is activated by internal apoptotic stimulus [54]. Eventually, both pathways lead to activation of caspase 3 and caspase 7, and apoptosis. Mitochondria play a central role in the intrinsic pathway. Upon apoptotic stimulus, the mitochondrial outer membrane permeabilization (MOMP) triggered by activation and dimerization of pro-apoptotic proteins (BCL2 associated X / BCL2 homologous antagonist/killer (Bax/Bak)) results in the release of the soluble IMS into the cytoplasm, including proteins such as cytochrome C, SMAC (second mitochondria-derived activator of caspase), OMI (Serine protease HTRA2) and others. Cytochrome C can, therefore, bind to the cytosolic APAF1 (apoptotic peptidase activating factor 1) forming a protein complex called apoptosome, which activate caspases and lead to apoptosis. Together, the liberation of proteins such as SMAC and OMI, enable the blockage of caspase inhibitors like XIAP (E3 ubiquitin-protein ligase) and facilitate the apoptosis [54].



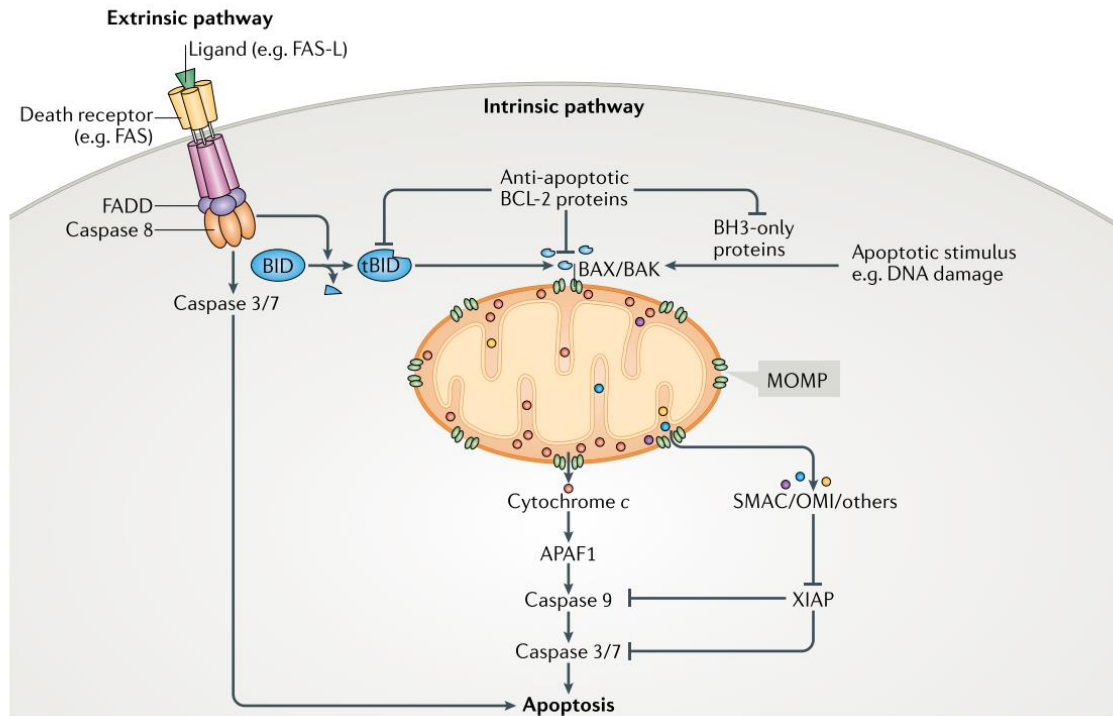
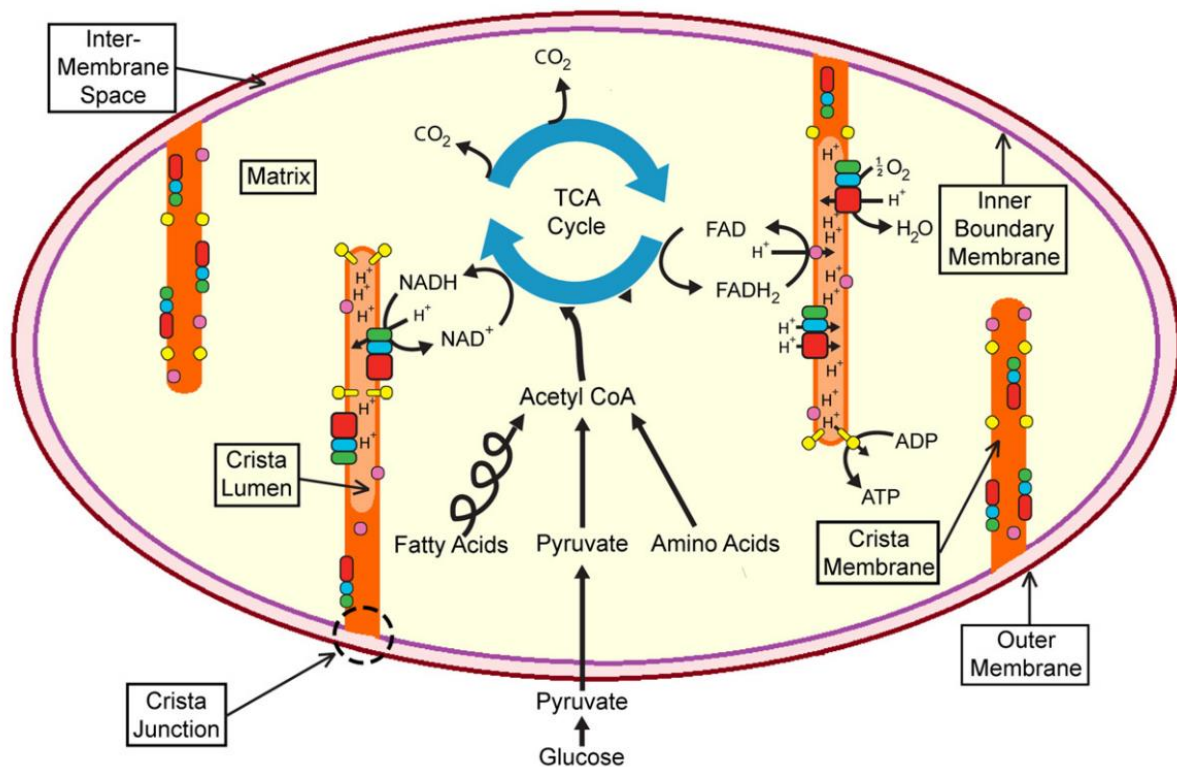


Figure 6 : *The extrinsic and intrinsic apoptosis signaling pathways. Extrinsic pathway is triggered by fixation of a ligand on the death receptor at the cellular surface. Intrinsic pathway process intracellular apoptosis signals around mitochondria, which is the central actor of apoptosis. (Taken from Bock et al., 2019) [54]*

### 2.1.6.2 Aerobic respiration

Mitochondria take a central role in the cellular metabolism by efficiently generating ATP through aerobic respiration, and are thus considered as ‘powerhouses of the cell’ [40]. First, the glycolysis occurring in the cytosol converts glucose into pyruvate, which will be transported into the mitochondrial matrix and oxidized as Acetyl-Coenzyme A (Acetyl CoA). The latest molecule, which is also a product of the  $\beta$ -oxidation of fatty acids and metabolization of amino acids, will be processed in the Krebs cycle (also named citric acid cycle or tricarboxylic acid cycle (TCA)), resulting in the production of NADH and FADH<sub>2</sub> molecules. The two high energy electron carriers will be used to produce ATP through the OXPHOS process, involving the mitochondrial electron transport chain (ETC) and the ATP synthase, densely packed in cristae (Figure 7). The ETC is composed of four protein complexes embedded in the MIM (Figure 8). Complexes I and II are loading the chain with electrons by the utilization of NADH and FADH<sub>2</sub> respectively. Electrons are transferred to complex III via ubiquinone, and will be used for the reduction of cytochrome C. The soluble cytochrome C

will finally transfer electrons to complex IV where they will be used to catalyze the formation of  $H_2O$  from proton and oxygen. The ETC results in the pumping of protons from the mitochondrial matrix to the cristae lumen, part of the IMS, via complexes I, III and IV. As protons are trapped in the cristae lumen, a proton gradient is created across the MIM. The ATP synthase complex, also named complex V, uses the proton gradient to catalyze in the matrix the formation of ATP from ADP and inorganic phosphate (Pi) [56–58].



*Figure 7 : Aerobic respiration. Acetyl-CoA originating either from glycolysis, fatty acid or amino acid metabolisms is processed in the Krebs (TCA) cycle in the mitochondrial matrix to release NADH and FADH<sub>2</sub>. The two high energy electron carriers are used in the ETC to pump protons from matrix to cristae lumen, via the consumption of oxygen. The return of protons in the matrix is used to generate ATP. (Taken from Ikon et al., 2017) [58]*

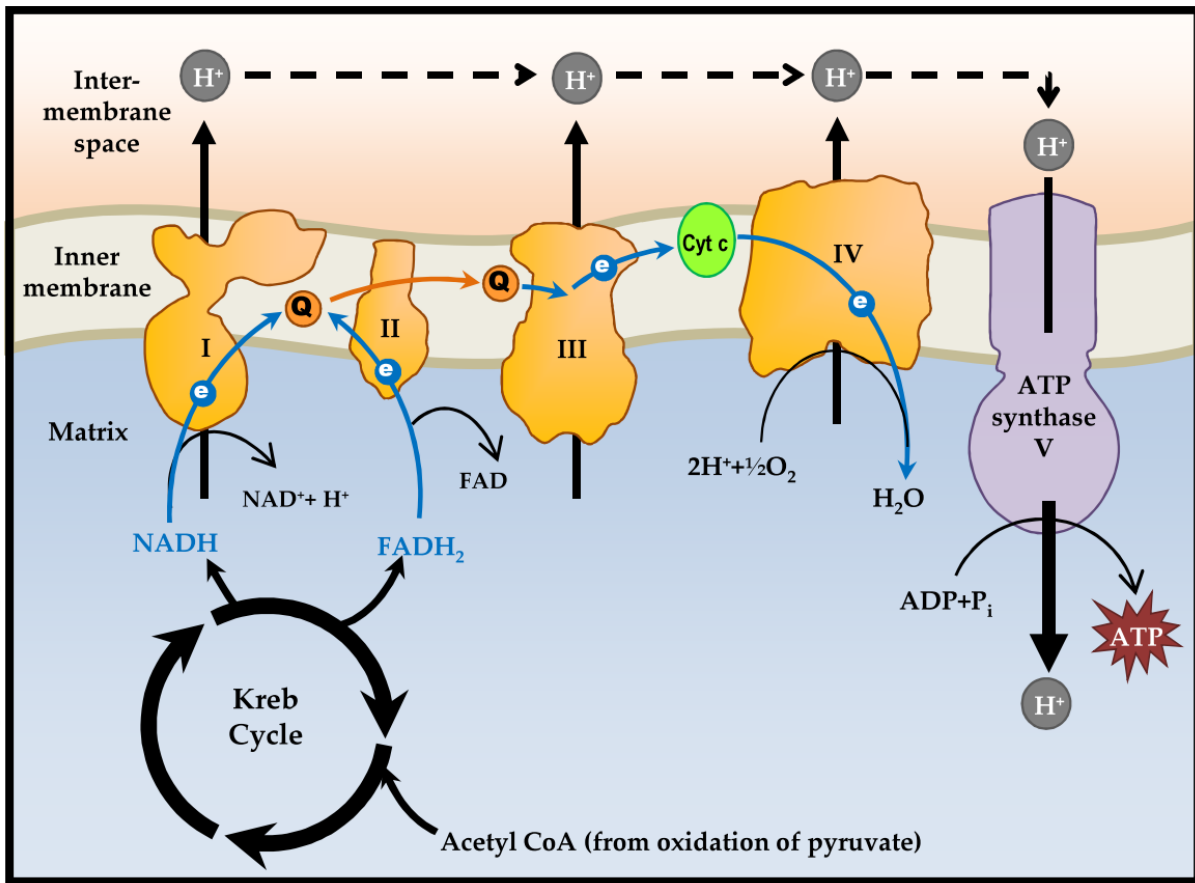


Figure 8 : *Electron transport chain and oxidative phosphorylation.* Electrons ( $e$ ) fueled by NADH and  $FADH_2$  to complex I and II are transferred along the chain via the ubiquinone (Q) and cytochrome C (CytC) proteins until complex IV, where oxygen is reduced to water. The process generates the pumping of protons ( $H^+$ ) from the matrix to the cristae lumen (part of IMS). The proton gradient created is used by the ATP synthase to catalyze the production of ATP. (Taken from Yusoff et al., 2015) [59]

## 2.2 NDPK activity

Nucleoside diphosphate kinases are characterized by their NDPK domain, a specific protein sequence and structure that accommodates the center for NDPK activity. NDPK activity was described as the reversible transfer of the terminal  $\gamma$ -phosphate group from nucleoside triphosphate, mostly ATP, to nucleoside diphosphate [60], thus responsible for the maintenance of cellular nucleotide pool [61]. The NDPK domain catalyzes the reaction through a ping-pong mechanism [60,62,63], schematized on Figure 9. First the ATP enters the NDPK catalytic site and its  $\gamma$ -phosphate group is transferred to the main catalytic histidine (H118 for human

NME1). The histidine is phosphorylated on the first nitrogen atom of the imidazole group (1-pHis), characteristic for NME proteins [64]. This represents the “ping” part of the reaction, also named autophosphorylation. The NME protein is, thus, in a transient, high energy phospho-histidine state. The product of the “ping” reaction is released (ADP), and another NDP takes place in the catalytic site. The phosphate group is then transferred to NDP as a  $\gamma$ -phosphate group, to form NTP, which represents the “pong” part of the reaction. The reaction takes place in the catalytic site, that forms a structural pocket accommodating the ATP substrate (Figure 10).

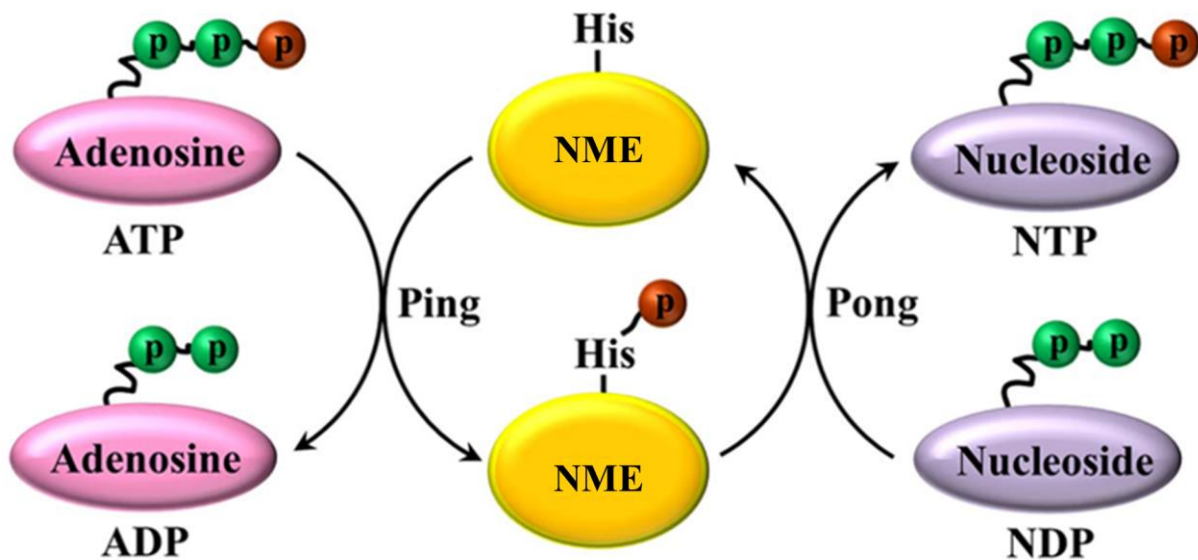
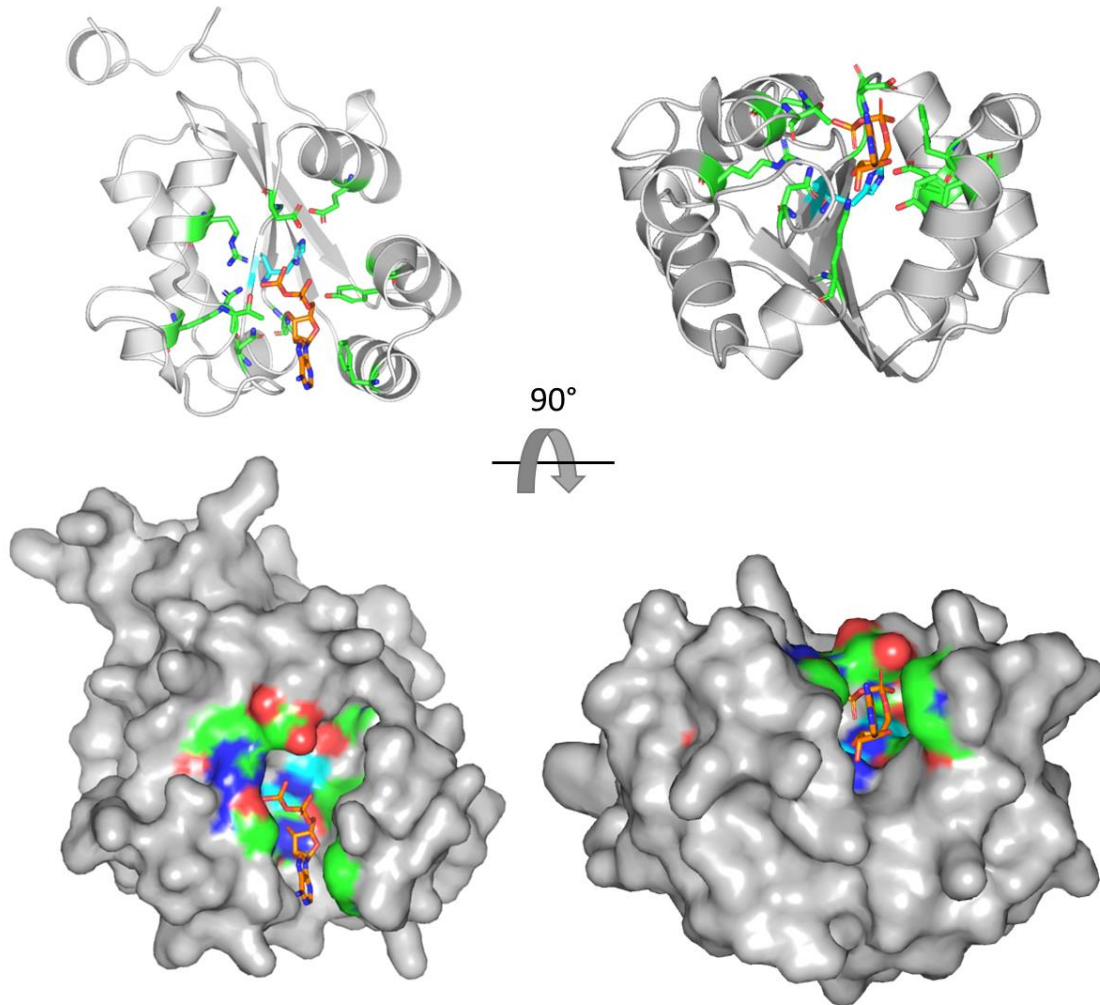
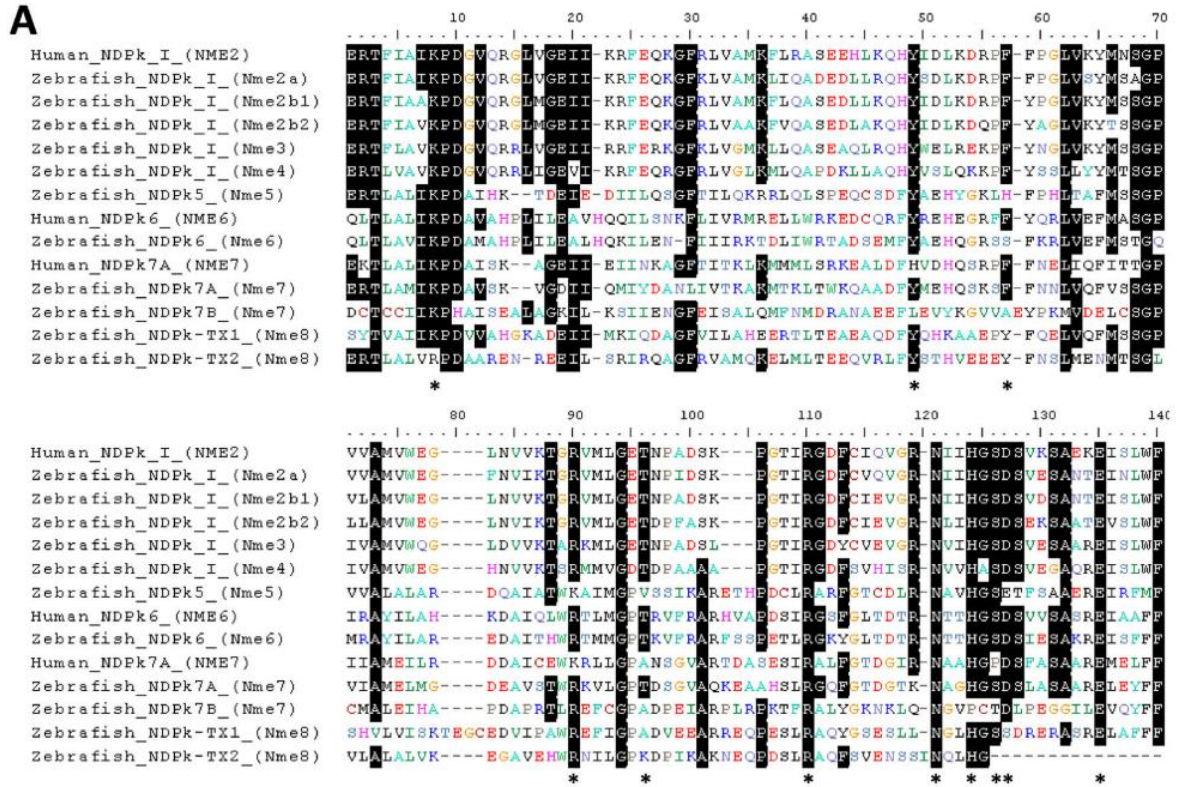


Figure 9 : *Schematic representation of the NDPK reaction.* NME proteins transfer the  $\gamma$ -phosphate group from NTP (mostly ATP) to NDP. The ping-pong reaction involves the phosphorylation of the specific histidine residue in the catalytic site (“ping”, autophosphorylation), prior to the transfer of the mentioned phosphate group to any NDP to form NTP (“pong”). (Adapted from Yu et al., 2017) [65]



*Figure 10 : Representation of the human NME1 protein bound with ADP (PDB structure: 2HVD). The protein is displayed as cartoon (up) and surface (down) representations, in the same orientation. A 90° rotation along the X axis is applied between the left and the right molecule. The amino acids deemed essential for enzymatic activity are represented in green. The main histidine H118 is represented in cyan. The ADP molecule is represented in orange and is fitted in the NDPK catalytic pocket.*

The alignment of the NDPK domains from human and other species revealed several amino acid residues thoroughly conserved through evolution (Figure 11) [1]. Those residues, mainly components of the catalytic site including the main histidine responsible for the ping-pong reaction, are represented in green and cyan on Figure 10. They are deemed essential for the NME structure and enzymatic activity.



*Figure 11 : Sequence alignment of zebrafish and human NME protein domains. Residues identified as important for the catalytic mechanism are indicated by an \*. (Taken from Desvignes et al., 2009) [1]*

Interestingly, all NME proteins displaying enzymatic activity are oligomers [13,66], and denaturation into monomers impairs their NDPK activity [67]. NME proteins can form homohexamers or heterohexamers as reported in eukaryotes [17,68–70], archaea and some bacteria [71,72]. In some other bacteria, NME’s have been reported to oligomerize as tetramers [73–75]. Structures, folding and stability of NME proteins from a wide range of species was nicely reviewed by Georgescauld et al. [13]. It is accepted that the monomers first assemble as head to tail dimers before aggregating as tetramers or hexamers, as represented in Figure 12. The oligomerization helps the formation of the catalytic site and the stabilization of NME complexes [13].

Several structures of the NME proteins are important for oligomer assembly and enzymatic activity, of which the *Kpn* loop and the C-terminal extension are the most studied. The *Kpn* loop participates in the stabilization of the NME complexes at the trimer interface upon the formation of hexamers [76]. The *Kpn* loop is named after the “Killer of prune” mutation of the *Drosophila awd* gene, which encodes for an orthologue of human NME1 [69]. In *Drosophila*,

the mutation does not trigger particular phenotype, but is lethal when associated with a null mutation of the *plum* gene that encodes for a phosphodiesterase [77]. The P96S mutation (human NME1 numbering) was shown to increase the flexibility of the *Kpn* loop [12], which consequently destabilized the hexameric structure of NME proteins. In human cells, the mutated NME1<sup>P96S</sup> displayed autophosphorylation and NDPK activity, but lost its antimetastatic characteristic [78]. The C-terminal part is highly variable in sequence when comparing the different NME proteins. It was shown to be important in the oligomerization of hexamers. A *Kpn* mutation combined with C-terminal shortage is often associated with oligomer dissociation and loss of enzymatic activity [12,76,79].

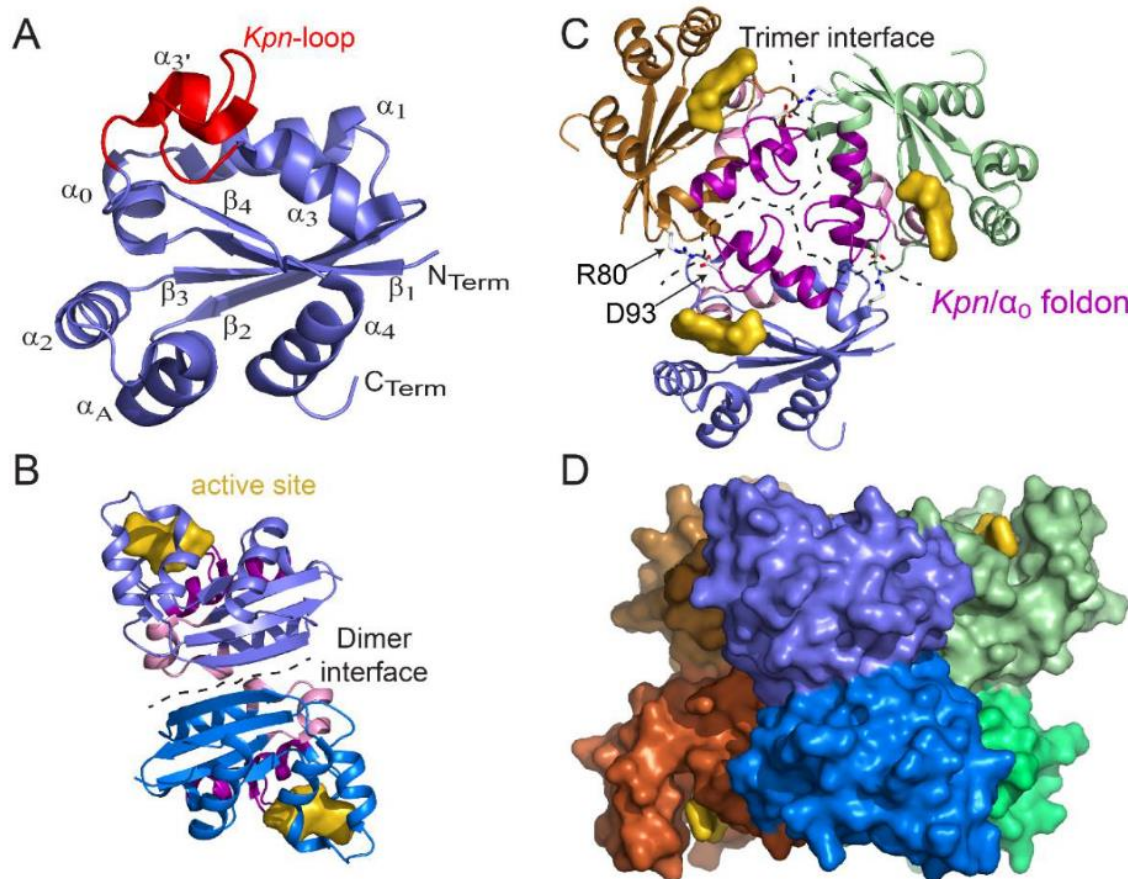


*Figure 12 : Structure of the monomer, dimer, trimer, and hexamer of the NDPK from Mycobacterium tuberculosis (Mt). (A) View of the monomer with labeled secondary structural elements. (B) Side view of a dimer showing the dimer interface and the active site pocket. (C) Top view of a trimer. At the trimer interface, the *Kpn*/ $\alpha_0$  foldon and the R80–D93 salt bridge are involved in hexamer assembly. (D) Side view of the surface of the six-color hexamer Mt-NDPK. The active site is colored in yellow. (Taken from Georgescauld et al., 2020) [13]*

To summarize, the NDPK activity, described as a reversible ping-pong reaction, takes place in the catalytic pocket of the NDPK domain. The oligomerization of NME proteins is essential for NDPK activity. The *Kpn* loop and the C-terminal extension are critical structures for the stability of the NME oligomer.

## 2.3 Human NME family

In vertebrate, ten NME genes are recorded to date, divided into two groups based on their structures and phylogenetic analysis [1]. The human Group I is composed of NME1, NME2, NME3 and NME4, four genes/proteins that seems to have emerged from a common ancestor gene around teleost radiation [1]. They are highly conserved in their amino acid sequence (58-88% aa homology [80]), possess a single NDPK domain and all display NDPK activity. The human Group II members (NME5, NME6, NME7, NME8, NME9) arose earlier in the course of evolution, i.e. they are more “ancient”. Phylogenetic analysis indicates that they emerged from a common ancestor after a duplication event that occurred before the chordate radiation [1]. The related proteins are more divergent among themselves in their amino acid sequence and structure (28-45% aa identity), and differ from Group I proteins (25-34% amino acid identity) [24]. They possess one or several NDPK domains, and display additional domains such as DPY-30, DM10 and Thioredoxin (Figure 13). Except for NME6, Group II NMEs are all related to ciliary function [80]. The NME10 does not belong to any of the groups, since its partial NDPK domain was inserted in the gene much more recently, before the gnathostome radiation [1].

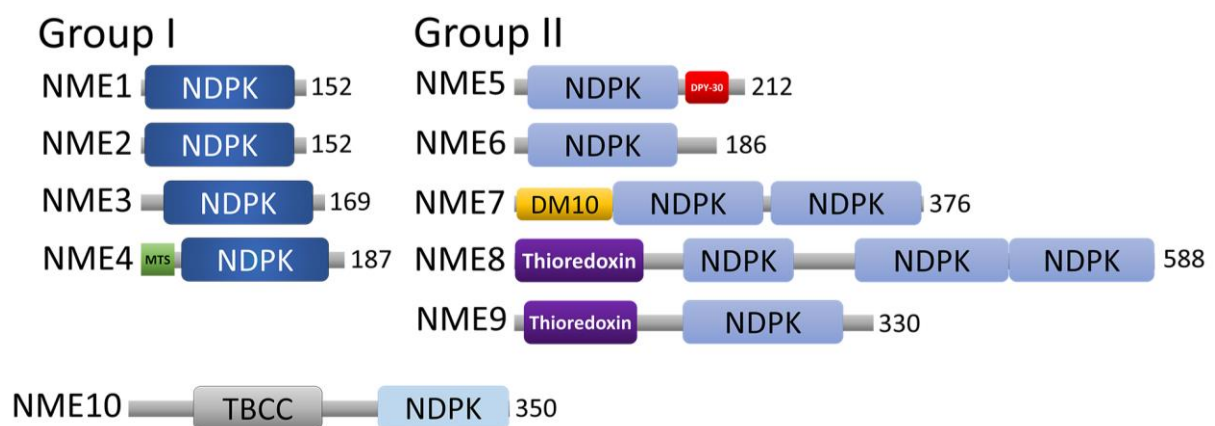


Figure 13 : Schematic representation of human NME proteins. The total amino acid length of the protein is shown at the end of each protein. Protein domains have been indicated with



*boxes, and each protein has been searched against SMART/Pfam databases. Abbreviations of domain names are retrieved from SMART/Pfam databases and indicated in the figure. Shortened name MTS stands for mitochondrial targeting sequence domain. (Taken from Proust et al., 2021) [81]*

NME1 is by far the most studied protein of the family. In 1988, Steeg et al. demonstrated the association of NME1 protein high expression with low metastatic potential of the tumor [9], highlighting NME1 as a metastasis suppressor protein. After this breakthrough, a large number of studies confirmed that NME1 downregulation or loss of expression is correlated with metastasis onset and poor clinical outcome in many tumor types [82], however the detailed mechanism of this phenomenon is still under investigation. NME2, although less described, seems to have a role in the metastatic process as well [83]. Furthermore, NME2 was shown to be involved in heart diseases through its critical role in cardiac contractility [84]. NME1 and NME2 are highly homologous (88% aa identity), share the same cellular localization and have been shown to interact in hetero-hexameric structures [17,85]. They are involved in several processes such as apoptosis [86,87], proliferation [88], differentiation and development [23,89,90], vesicular trafficking [18], adhesion and migration [91,92]. They are both enzymatically active, and besides the NDPK activity, they are associated, together or individually, with other biochemical activities [17] such as histidine kinase activity [14], transcriptional regulatory functions [15], and 3'-5' exonuclease activity [16].

The two remaining members of the Group I, NME3 and NME4, are both colocalizing with mitochondria. NME3 displays a short N-terminal hydrophobic peptide likely anchoring the protein to the MOM [19]. The homozygous mutation of NME3 is associated with fatal mitochondrial neurodegenerative disorder, where the mitochondrial fusion is impaired [19]. Similarly, downregulation of NME3 increases mitochondrial fragmentation and oxidative stress [20]. In cancer, downregulation of NME3 is generally associated with poor prognosis [93].

NME4 is the only member of the human NME family to display a N-terminal MTS. This typical sequence helps the protein's entry to the mitochondria, and is cleaved after protein import. The shorter, mature NME4 binds cardiolipins of the MIM, and is either facing the IMS or the matrix [94]. NME4 was shown to interact with OPA1 in the IMS, thus affecting mitochondrial fusion and dynamics [5,18]. It was also shown to transfer the cardiolipin between MIM and MOM, thus triggering apoptosis or mitophagy [95,96]. More recently, NME4 was demonstrated as a

novel metastasis suppressor gene, where the NME4 mutations or the NME4 depletion increased epithelial-mesenchymal transition, but also migratory and invasive potential of human cells [97]. In cancer, high NME4 expression is generally associated with good prognosis [97].

To this date Group II members are scarcely studied and thus poorly described. The human NME5 expression seems to be tissue dependent, as it was almost exclusively found in testis [11]. The protein displays a NDPK domain and a DPY-30 domain of generally unknown function. Its NDPK domain conserved most of the residues important for enzymatic activity. However, NME5 is lacking measurable NDPK activity probably due to a three amino acid insertion in the *Kpn* loop, as compared to NME1 [98]. Lately, the protein was associated with motile cilia function, when a homozygous mutation of NME5 was found as the cause of primary ciliary dyskinesia in human patients [99].

NME7 displays one DM10 domain in the N-terminal, followed by two NDPK domains. As described for NME5, both NDPK domains of NME7 show a three amino acid insertion in the *Kpn* loop compared to NME1. The protein is devoid of NDPK activity [6]. Recently, two impressive cryo-electron microscopy studies resolving structures of the ciliary doublet of microtubules revealed the presence of NME7 (bovine) and its homologue FAP67 (*Chlamydomonas reinhardtii*) within the microtubule. The protein interacts with microtubules through its DM10 domain, leaving the NDPK domains accessible [22,100].

NME8 and NME9 are very similar since NME9 arose through duplication of NME8 gene around the appearance of mammals [1]. They possess a thioredoxin domain and one or several NDPK domains. NME8 was shown to be involved in cilia motility, as NME5 and NME7. Mutation of NME8 was correlated with primary ciliary dyskinesia, left–right asymmetry randomization, and male infertility [101]. NME9 was shown to associate with microtubule structures in lung and testis tissues [102]. Its expression was recently associated with poor outcome in a specific type of lymphoma [103].

## 2.4 Human NME6 protein

Similar to other Group II members, very few studies addressed NME6. The human gene/protein was first described in 1999 by two independent research groups. Mehus et al. [28] described the human NME6 gene located on the chromosome 3p21.3. They predicted a protein product of 186 amino acids, with a molecular mass of 21.142 kDa and a calculated isoelectric point of 8.5. By comparing the protein with NME1, the authors reported additional sequences at the N-terminus (7 aa) and at the C-terminus (22 aa) of NME6, an extra amino acid at the position L30 and a 3 amino acid insertion in the *Kpn* loop. By semiquantitative RT-PCR followed by northern blot analysis, the group revealed that NME6 is expressed in every tissue studied, with a mRNA abundance considered as moderately low. They pinpointed that NME6 conserved all of the amino acids essential for enzymatic structure and activity, but mentioned that they were unable to measure NDPK activity from the recombinant protein they produced. Tsuiki et al. [8] described the same gene found on the chromosome location 3p21.3. They predicted an NME6 protein of 194 aa, with 8 extra amino acid on the N-terminus compared to the protein described by Mehus et al. By northern blot analysis, they showed that NME6 expression levels vary depending on human tissue or cell line studied, with the highest mRNA levels found in placenta, heart and skeletal muscles. A Western blot analysis of human cell lines revealed a single band when probed with NME6 antibody, with expression levels that can vary from one cell line to another. They tried to uncover the NDPK activity of their recombinant GST-NME6 by following a radioactive  $\gamma$ -phosphate along the NDPK ping-pong process. They described that GST-NME6 is able of autophosphorylation (“ping”), i.e. to transfer the  $\gamma$ -phosphate from an NTP to the main histidine of the NME6’s catalytic site. However, this autophosphorylation was very low, 30 time lower than the positive control GST-NME1. They further studied the ability of the phosphorylated GST-NMEs to transfer their phosphate to a “cold” NDP (“pong”). They showed that both recombinant GST-NME6 and GST-NME1 were able to transfer their radioactive phosphate to NDP. By this unusual method, they argued that the human NME6 protein could display some NDPK activity. By immunocytochemistry and cell fractionation, they co-localized NME6 with mitochondria. Further, they showed that NME6 overexpression led to SAOS2 cells growth suppression, together with apparition of multinucleated cells due to mitosis failure. Later in 2005, Yoon et al. [6] aimed to describe the enzymatic properties of human NME proteins (NME1 to NME8). In this attempt, they produced and analyzed a recombinant His-tagged NME6 protein of 194 aa. By studying the transfer of radioactive  $\gamma$ -phosphate from NTP to NME’s, they showed that NME6 was not able to autophosphorylate

(“ping”). Similarly, the classical NDPK activity assay they performed revealed a lack of NDPK activity for NME6, while it was detectable for NME1, NME2 and NME4. Authors also studied the ability of NME’s to bind and cleave DNA through a 3’ 5’ exonuclease activity. While they found it for NME1, NME5, NME7 and NME8, such activity was absent from NME6 recombinant proteins. Altogether, the three main sources of information for the human NME6 protein led to contradictory results that are summarized in Table 1.

*Table 1 : Information summary from the three major publications describing the human NME6 protein*

	<b>Mehus 1999</b> [28]	<b>Tsuiki 1999</b> [8]	<b>Yoon 2005</b> [6]
<b>NME6 length</b>	186 aa	194 aa	194 aa
<b>NME6 mRNA expression</b>	Ubiquitous	Tissue specific	/
<b>Localization</b>	/	Mitochondria	/
<b>Autophosphorylation (Ping)</b>	/	Yes (but weak)	No
<b>Phosphate transfer (Pong)</b>	/	Yes	/
<b>NDPK activity</b>	No	Probable	No
<b>3’ 5’ exonuclease activity</b>	/	/	No
<b>Biological role</b>	/	Growth suppression	/

Nowadays, the Ensembl database [104] contains several predicted transcripts for the human NME6 gene, coding for different isoforms of the NME6 protein (Figure 14). NME6 gene contains four start codons in line with the accepted open reading frame. The transcripts following the usual intron splicing theoretically lead to expression of NME6-194, NME6-186, NME6-141 and NME6-88 (named after the aa length of each protein). Alternative splicing is also predicted, and could result in the production of NME6-114 from the first start codon, or NME6-163 and NME6-119 from the second start codon. It is to note that with the exception of NME6-163, all predicted NME6 isoforms are in the same reading frame, thus sharing the amino acid sequences and the stop codon. The alternative splicing predicted for NME6-163 changes the reading frame after splicing, leading to a different protein sequence and a different stop codon used. Other NME6 isoforms are predicted but not represented on Figure 14, namely NME6-174, NME6-111, NME6-61, due to the lack of a predicted stop codon for the mentioned isoforms. Since NME6 Western blots available in the literature and in our early experiments display a single band with a protein size around 20 kDa [8], the isoforms NME6-194 and

NME6-186 are the best candidate to be expressed endogenously. Moreover, among the predicted isoforms, only NME6-194, NME6-186, NME6-141 and NME6-114 possess the immunogenic sequence used to produce the highly specific anti-NME6 antibody used in this study.

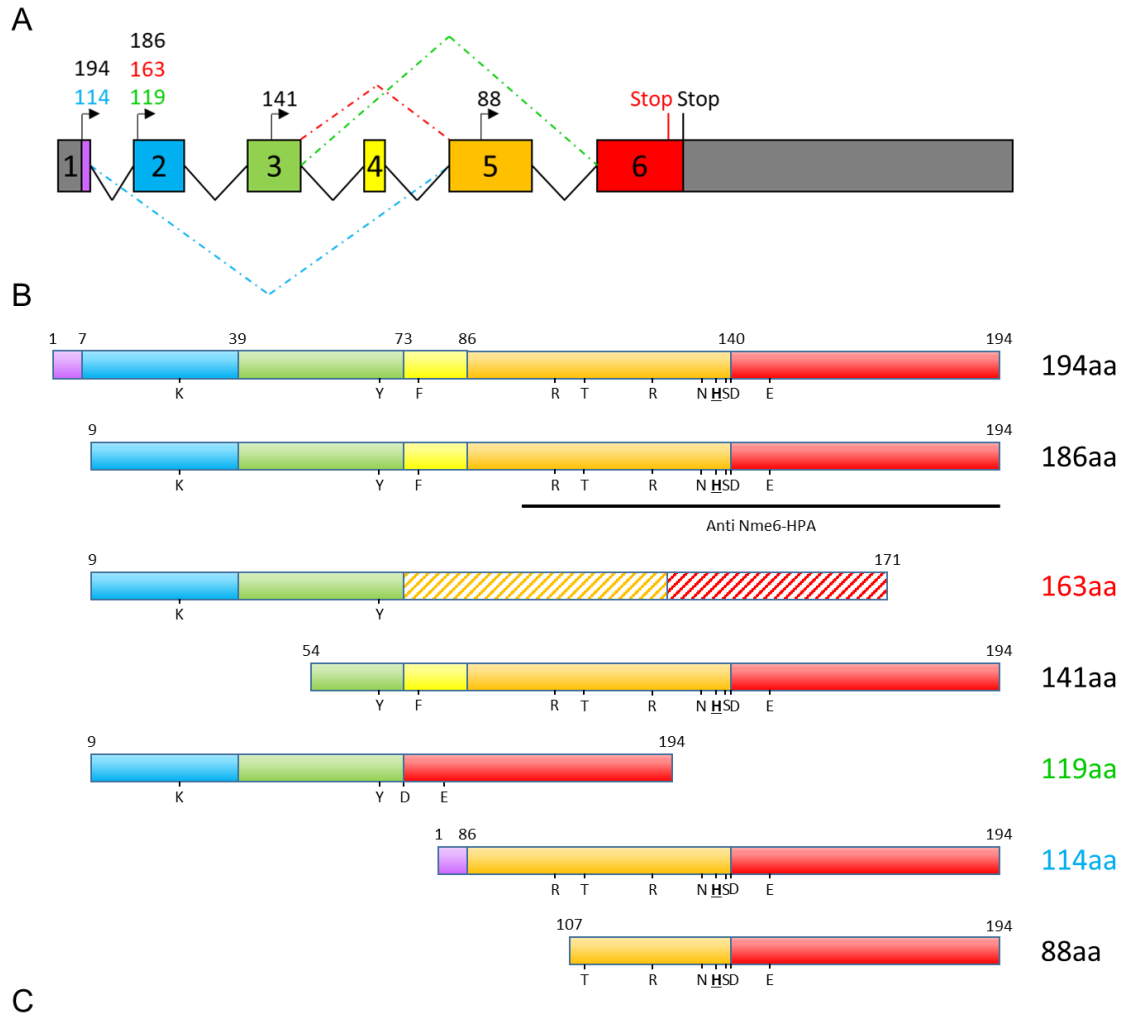


*Figure 14 : Schematic representation of the human NME6 gene and predicted protein isoforms associated. A The human NME6 gene structure: four predicted start codons (↑) combined with classical (^) or alternative (∧) splicing lead to the predicted expression of several NME6 isoforms. Exons are represented by colored boxes and enumerated. Numbers above start codons refer to the amino acid length of the predicted NME6 protein isoforms. B Predicted NME6 protein isoforms: Colors are associated to exons presented in A. Isoforms are labelled*

on the right according to their amino acid length (194aa). The amino acid numeration of NME6-194 is used for all isoforms. The hatched pattern represents a different amino acid sequence as compared to isoform 194. Letters refer to the conserved amino acids deemed essential for enzyme structure and activity. The main histidine of the catalytic site is highlighted in bold and underlined. The immunogenic sequence used to produce the highly specific NME6 antibody used in this study is represented as a black line (anti NME6-HPA). **C** Amino-acid sequence of the NME6-194 isoform. Colors are associated to exons presented in A. Conserved amino acids deemed essential for enzyme structure and activity are displayed in bold, and the main histidine is underlined.

The structure of NME6 protein is not resolved to date. Nevertheless, the recent advance in structure prediction based on amino acid sequence and boosted by artificial intelligence generated a high confidence model for the human NME6-186 isoform [105–107]. When superimposed on human NME1 structure (PDB structure: 2HVD), the NME6 model revealed that the conserved amino acid of the catalytic site shares the same 3D position (Figure 15). Moreover, the superimposition pinpointed the presence of two arginines in the *Kpn* loop of NME6 (R103, R106), oriented towards the protein surface (Figure 16). As a result, the *Kpn* loop turned strongly positively charged as compared to NME1. Another arginine of the  $\alpha 2$  helix of NME6 (R71) obstructs the entrance of the catalytic pocket, as compared to the NME1 structure. This predicted NME6 structure represents a great help for studying NME6, but still, needs to be considered with caution and proved experimentally.

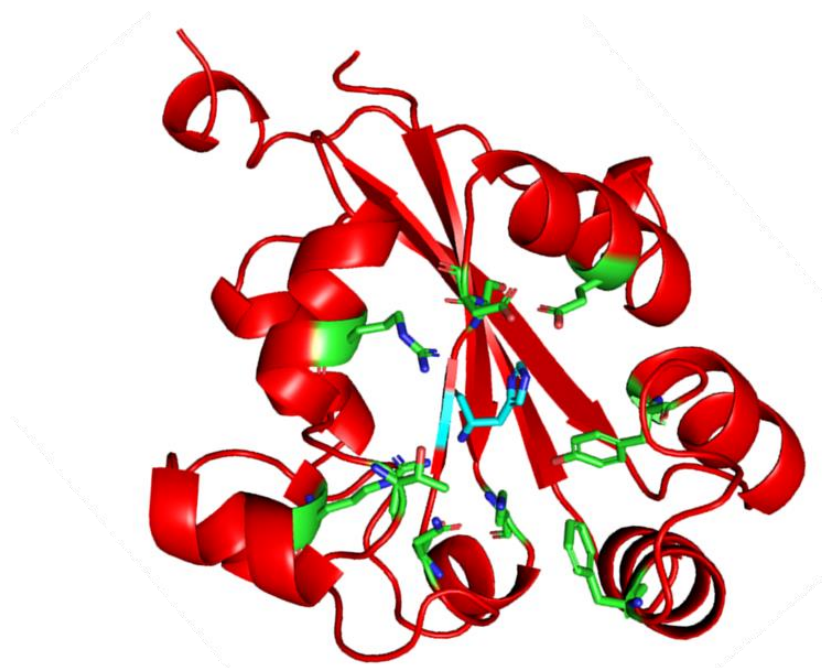


*Figure 15 : The NME6 catalytic site. Predicted structure of the human NME6-186 protein is represented as cartoon. The conserved amino acids of the catalytic site deemed important for enzyme structure and activity are represented as stick in green. The main histidine H129 is represented in cyan.(NME6 AlphaFold predicted structure AF-O75414-F1) [105–107]*

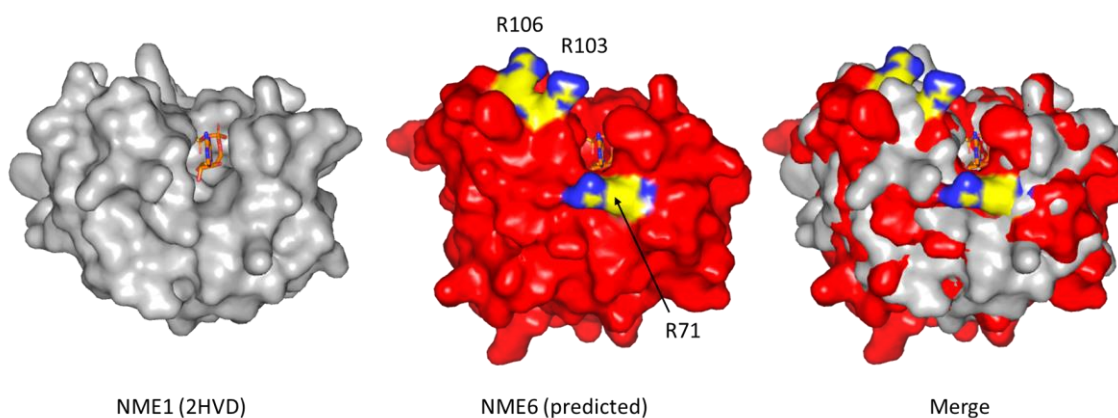


*Figure 16 : Superimposition of the resolved NME1 structure and the predicted NME6-186 structure from human. Structures are displayed as surface, and the ADP from NME1 structure is represented as stick in orange, in both NME1 and NME6 structures. Positively charged arginines from the NME6 Kpn loop (R103, R106, NME6-186 numbering) and obstructing the catalytic pocket (R71, NME6-186 numbering) are represented in yellow, with nitrogen in blue. Molecules were superimposed in Pymol. (NME1 PDB structure 2HVD; NME6 AlphaFold predicted structure AF-O75414-F1) [105–107]*

In the years following its discovery, scarce information was added to NME6 functions. First, NME6 together with NME4 and NME7 were found to be overexpressed at the protein level in primary colon and gastric carcinomas compared to normal tissues [108]. Similarly, another study revealed that NME6 expression was higher in colorectal cancer tissues in the Chinese population [109]. In a shRNA screen, NME6 and NME7 were found as essential genes for embryonic stem cells (ESC) renewal. Downregulation of NME6 or NME7 triggered the differentiation of ESC into embryoid body, and was associated with downregulation of ESC renewal-related genes expression at the protein level. Interestingly the protein abundance of both NME6 and NME7 was decreased after differentiation [110]. More recently, a group pinpointed a potential role of NME6 in the regulation of inflammation in mice [111]. Another enzymatic information of NME6 was revealed by a team working on the production of antibodies that specifically recognize phosphorylated histidine in two conformations (1-pHis and 3-pHis). The testing of 1-pHis antibody on recombinant human and mouse NME proteins revealed that NME1, NME2, NME4, NME5 and NME7 display histidine phosphorylation, i.e. they are able of autophosphorylation (“ping”). The human NME6 was the only NME tested that failed to display the 1-pHis signal, indicating that the recombinant GST-NME6 they produced was unable to autophosphorylate, which is the first step of NDPK activity [64]. Information of NME6 localization was released by Pagliarini et al., where they listed NME6 as a mitochondrial protein [112], even though NME6 is devoid of a typical cleavable MTS. The analyze of large-scale studies mapping proteins presence within the different mitochondrial compartments revealed the detection of NME6 within the mitochondrial matrix proteome [113], and its absence from the mitochondrial IMS proteome [114] or the MOM facing cytosol proteome [115]. Finally, data from large-scale protein-protein interactions pinpointed several mitochondrial interactors for NME6. The only consistent “hit” among the studies was RCC1L (RCC1-like G exchanging factor-like protein), also named WBSR16 (Williams-Beuren Syndrome Chromosomal Region 16) [116–120].

## 2.5 RCC1L protein

RCC1L belongs to the regulator of chromosome condensation 1 (RCC1) family, a group of proteins characterized by their RCC1-like domain (RLD), that consist of a specific seven-bladed  $\beta$ -propeller fold [121]. The most studied member of the family, the RCC1 protein, is localized in the nucleus and acts as a chromosome condensation regulator through its



interaction with chromatin [122]. RCC1 is also a guanine exchange factor (GEF) for the Ran GTPase protein [123].

RCC1L protein description was addressed only very recently, even though the gene was previously described. RCC1L is located on chromosome 7q11.23, at the periphery of the Williams-Beuren syndrome (WBS) critical region. The large WBS region covers at least 25 genes, and its heterozygous deletion is responsible for a neurodevelopmental disorder associated with cardiovascular malformation, mental retardation and facial dysmorphism [124]. In 2017, four research groups published independently the first bricks of the RCC1L protein knowledge. Arroyo et al. identified RCC1L as an essential gene for oxidative phosphorylation. They described that it is part of a module that regulates 16S rRNA and intra-mitochondrial translation [117]. Later, Antonicka et al. associated RCC1L with the same module by proximity biotinylation assay. They characterized it as the pseudouridine synthase module, localized in the RNA granules of the mitochondria (matrix). Moreover, they confirmed the mitochondrial localization of RCC1L by immunofluorescence [125]. A few months later, the structure of RCC1L was resolved by Koyama et al., bringing a detailed structure comparison with other proteins from the RCC1 family. They also confirmed its mitochondrial localization by immunofluorescence [126]. Finally, Huang et al. explored the protein function. They reported that RCC1L can interact with, and act as a GEF for OPA1, in mitochondria. The RCC1L heterozygous mutation exerted mitochondrial dysfunction and fragmentation in mice while homozygous mutation was lethal at the early embryonic stage [127]. In 2020, an extensive description of RCC1L was performed by Reyes et al., where a few isoforms of the protein were described, all possessing a cleavable MTS. RCC1L was shown to interact with the MIM, and was strongly associated with mitoribosome biogenesis in the mitochondrial matrix through direct interaction with mitoribosome proteins [128].

### 3 MATERIALS AND METHODS

#### 3.1 Materials

##### 3.1.1 Chemicals and buffers

Table 2 : Chemicals

<b>Chemical</b>	<b>Manufacturer</b>
Acrylamide/Bis-acrylamide	Sigma Aldrich, USA
ADP (adenosine diphosphate)	Sigma Aldrich, USA
Agar	Merck, USA
Agarose	Roche, Switzerland
Ampicillin	Pliva, Croatia
APS (ammonium persulfate)	Sigma Aldrich, USA
ATP (adenosine triphosphate)	Sigma Aldrich, USA
Bromophenol blue	Sigma Aldrich, USA
BSA (bovine serum albumin)	Thermo Fisher Scientific, USA
Camptothecin	Sigma Aldrich, USA
Cytochrome C	Sigma Aldrich, USA
Digitonin	Acros Organics, Belgium
dTDP (deoxythymidine diphosphate)	Sigma Aldrich, USA
DTT (Dithiothreitol)	Sigma Aldrich, USA
EDTA (ethylenediaminetetraacetic acid)	Kemika, Croatia
EGTA (ethylene glycol-bis(2-aminoethylether)-N,N,N',N'-tetraacetic acid)	Sigma Aldrich, USA
FBS (fetal bovine serum)	Sigma Aldrich, USA
G418 disulfate salt	Sigma Aldrich, USA
Glutamate	Sigma Aldrich, USA
Glutaraldehyde	Sigma Aldrich, USA
HEPES (4-(2-hydroxyethyl)-1-piperazineethanesulfonic acid)	Sigma Aldrich, USA
Imidazole	Sigma Aldrich, USA
Inorganic Phosphate (phosphoric acid)	Honeywell Fluka, USA
IPTG (Isopropyl $\beta$ -D-1-thiogalactopyranoside)	Sigma Aldrich, USA

Table 2 : - Continued - Chemicals

<b>Chemical</b>	<b>Manufacturer</b>
<b>Kanamycin</b>	Pliva, Croatia
<b>KH<sub>2</sub>PO<sub>4</sub> / Na<sub>2</sub>HPO<sub>4</sub> / KCl / NaCl / CaCl<sub>2</sub> / MgCl<sub>2</sub></b>	Kemika, Croatia
<b>L-Glutamine</b>	Sigma Aldrich, USA
<b>LB (Luria-Bertani broth)</b>	Sigma Aldrich, USA
<b>Lysozyme</b>	Sigma Aldrich, USA
<b>Malate</b>	Sigma Aldrich, USA
<b>Mannitol</b>	Sigma Aldrich, USA
<b>Methanol / Ethanol / DMSO (Dimethyl sulfoxide) / Acetic Acid / 2-Propanol / glycine / glycerol / formaldehyde</b>	Kemika, Croatia
<b>NADH (nicotinamide adenine dinucleotide)</b>	Sigma Aldrich, USA
<b>Naphthol Blue</b>	Kemika, Croatia
<b>NP-40</b>	Calbiochem, USA
<b>Penicillin-streptomycin</b>	Thermo Fisher Scientific, USA
<b>PEP (phosphoenolpyruvate)</b>	Sigma Aldrich, USA
<b>Percoll</b>	Sigma Aldrich, USA
<b>Propidium iodide</b>	Molecular probes, USA
<b>RNAse</b>	Sigma Aldrich, USA
<b>Rotenone</b>	Sigma Aldrich, USA
<b>SDS (sodium dodecyl sulfate)</b>	Sigma Aldrich, USA
<b>Sodium Pyruvate</b>	Thermo Fisher Scientific, USA
<b>Succinate</b>	Sigma Aldrich, USA
<b>Sucrose</b>	Sigma Aldrich, USA
<b>TEMED (Tetramethylethylenediamine)</b>	Sigma Aldrich, USA
<b>Tris base</b>	Sigma Aldrich, USA
<b>Trypan Blue</b>	Sigma Aldrich, USA
<b>Trypsin</b>	Sigma Aldrich, USA
<b>Tween20</b>	Sigma Aldrich, USA
<b>Xylene cyanol</b>	Sigma Aldrich, USA

Table 3 : List of buffers

<b>Solution</b>	<b>Composition</b>
<b>1× Bradford</b>	20% (v/v) Protein Assay Dye Reagent Concentrate in dH <sub>2</sub> O
<b>2× LB: Protein loading buffer</b>	50% 4× LB (v/v) diluted in qH <sub>2</sub> O
<b>4× LB: Protein loading buffer</b>	0.2 M Tris-HCl pH 6.8, 0.4 M DTT, 8% (v/v) SDS, 40% (v/v) glycerol, 0.001% (w/v) bromophenol blue
<b>5× LB: Polynucleotide loading buffer</b>	0.25% (w/v) bromophenol blue, 0.25% (w/v) xylene cyanol, 35% (v/v) glycerol
<b>5× TKM buffer</b>	250 mM Tris HCL pH 7.5, 375 mM KCl, 25mM MgCl <sub>2</sub> , 5mg/mL BSA
<b>AAS 30%</b>	29.2% (w/v) acrylamide, 0.8% (w/v) bis-acrylamide
<b>APS 10%</b>	10% ammonium persulfate (w/v)
<b>Blocking BSA buffer</b>	5% BSA (w/v) in TBST, pH 8.5
<b>Blocking milk buffer</b>	5% milk powder (w/v) in TBST
<b>Buffer A</b>	210 mM mannitol, 70 mM sucrose, 0.2 mM EDTA, 10 mM HEPES pH 7.5
<b>Buffer B</b>	210 mM mannitol, 70 mM sucrose, 0.1 mM EGTA, 10 mM HEPES pH 7.5
<b>Crosslinking buffer</b>	25 mM HEPES, pH 7.4, 300 mM NaCl, 5 mM DTT and 5 mM MgCl <sub>2</sub>
<b>Distaining solution</b>	50% (v/v) methanol, 7% (v/v) acetic acid
<b>Elution buffer</b>	50 mM HEPES pH 7.4, 300 mM NaCl and 150 mM imidazole
<b>Formaldehyde 2%</b>	2% formaldehyde in PBS (v/v)
<b>IF blocking buffer</b>	10% BSA (w/v) in PBS
<b>KET buffer</b>	150 mM KCl, 1 mM EGTA, 20 mM Tris pH 7,2
<b>Naphthol blue (Staining)</b>	10% (v/v) methanol, 2% (v/v) acetic acid, 0.1% (w/v) naphthol blue
<b>PBS (Phosphate-buffered saline)</b>	137 mM NaCl, 2.7 mM KCl, 1.4 mM KH <sub>2</sub> PO <sub>4</sub> , 4.3 mM Na <sub>2</sub> HPO <sub>4</sub> × 7H <sub>2</sub> O, pH 7.4
<b>PBS-Tween</b>	0.02% (v/v) Tween20 in PBS

Table 3 : - Continued - List of buffers

<b>Solution</b>	<b>Composition</b>
<b>pHis-5× LB: pHis protein loading buffer</b>	10% SDS, 250 mM Tris-HCl, 0.02% bromophenol blue, 50% glycerol, 50 mM EDTA, 500 mM DTT, pH8.8
<b>RB: running buffer</b>	1 M glycine, 50 mM Tris, 1% (v/v) SDS
<b>Resuspension buffer</b>	5 mM MgCl <sub>2</sub> , 50 mM HEPES pH 7.4, 400 mM NaCl, 10 % glycerol
<b>Resuspension buffer supplemented with imidazole</b>	5 mM MgCl <sub>2</sub> , 50 mM HEPES pH 7.4, 400 mM NaCl, 10 % glycerol, 5 mM imidazole
<b>SDS 10%</b>	10% (w/v) sodium dodecyl sulfate
<b>Storage buffer</b>	25 mM HEPES, pH 7.4, 300 mM NaCl and 5 mM DTT
<b>SW1: swelling buffer</b>	10 mM KH <sub>2</sub> PO <sub>4</sub> pH 7.4
<b>SW2: shrinking buffer</b>	10 mM KH <sub>2</sub> PO <sub>4</sub> pH 7.4, 30% sucrose, 30% glycerol, 10 mm MgCl <sub>2</sub> , 4 mM ATP
<b>TAE buffer</b>	40 mM TRIS, 20 mM acetic acid, 1 mM EDTA
<b>TB: transfer buffer</b>	200 mM Tris, 1.5 mM glycine, 10% (v/v) methanol
<b>TBST</b>	50 mM Tris, 150 mM NaCl, 0.05% (v/v) Tween20, pH 7.5
<b>TEEN buffer</b>	50 mM Tris pH 7.4, 5 mM EDTA, 150 mM NaCl, 0.5% (v/v) NP-40
<b>Thrombin buffer</b>	50 mM Tris pH 8.0, 0.1 M NaCl
<b>Tris running</b>	1.5 M Tris pH 8.8
<b>Tris stacking</b>	1.0 M Tris pH 6.8
<b>Triton X-100 0.1%</b>	0.1% (v/v) Triton X-100 in PBS
<b>Washing buffer</b>	5 mM MgCl <sub>2</sub> , 50 mM HEPES pH 7.4, 400 mM NaCl, 10 % glycerol, 10 mM imidazole

### 3.1.2 Instruments and material

Table 4 : Instruments

<b>Instruments</b>	<b>Manufacturer</b>
<b>5414 R centrifuge</b>	Eppendorf, Germany
<b>Agarose gel electrophoresis system Sub-Cell GT</b>	Bio-Rad, USA
<b>Bacteria incubator New Brunswick™ Innova® 40</b>	Eppendorf, Germany
<b>BD FACSCalibur™ flow cytometer</b>	BD Biosciences, USA
<b>Cell incubator</b>	Kambič, Slovenia
<b>Clark electrode oxygraph MS200A</b>	Strathkelvin Instruments, UK
<b>Confocal microscope Leica TCS SP8 X FLIM</b>	Leica Microsystems, Germany
<b>Electroporation system gene pulser xCell</b>	Bio-Rad, USA
<b>GeneAmp PCR system 2700</b>	Applied Biosystems, USA
<b>Gyro-rocker SSL3</b>	Stuart®, Cole-Parmer Ltd., UK
<b>Harrier 18/80 refrigerated centrifuged digital</b>	MSE, UK
<b>Mini protean casting stand</b>	Bio-Rad, USA
<b>Mini protean II and III electrophoresis and transfer system</b>	Bio-Rad, USA
<b>Nanophotometer® N60</b>	Implen, Germany
<b>Rotator Multi Bio RS-24</b>	Biosan, Latvia
<b>Spectrophotometer Multiskan MS</b>	Labsystems, Finland
<b>Sterile hood</b>	Iskra, Slovenia
<b>Thermo-shaker TS-100</b>	Biosan, Latvia
<b>Ultracentrifuge Optima XL 100K, rotors 60Ti and 70.1Ti fixed angle</b>	Beckman Coulter, USA
<b>Ultrasonic homogenizer CP 130 and 6mm probe</b>	Cole-Palmer Ltd., UK
<b>Ultrasonic homogenizer Labsonic® M and 1mm probe</b>	Montreal Biotech, Canada
<b>Ultrasonic homogenizer Sonopuls®</b>	Bandelin, Germany
<b>Ultrospec 2100 pro spectrophotometer</b>	Amersham biosciences, UK
<b>UVItec: Western blot imaging system Alliance 4.7</b>	UVItec Cambridge, UK

Table 5 : Material

<b>Material</b>	<b>Manufacturer</b>
<b>0.2µm nitrocellulose membrane</b>	Amersham Biosciences, UK
<b>8 well chamber slide</b>	Ibidi, Germany
<b>Amicon® Ultra-15 centrifugal filter units, 10kDa cutoff</b>	Merck, USA
<b>Confocal 4-chamber 35mm glass bottom dish</b>	Cellvis, USA
<b>Cryotubes</b>	Greiner Bio-One, Austria
<b>Electroporation cuvette 2mm</b>	Sigma Aldrich, USA
<b>Glasstic™ slides cell counter</b>	KOVA International, USA
<b>Microcon® centrifugal filter unit YM-3, 3kDa cutoff</b>	Merck, USA
<b>Poly-Prep chromatography columns</b>	Bio-Rad, USA
<b>Parafilm M</b>	Sigma Aldrich, USA

### 3.1.3 Commercial products

Table 6 : List of commercial kit, enzymes and standards

<b>Product</b>	<b>Manufacturer</b>
<b>1 Kb plus DNA ladder</b>	Thermo Fisher Scientific, USA
<b>Annexin-V-FLUOS staining kit</b>	Roche, Switzerland
<b>Cell fractionation kit - standard (ab109719)</b>	Abcam, UK
<b>CIP: calf-intestinal alkaline phosphatase</b>	New England Biolabs, USA
<b>Complete mini EDTA-free protease inhibitor cocktail tablets</b>	Roche, Switzerland
<b>Dharmafect transfection reagent 4</b>	Dharmacon, USA
<b>Dynabeads protein G</b>	Invitrogen, USA
<b>EmeraldAmp MAX PCR master mix</b>	TakaraBio, Europe
<b>Expand™ long template PCR system</b>	Sigma Aldrich, USA
<b>FastDigest green buffer FD10×</b>	Thermo Fisher Scientific, USA
<b>FLAG agarose</b>	Sigma Aldrich, USA
<b>Fluorescence mounting medium</b>	Dako, Denmark
<b>GenElute™ plasmid miniprep kit</b>	Sigma Aldrich, USA
<b>LDH, Lactate dehydrogenase enzyme</b>	Sigma Aldrich, USA

Table 6 : - Continued - List of commercial kit, enzymes and standards

<b>Product</b>	<b>Manufacturer</b>
<b>Midori green</b>	Bulldog-Bio, USA
<b>MitoTracker™ Deep Red FM</b>	Thermo Fisher Scientific, USA
<b>NEBuffer 3</b>	New England Biolabs, USA
<b>NME6 human gene knockout kit (CRISPR) KN200541BN</b>	Origene, USA
<b>Pierce BCA protein assay kit</b>	Thermo Fisher Scientific, USA
<b>PK, Pyruvate kinase enzyme</b>	Sigma Aldrich, USA
<b>Precision plus protein dual color standard</b>	Bio-Rad, USA
<b>Protein assay dye reagent concentrate</b>	Bio-Rad, USA
<b>QIAprep spin miniprep kit</b>	Qiagen, Germany
<b>QIAquick gel extraction kit</b>	Qiagen, Germany
<b>QIAquick PCR purification kit</b>	Qiagen, Germany
<b>Restriction enzymes (XhoI, EcoRI, NdeI, BamHI)</b>	Thermo Fisher Scientific, USA
<b>Supersignal west femto maximum sensitivity substrate</b>	Thermo Fisher Scientific, USA
<b>Supersignal west pico chemiluminescent substrate</b>	Thermo Fisher Scientific, USA
<b>T4 DNA ligase</b>	New England Biolabs, USA
<b>T4 DNA ligase reaction buffer 10×</b>	New England Biolabs, USA
<b>Talon metal affinity resin</b>	TakaraBio, Europe
<b>Thrombin sepharose beads</b>	BioVision, USA
<b>Turbofect transfection reagent</b>	Thermo Fisher Scientific, USA
<b>Western lighting plus ECL enhanced chemiluminescent substrate</b>	PerkinElmer, USA



Table 7 : Primary antibodies

<b>Primary Antibodies</b>	<b>Host</b>	<b>Reference</b>	<b>Manufacturer</b>
<b>1-pHis</b>	Rabbit	SC1-1	Hunter Lab, La Jolla, CA, USA, Salk
<b>3-pHis</b>	Rabbit	SC44-1	Hunter Lab, La Jolla, CA, USA, Salk
<b>6× His-tag</b>	Mouse	ab18184	Abcam, UK
<b>AK2</b>	Rabbit	AP8134B	Abgent, USA
<b>ANT</b>	Mouse	ab110322	Abcam, UK
<b>Antibody cocktail apoptosis (Cytochrome C, GAPDH, PDH-E1 <math>\alpha</math>, ATP synthase <math>\alpha</math>)</b>	Mouse	ab110415	Abcam, UK
<b>Antibody cocktail OXPHOS (CI-NDUFA9, CII-SDHA, CIII-UQCRC2, CIV-COX IV, CV-ATP5A)</b>	Mouse	ab110412	Abcam, UK
<b>Calreticulin</b>	Mouse	C41720	BD Biosciences, USA
<b>Drp1</b>	Rabbit	8570s	Cell Signaling Technology, USA
<b>FLAG M2</b>	Mouse	F1804	Sigma-Aldrich, USA
<b>FLAG M2</b>	Mouse	8146s	Cell Signaling Technology, USA
<b>Histone H3</b>	Rabbit	ab1791	Abcam, UK
<b>Histone H3</b>	Mouse	#14269	Cell Signaling Technology, USA
<b>Irrelevant IgG</b>	Mouse	556648	BD Biosciences, USA
<b>Irrelevant IgG</b>	Rabbit	2729p	Cell Signaling Technology, USA
<b>Lamp1</b>	Mouse	15665	Cell Signaling Technology, USA
<b>MFN1</b>	Mouse	ab56889	Abcam, UK
<b>MFN2</b>	Mouse	ab57602	Abcam, UK
<b>Na<sup>+</sup>K<sup>+</sup> ATPase</b>	Mouse	05-369	Merck Millipore, USA
<b>NME1</b>	Mouse	OP48	Calbiochem, USA
<b>NME1</b>	Mouse	UM800025	Origene, USA
<b>NME1/2</b>	Rabbit	/	Gift from Dr. I. Lascu and Dr. S. Volarević

Table 7 : - Continued - Primary antibodies

<b>Primary Antibodies</b>	<b>Host</b>	<b>Reference</b>	<b>Manufacturer</b>
<b>NME3</b>	Rabbit	PA5-49708	Invitrogen, USA
<b>NME4</b>	Rabbit	/	Homemade
<b>NME4</b>	Rabbit	HPA072588	Sigma-Aldrich, USA
<b>NME6</b>	Rabbit	HPA017909	Sigma-Aldrich, USA
<b>OPA1</b>	Mouse	612607	BD Biosciences, USA
<b>RCC1-L</b>	Mouse	SAB140186 0	Sigma-Aldrich, USA
<b>RCC1-L</b>	Rabbit	ab247142	Abcam, UK
<b>TOM22</b>	Mouse	sc-58308	Santa Cruz Biotechnology, USA
<b>VDAC</b>	Rabbit	/	gift from Dr. Marco Colombini
<b><math>\beta</math> Actin</b>	Mouse	60008-1-Ig	Proteintech, USA
<b><math>\beta</math> Tubulin</b>	Rabbit	2128S	Cell Signaling Technology, USA

Table 8 : Secondary antibodies

<b>Secondary Antibodies</b>	<b>Host</b>	<b>Reference</b>	<b>Manufacturer</b>
<b>Alexa Fluor488-Rabbit</b>	Goat	A11008	Invitrogen, USA
<b>Dylight 488-Rabbit</b>	Goat	ab96899	Abcam, UK
<b>HRP-Mouse</b>	Horse	7076	Cell Signaling Technology, USA
<b>HRP-Rabbit</b>	Goat	7074	Cell Signaling Technology, USA
<b>IgG-Cy5-Mouse</b>	Goat	ab-2338714	Jackson ImmunoResearch, USA

### 3.1.4 Cell culture

Table 9 : Media for cell culture and bacteria proliferation

<b>Media</b>	<b>Composition</b>
<b>Cryoprotective medium</b>	45% (v/v) DMEMcomp, 45% (v/v) FBS, 10% (v/v) DMSO
<b>DMEMcomp</b>	Gibco, Thermo Fisher Scientific, USA, supplemented with 10% (v/v) FBS, 100 µg/mL penicillin, 100 µg/mL streptomycin, 1 mM L-glutamine, 1 mM sodium pyruvate
<b>DMEMg418</b>	Gibco, Thermo Fisher Scientific, USA, supplemented with 10% (v/v) FBS, 1mg/mL G418, 1 mM L-Glutamine, 1 mM Sodium pyruvate
<b>Lebovitz's L-15</b>	Thermo Fisher Scientific, USA, supplemented with 10% (v/v) FBS, 100 µg/mL penicillin, 100 µg/mL streptomycin, 1 mM L-glutamine, 1 mM sodium pyruvate
<b>Liquid LB+Amp</b>	5 g/L yeast extract, 10 g/L NaCl, 10 g/L tryptone, 100 mg/L ampicillin
<b>Liquid LB+Kan</b>	5 g/L yeast extract, 10 g/L NaCl, 10 g/L tryptone, 50 mg/L kanamycin
<b>Opti-MEM</b>	Gibco, Thermo Fisher Scientific, USA
<b>RPMIcomp</b>	Lonza, Switzerland, supplemented with 10% (v/v) FBS, 100 µg/mL penicillin, 100 µg/mL streptomycin, 1 mM L-glutamine, 1 mM sodium pyruvate
<b>Solid LB+Amp</b>	5 g/L yeast extract, 10 g/L NaCl, 10 g/L tryptone, 13 g/L agar, 100 mg/L ampicillin
<b>Solid LB+Kan</b>	5 g/L yeast extract, 10 g/L NaCl, 10 g/L tryptone, 13 g/L agar, 50 mg/L kanamycin
<b>Trypsin solution</b>	0.05% (w/v) trypsin, 1 mM EDTA

Table 10 : Cells and Media

Cell line	Cell type	Media	Origin
<b>Mel 224</b>	Melanoma	DMEMcomp	Kind donation of Dr. Bergamaschi (Barts and The London School of Medicine and Dentistry, London, UK)
<b>Mel 501</b>	Melanoma	DMEMcomp	
<b>Mel 505</b>	Melanoma	DMEMcomp	
<b>A375</b>	Melanoma	DMEMcomp	
<b>A375M</b>	Melanoma	DMEMcomp	
<b>WM793B</b>	Melanoma	DMEMcomp	
<b>WM983B</b>	Melanoma	DMEMcomp	
<b>LM6</b>	Melanoma	DMEMcomp	
<b>CHL1</b>	Melanoma	DMEMcomp	
<b>RPMI7951</b>	Melanoma	DMEMcomp	
<b>HTB82</b>	Rhabdomyosarcoma	RPMIcomp	Kind donation of Dr. Neda Slade (Laboratory for Protein Dynamics, Ruđer Bošković Institute, Zagreb, Croatia)
<b>HTB92</b>	Liposarcoma	RPMIcomp	Kind donation of Dr. Neda Slade (Laboratory for Protein Dynamics, Ruđer Bošković Institute, Zagreb, Croatia)
<b>HTB93</b>	Synovial sarcoma	RPMIcomp	
<b>WT</b>	Variant of HT1080 fibrosarcoma	DMEMcomp	
<b>H1299</b>	Lung Carcinoma	RPMIcomp	
<b>Detroit 562</b>	Pleural effusion of pharyngeal carcinoma	DMEMcomp	Kind donation of Dr. Jeannine Gioanni, (Centre Antoine Lacasagne, Nice, France)
<b>Cal165</b>	Spinocellular pharyngeal carcinoma	DMEMcomp	
<b>MDA-MB-231T</b>	Pleural effusion of breast carcinoma	DMEMcomp	Kind donation of Dr. Patricia S. Steeg (Center for Cancer Research, National Cancer Institute, USA)

Table 10 : - Continued - Cells and Media

<b>Cell line</b>	<b>Cell type</b>	<b>Media</b>	<b>Origin</b>
<b>H460</b>	Lung carcinoma	RPMIcomp	Kind donation of Dr. Marijeta Kralj (Laboratory of Experimental Therapy, Ruđer Bošković Institute, Croatia)
<b>MJ90</b>	Human skin fibroblast	DMEMcomp	Pereira-Smith laboratory
<b>MDA-MB-436</b>	Pleural effusion of breast carcinoma	DMEMcomp	ATCC® CCL-2™
<b>C33</b>	Cervix carcinoma	DMEMcomp	
<b>LNCaP</b>	Prostate adenocarcinoma metastatic	RPMIcomp	
<b>PC3</b>	Prostate adenocarcinoma metastatic	DMEMcomp	
<b>Du145</b>	Prostate carcinoma metastatic	DMEMcomp	
<b>MCF7</b>	Pleural effusion of breast carcinoma	DMEMcomp	
<b>SKOV 3</b>	Ovary adenocarcinoma	RPMIcomp	
<b>RD</b>	Rhabdomyosarcoma	DMEMcomp	
<b>HCT 116</b>	Colorectal carcinoma	RPMIcomp	
<b>SW620</b>	Colorectal carcinoma, lymph node metastasis	DMEMcomp	
<b>HeLa</b>	Cervix adenocarcinoma	DMEMcomp	
<b>HACAT</b>	Human keratinocyte	DMEMcomp	
<b>WPMY-1</b>	Human prostate fibroblast	DMEMcomp	
<b>HEK293</b>	Human embryonic kidney	DMEMcomp	
<b>MDA-MB-435</b>	Melanoma	DMEMcomp	
<b>RKO</b>	Rectal Carcinoma	DMEMcomp	

### 3.1.5 Plasmids, primers and silencers

Table 11: Plasmids and associated primers used in the study

<b>Plasmid Name</b>	<b>Plasmid of origin</b>	<b>Cloned in</b>	<b>Primers (Table 12)</b>	<b>TAG</b>
<b><i>pNME6-194-GFP</i></b>	<i>RG200541, Origene</i>	/	/	<i>GFP, C-ter</i>
<b><i>pEGFPN1-NME6-186-GFP</i></b>	<i>RC200541, Origene</i>	<i>pEGFPN1</i>	<i>Pr-186-GFP</i>	<i>eGFP, C-ter</i>
<b><i>pET28b-NME6-194-His</i></b>	<i>RC200541, Origene</i>	<i>pET28b</i>	<i>Pr-194-His</i>	<i>6xHis, N-ter</i>
<b><i>pET28b-NME6-186-His</i></b>	<i>RC200541, Origene</i>	<i>pET28b</i>	<i>Pr-186-His</i>	<i>6xHis, N-ter</i>
<b><i>pcDNA3.1-NME6-194-FLAG</i></b>	<i>RC200541, Origene</i>	<i>pcDNA3.1</i>	<i>Pr-194-FLAG</i>	<i>FLAG, C-ter</i>
<b><i>pcDNA3.1-NME6-186-FLAG</i></b>	<i>RC200541, Origene</i>	<i>pcDNA3.1</i>	<i>Pr-186-FLAG</i>	<i>FLAG, C-ter</i>
<b><i>pcDNA3.1-NME4-FL-FLAG</i></b>	<i>pET28a(+)-Nme4-FL (Millon et al., 2000)</i>	<i>pcDNA3.1</i>	<i>Pr-NME4-FLAG</i>	<i>FLAG, C-ter</i>
<b><i>pcDNA3.1-NME3-FLAG</i></b>	<i>pCMVTag3-Nme3-tetra-cys-tag (Kind donation of Prof. Thomas Wieland)</i>	<i>pcDNA3.1</i>	<i>Pr-NME3-FLAG</i>	<i>FLAG, N-ter</i>
<b><i>pCFPmito</i></b>	<i>Kind donation of Dr. Yaron Shav-Tal, Bar-Ilan University, Ramat-Gan, Israel)</i>	/	/	<i>CFP, mitochondria targeted</i>

Table 12 : Primers used for plasmids cloning

Primers name	Sequences	Restriction enzymes
<b>Pr-186-GFP</b>	5'-GTCTAGCTCGAGTAATGGCCTCAATCTTGCG-3' 5'-CTAGACGAATTCGGCTGGTCCTAGGCC-3'	XhoI EcoRI
<b>Pr-194-His</b>	5'-GTCTAGCATATGACCCAGAATC-3' 5'-CTAGACGGATCCTCAGGCTGGTCCTAGGCC-3'	NdeI BamHI
<b>Pr-186-His</b>	5'-GTCTAGCATATGGCCTCAATC-3' 5'-CTAGACGGATCCTCAGGCTGGTCCTAGGCC-3'	NdeI BamHI
<b>Pr-194-FLAG</b>	5'-GTCTAGGGATCCACGAGATGACCCAGAATCTG GGG-3' 5'-CTAGACGAATTCCTTAAACCTTATCGTCGTCATC CTTGTAATCGGCTGGTCCTAGGCC-3'	BamHI EcoRI
<b>Pr-186-FLAG</b>	5'-GTCTAGGGATCCACGAGATGGCCTCAATCTTG CG-3' 5'-CTAGACGAATTCCTTAAACCTTATCGTCGTCATC CTTGTAATCGGCTGGTCCTAGGCC-3'	BamHI EcoRI
<b>Pr-NME4- FLAG</b>	5'-GTCTAGGGATCCACGAGATGGGCGGCCTCTTC TGGCGCTCC-3' 5'-CTAGACGAATTCCTTACTTATCGTCGTCGTCCTT GTAGTCGGCTGGGTGGATGCTGCTGTG-3'	BamHI EcoRI
<b>Pr-NME3- FLAG</b>	5'-GTCTAGGGATCCACGAGATGGACTACAAGG ACGACGACGATAAGATGATCTGCCTGGTGCTGA CC-3' 5'-CTAGACGAATTCCTTACTCATAACAGCCAGTG CC-3'	BamHI EcoRI

Table 13 : Primers used for the control of NME6-KO and the assessment of correct left and right integration junctions.

Primers	Sequence
NME6-KO and NME6-WT screen	LF: 5'-GACACGTGAAAGGCCGTTAT-3' RR: 5'-CTTTCTCTGGTTGCCTCCTG-3'
Left integration junction screen	LF: 5'-GACACGTGAAAGGCCGTTAT-3' LR: 5'-GGGTGTGGTTGATGAAGGTC-3'
Right integration junction screen	RF: 5'-CGTTGGCTACCCGTGATATT-3' RR: 5'-CTTTCTCTGGTTGCCTCCTG-3'

Table 14 : Small interfering RNA used in the study

<b>Silencers</b>	<b>Reference</b>	<b>Manufacturer</b>
<b>siNME6</b>	ON-TARGETplus Human NME6 siRNA - SMARTpool	Dharmacon, USA
<b>siCTRL</b>	ON-TARGETplus Non-targeting siRNAs	Dharmacon, USA

### 3.1.6 Software

Table 15 : Software used in the study

<b>Software</b>	<b>Manufacturer</b>
<b>FlowJo</b>	FlowJo LLC, USA
<b>Image Lab 6.1.0</b>	Bio-Rad, USA
<b>ImageJ Fiji</b>	National Institutes of Health, USA
<b>Leica application suite X (LAS X) 3.3.0.16799</b>	Leica Microsystems, Germany
<b>Microsoft Office Professional plus 2019</b>	Microsoft Corporation, USA
<b>Photoshop CS4</b>	Adobe Inc., USA
<b>Prism 8.3.0</b>	GraphPad, USA
<b>PyMol 2.4.0</b>	Schrödinger LLC, USA
<b>SnapGene</b>	GSL Biotech LLC, USA



## 3.2 Methods

### 3.2.1 Preparation

#### 3.2.1.1 Cloning of specific plasmids

Plasmids used for the overexpression of human NME6 isoforms, NME3 and NME4 in human and bacterial systems were produced in-house by plasmid cloning. A sequence of interest was extracted from one existing plasmid by PCR using specific primers. The resulting DNA sequence of interest (insert) as well as the plasmid of destination were separately digested with specific couple of enzymes to expose single stranded complementary sequences. Ligation was performed by incubating both the insert and the opened plasmid with T4 DNA ligase. Primers, plasmids and enzymes used for each cloning are listed in Table 11 and Table 12.

##### 3.2.1.1.1 PCR

PCR was used to extract and amplify a DNA sequence of interest from an existing plasmid using specific primers. Primers and plasmids are listed in Table 11 and Table 12. The PCR was performed on the Geneamp 2700, using the reaction mix and PCR parameters (Table 16 and Table 17):

*Table 16 : PCR reaction mix used for plasmid cloning*

Plasmid	50 ng
Primer -forward 10uM, diluted in qH <sub>2</sub> O	2 $\mu$ L
Primer -reverse 10uM, diluted in qH <sub>2</sub> O	2 $\mu$ L
EmeraldAmp master mix	25 $\mu$ L
qH <sub>2</sub> O	Up to 50 $\mu$ L
Total volume	50 $\mu$ L

*Table 17 : PCR parameters used for plasmid cloning*

	95 °C	1 min	
<b>Denaturation</b>	<b>95 °C</b>	<b>30 s</b>	<b>30×</b>
<b>Annealing</b>	<b>65 °C</b>	<b>30 s</b>	
<b>Elongation</b>	<b>72 °C</b>	<b>1 min</b>	
	72 °C	5 min	
	4 °C	$\infty$	

#### **3.2.1.1.2 Agarose gel electrophoresis**

A fresh 1,2 % agarose gel was produced according to the following recipe (100 mL TAE buffer, 1.2 g agarose, 3  $\mu$ L Midori Green). The mixture was boiled in a microwave and poured into a cast system. After polymerization, the DNA was loaded onto the gel after being diluted in 5 $\times$ LB to 1 $\times$  (50  $\mu$ L of the above PCR product + 12.5  $\mu$ L 5 $\times$ LB). One microliter of 1kb plus DNA ladder was loaded, as well, to assess the size of different DNAs. The electrophoresis was performed in Sub-Cell GT system at 100 V for 1 h. DNA fragments were visualized using Uvitec alliance 4.7 system.

#### **3.2.1.1.3 Gel extraction**

The gel was illuminated using the UV lamp and the band of interest produced by PCR was cut out. The PCR product was extracted using QIAquick Gel Extraction Kit according to manufacturer's instructions, and eluted in qH<sub>2</sub>O. The product's concentration was determined by nanodrop (section 3.2.1.1.4) and saved on ice for the next step.

#### **3.2.1.1.4 Determination of DNA concentration**

The concentration of DNA was determined using Nanophotometer N60 spectrophotometer. One microliter of elution buffer was used as a blank to calibrate the instrument, and 1  $\mu$ L of the sample was used to determine DNA concentration, by measuring the absorbance at 260 nm. The absorbance at 280 and 230 nm was measured as well, and the ratio A<sub>260</sub>/A<sub>280</sub> and A<sub>260</sub>/A<sub>230</sub> were used to assess the purity of DNA. A ratio A<sub>260</sub>/A<sub>280</sub> about 1.8 and A<sub>260</sub>/A<sub>230</sub> between 2.0 and 2.2 were considered to be acceptable for future experiments.

#### **3.2.1.1.5 Digestion of the PCR products and plasmids of interest**

The digestion of a PCR fragment and a plasmid with specific enzymes exposes complementary single stranded DNA sequences to allow proper ligation. PCR fragment and plasmid digestions were realized separately, using the reaction mix as described in Table 18. The digestion was carried on for 40 min at 37 °C using restriction enzymes listed in Table 12, specific for each plasmid (Table 11).

Table 18 : Digestion reaction mix

PCR fragment or plasmid	3 $\mu\text{g}$
Enzyme 1	1.5 $\mu\text{L}$
Enzyme 2	1.5 $\mu\text{L}$
Buffer FD10 $\times$	3.5 $\mu\text{L}$
qH <sub>2</sub> O	Up to 36 $\mu\text{L}$
Total volume	36 $\mu\text{L}$

### 3.2.1.1.6 Purification of the digested PCR fragment and plasmid

The purifications were performed separately using QIAquick PCR purification Kit according to manufacturer's instructions. PCR fragments were eluted in 30  $\mu\text{L}$  while the plasmids were eluted in 50  $\mu\text{L}$  of qH<sub>2</sub>O.

### 3.2.1.1.7 CIP procedure of the digested plasmid

Plasmids were digested with CIP (calf intestinal alkaline phosphatase) to remove the terminal phosphate of the open plasmid and reduce the re-ligation of linearized plasmids. The procedure was performed with the reaction mix described in Table 19. The incubation was carried at 37 °C for 1 h.

Table 19 : CIP reaction mix

Open plasmid	50 $\mu\text{L}$
CIP (10 U/ $\mu\text{L}$ )	1 $\mu\text{L}$
qH <sub>2</sub> O	3 $\mu\text{L}$
NEBuffer 3	6 $\mu\text{L}$
Total volume	60 $\mu\text{L}$

Purification of the plasmid was carried out as described in section 3.2.1.1.6. The plasmid concentration was measured as described in section 3.2.1.1.4.

PCR fragment and CIP-digested open plasmid were loaded on 1.2% agarose gel as described in section 1.1.2 using a mix of 1  $\mu\text{L}$  of sample, 2  $\mu\text{L}$  of 5 $\times$ LB and 7  $\mu\text{L}$  of qH<sub>2</sub>O to control the presence and purity of each component before ligation.

### 3.2.1.1.8 Ligation

The ligation mixture was calculated using the NEB calculator service, with a plasmid mass of 100 ng and plasmid to insert mass ratio of 3:1. (<https://nebiocalculator.neb.com/#!/ligation>). volumes were dependent on the length of the insert and of the linearized plasmid. The reaction mixture was performed as described in Table 20. The ligation reaction started by adding the ligase and was allowed to perform for 10 min at room temperature. The reaction was heat inactivated by 10 min incubation at 65°C. The reaction mix was chilled on ice and 1  $\mu$ L was immediately used to transform electrocompetent bacteria as described in section 3.2.1.2.

Table 20 : Ligation reaction mix

Insert (NEB calculated)	X ng (Roughly 34 ng)
Plasmid	100 ng
T4 DNA Ligase Reaction Buffer (10 $\times$ )	2 $\mu$ L
qH <sub>2</sub> O	Up to 19 $\mu$ L
T4 DNA Ligase	1 $\mu$ L
Total volume	20 $\mu$ L

### 3.2.1.2 Transformation of bacteria by electroporation

Freshly produced plasmids were immediately used to transform bacteria and produce stable bacterial colonies carrying the plasmid of interest. Selected bacteria were stored at -80 °C and used for plasmid production or for recombinant protein production. Every step involving bacteria was performed under sterile environment near a benzene burner.

DH5 $\alpha$  electrocompetent bacteria were a kind gift of Dr. sc. Nikolina Škrobot Vidaček. The concentration of the plasmid of interest was measured (section 3.2.1.1.4), and diluted in dH<sub>2</sub>O at 20 ng/ $\mu$ L. Electroporation cuvette was cooled down at -20 °C overnight. Under the sterile environment of a benzene burner, 1  $\mu$ L of diluted plasmid was pipetted on top of 40  $\mu$ L of electrocompetent bacteria, and the mixture was directly transferred into the electroporation cuvette. Electroporation was performed using the gene pulser xCell system and the preset bacterial protocol 2 (*E. coli*, exponential decay, 25  $\mu$ F, 200  $\Omega$ , 2500 V, 2 mm cuvette). Bacteria were immediately transferred into 1 mL of liquid LB without antibiotic in 1.5 mL tube for recovery, and mixed by inversion. The tube was incubated on a thermoshaker for 1 h at 37 °C, 200 rpm. Bacteria were plated on solid LB complemented with a specific antibiotic (LB+Kan

for selection of the pET28b and pEGFP plasmids, LB+Amp for pcDNA 3.1 plasmids) at low density (50  $\mu$ L of transformed bacteria) and high density (300  $\mu$ L of transformed bacteria). Plates were incubated overnight at 37 °C. The next day, single colonies were selected, inoculated in 5 mL of liquid LB+antibiotic and incubated overnight at 37 °C with vigorous shaking. Colonies were stored in a bank at -80 °C after mixing 1.4 mL of the overnight liquid culture with 0.6 mL of sterile 50 % glycerol. The rest of the overnight culture was used to extract plasmid using QIAprep spin miniprep kit according to the manufacturer's instructions. DNA concentration was measured as described earlier (section 3.2.1.1.4). The presence of the plasmid of interest within the colony was crosschecked by enzymatic digestion (section 3.2.1.1.5) using relevant restriction enzymes listed in Table 12. Digested plasmids were subjected to gel electrophoresis (section 3.2.1.1.2) using a mix of 1  $\mu$ L of sample diluted in 2  $\mu$ L 5 $\times$ LB and 7  $\mu$ L qH<sub>2</sub>O. Plasmids were sent to sequencing to control the cloning.

### **3.2.1.3 Production of recombinant proteins**

For enzymatic and structural analysis of NME6, human NME6-186-His and NME6-194-His proteins were produced in bacterial systems. Proteins were extracted and purified by immobilized metal affinity chromatography (IMAC), using the natural affinity of the His-tag for the positively charged metal ions (Ni<sup>2+</sup>, Co<sup>2+</sup>, Cu<sup>2+</sup> and Zn<sup>2+</sup>) immobilized in the resin. Pure eluted NME6-His proteins underwent buffer exchange and concentration before storage in - 80 °C. The human NME1-His purified protein, already prepared following the same protocol, was a kind gift from Dr. sc. Helena Četković.

#### **3.2.1.3.1 Large scale production of NME6-His recombinant proteins**

Glass material, LB, tips and pipettes were sterilized and used under the sterile environment of a benzene burner until the harvesting of the large-scale bacteria culture. After harvesting, the samples were constantly kept on ice to avoid protein degradation.

Bacteria carrying plasmid pET28b-NME6-194-His or pET28b-NME6-186-His were inoculated into 12 mL of liquid LB+Kan and incubated overnight (18 h) at 37 °C with vigorous shaking. The next day, 10 mL of the overnight culture was used to inoculate 1 L of liquid LB+Kan, and divided in two Erlenmeyer of 2 L volume (i.e. 0.5 L of bacterial culture per Erlenmeyer). Bacterial cultures were incubated at 37 °C with vigorous shaking until OD<sub>600</sub> of 0.7-0.8 was reached. Protein production was induced by addition of IPTG in the culture medium at 0.1 mM final concentration. The culture was immediately incubated at 16 °C overnight (20 h) with vigorous shaking using Innova 40 incubator. The next day, bacteria were

separately harvested by centrifugation at 4 000 g for 30 min, 4 °C (one tube per Erlenmeyer). Resulting pellets were separately resuspended in 40 mL of resuspension buffer and transferred in two 50 mL centrifugation tubes. Bacteria were centrifuged at 16 000 g, 4 °C, 5 min. The supernatant was discarded while the pellets were immediately stored at -80 °C overnight. The next day, each pellet was resuspended in 10 mL of resuspension buffer supplemented with imidazole and combined. Lysozyme was added at a final concentration of 1 mg/mL and sample was incubated on ice for 15 min. The sample was sonicated on ice using the CP 130 sonicator with 6 mm probe, 8 × 30 s with 1 min cooling period between each burst, amplitude 40, output 10 watt. Sample was centrifuged at 16 000 g for 30 min at 10 °C. The supernatant was saved in a new tube and filtered through a 0.20 µm pore filter, and named “Filtrate”. The “Filtrate” was saved on ice until IMAC purification (section 3.2.1.3.2).

#### **3.2.1.3.2 IMAC: immobilized metal affinity chromatography**

The purification process was performed in the cold room with buffers precooled at 4 °C to ensure preservation of the proteins. The Poly-Prep gravity-flow column was prepared by adding 400 µL of TALON resin on the filter. The column was equilibrated with 5 mL of washing buffer and the flow through was discarded. “Filtrate” sample (section 3.2.1.3.1) was loaded on the column and allowed to drain until the volume reaches the top of the resin bed (“Flow-through”). The column was washed three times with 10 mL of washing buffer (“W1”, “W2”, “W3”). The protein of interest was eluted using elution buffer. First 150 µL was applied for “E0”, that represent the buffer’s volume trapped in the resin, and not containing the protein of interest. The fraction was assayed by quick Bradford (section 3.2.1.3.4) to assess the absence of protein of interest. “E1” to “E10” were eluted with 1 mL of elution buffer and collected in separate tubes. The concentration of eluted protein was controlled visually by performing a quick Bradford (section 3.2.1.3.4). The elution process was stopped when no more proteins could be detected. Ten µL of fractions: “Filtrate”, “Flow-through”, “W1-3”, “E0-10” were saved to be analyzed by sodium dodecyl sulfate-polyacrylamide gel electrophoresis (SDS-PAGE), transferred on nitrocellulose membrane and stained with naphthol blue (3.2.3.3). All samples were saved on ice.

#### **3.2.1.3.3 Sample concentration and buffer exchange**

Amicon ultra centrifugal filters were used with a 10 kDa cutoff, according to the manufacturer’s instruction. The filter was equilibrated with 15 mL of storage buffer and centrifuged 4 000 g, 5 min, 10 °C. The flow through was discarded and elution fractions “E1”

to “E10” were loaded on the filter. “E0” was excluded since it should be devoid of protein of interest. Storage buffer was added to reach a final volume of 15 mL and the sample was centrifuged for 10 min, 4 000 g, 10 °C. The flow through was discarded and the concentrated sample was gently resuspended, directly in the filter, in storage buffer to reach a final volume of 15 mL. The sample was centrifuged again using the same parameters until 1 mL of concentrated sample remained (“Conc”). Concentrated sample was aliquoted and immediately stored at -80 °C until use. An aliquot was saved to perform protein concentration assay using the Bradford method (3.2.3.2.2).

#### **3.2.1.3.4 Quick Bradford**

On a clean sheet of parafilm, a series of 20 µL drops of 1× Bradford solution was disposed. A standard curve was created by pipetting in the drops 5 µL of bovine serum albumin (BSA) standard of 62.5, 125, 250, 375, 500, 750 and 1000 µg/mL. Five microliters of sample were assayed in a new drop of 1× Bradford while the concentration of protein was roughly estimated by comparing visually the sample’s blue color with the standard curve. This unprecise, but extremely quick method was used to assess in real-time the exit of proteins of interest from the column during protein purification.

### **3.2.2 Cell culture**

#### **3.2.2.1 Culture of cells in sterile conditions**

Cells listed in Table 10 were grown in complete media (RPMIcomp or DMEMcomp) according to ATCC and generous donators’ recommendation. Cells manipulations were processed in the environment of the Sterile Hood, while the cells were grown in humid atmosphere at 37 °C, 5 % CO<sub>2</sub> in the cell incubator. Every medium, solution and chemical were sterilized and material was disinfected prior to manipulation in the sterile environment. Solutions were prewarmed at 37 °C before use, unless otherwise specified. Volumes are indicated for a specific cell culture dish format. Upon the use of a different format, volumes were adjusted according to the dish surface.

#### **3.2.2.2 Maintenance/collection of cells**

In a 10 cm culture dish, the medium was removed and attached cells were washed with 5 mL phosphate-buffered saline (PBS). PBS was removed, 1 mL of trypsin solution was added on cells and dish was incubated for 3 min in the cell incubator. Trypsin was inactivated by diluting

it with 9 mL of complete medium. Cells were either maintained (section 3.2.2.2.1) or collected (section 3.2.2.2.2).

#### **3.2.2.2.1 Maintenance of cells**

Cells were resuspended, 1 mL was left in the dish and 9 mL of complete medium was added. The dish was returned in the cell incubator. Cells were maintained every 3-4 days when reaching 90 % of confluency.

#### **3.2.2.2.2 Collecting cells**

Cells were resuspended and collected in 15 mL centrifugal tube, cooled down on ice and centrifuged at 1 000 g, 5 min, 4 °C. Supernatant was discarded and cells were washed two times in 5 mL of PBS, using the same centrifugal parameters. During the wash, 20 µL of the sample was collected for counting (3.2.2.4). Supernatant was discarded and cell pellet was kept on ice.

#### **3.2.2.3 Freezing and thawing cells**

Cells were collected according to the protocol (section 3.2.2.2.2) and counted (section 3.2.2.4). Pellet was resuspended to reach  $3 \times 10^6$  cells/mL in cryoprotective medium. Cells were transferred in sterile Cryotubes, and stored at -80 °C for short term storage, or in liquid nitrogen for long term storage. When cells were needed, cryotubes were quickly thawed by incubation at 37 °C until the ice melted. Cells were immediately centrifuged at 1 000 g for 2 min, resuspended with complete medium, plated in 10 cm dish and placed in the cell incubator.

#### **3.2.2.4 Counting cells**

Cells were counted using the Glasstic™ slides according to the manufacturer's instruction. Briefly, 20 µL of cells resuspended in PBS (section 3.2.2.2.2) were collected and diluted in 80 µL trypan blue (dilution factor = 5). Few microliters were used to load the counting chamber and cells were counted under the microscope. The full grid of 81 squares was counted. The calculation was done as follow:

$$\frac{\text{Cell count}}{81} \times 90000 \times \text{Dilution factor} = \text{Cell concentration (cells/mL)}$$

#### **3.2.2.5 Transfection**

Cell transfections were realized with plasmids listed in Table 11 using Turbofect transfection reagent according to manufacturer's instructions. Briefly, for a 6 well culture plate format,  $10^5$



cells were seeded and placed in the cell incubator overnight. The next day, the cells were transfected with the transfection mixture (4 µg of plasmid and 6 µl of Turbofect reagent diluted in 400 µL of OptiMem) and incubated at room temperature for 20 min. The culture medium was changed during this time window with 3.6 mL of fresh complete medium, and transfection mix was applied to reach a final volume of 4 mL. Cells were immediately placed in the cell incubator. The medium was changed 6 h post transfection. Cells were used 48 h post transfection for the different analysis.

#### **3.2.2.6 Silencing**

Silencing was performed using Dharmafect 4 transfection reagent and Dharmacon silencers listed in Table 14, according to manufacturer's instructions. Briefly, for a 6-well plate format, cells were seeded at  $7 \times 10^4$  cells/well and placed in the cell incubator overnight. The next day, the transfection mix was prepared (10 µL Silencer (5 µM), 2 µL Dharmafect, and 388 µL OptiMem) and incubated for 20 min at room temperature. The cell medium was replaced during this time window, with 1.6 mL of fresh complete medium, after which the transfection mix was added. Cells were immediately placed in the cell incubator overnight and the medium was changed the next day. Cells were used for experiments 72 h post transfection for the different analysis.

#### **3.2.2.7 Production of NME6-KI (Knock-In) and NME6-KO (Knockout) clones**

##### **3.2.2.7.1 NME6-KI stable clones**

MDA-MB-231T cells were transfected with pcDNA3.1-NME6-194-FLAG and pcDNA3.1-NME6-186-FLAG using Turbofect transfection reagent according to section 3.2.2.5. The medium was changed 6 h post transfection with DMEMcomp. The selection of stable clones commenced 24 h post transfection in DMEMg418 for 14 days. During this period the medium was changed every 4 days (section 3.2.2.2.1). Selected cells underwent single-cell clone expansion as described in the section 3.2.2.7.3. The proper integration of the plasmid of interest in viable colonies was confirmed by Western blot (section 3.2.3.3) using anti-FLAG antibody for KI clones.

KI-negative control clones (Neg5, Neg6, Neg7) were previously prepared and used in the laboratory [129]. The negative controls are a result of the random integration of the empty pcDNA3.1 plasmid within the genome of MDA-MB-231T cell lines, conferring a resistance to G418 antibiotic.

### 3.2.2.7.2 NME6-KO stable clones

We tried to produce NME6-KO stable clones by CRISPR-Cas9 technique, using the NME6 Human Gene Knockout Kit according to manufacturer's instructions. The aim was to break both alleles of the NME6 gene by inserting-in a cassette containing the neomycin resistance gene. Briefly, MDA-MB-231T cells were co-transfected with the Donor construct and one of the gRNA constructs provided, using Turbofect transfection reagent according to manufacturer's instructions (section 3.2.2.5). The medium was changed 6 h post transfection and cells were passaged 7 times, every 3 days, to dilute the donor vector (section 3.2.2.2.1). Selection started on passage 8 (23 days post transfection) by growing cells in DMEMg418 medium for a 14 days period. Selected cells underwent single-cell clone expansion as described in the section 3.2.2.7.3. The surviving NME6-KO clones were verified by Western blot using anti-NME6 antibodies (section 3.2.3.3) and by PCR (section 3.2.2.7.4).

### 3.2.2.7.3 Single-cell clone expansion

Cells selected in DMEMg418 were counted (section 3.2.2.4), diluted and seeded at one cell per well in a 96-well plate. Single-cell clones were selected under the microscope 20 h after seeding and allowed to grow in DMEMg418. The wells containing either 0 cells or 2 cells and more were discarded. Cells were allowed to grow in DMEMg418 until the formation of a colony, all derived from the same parent cell (monoclonal cells), while the medium was changed every 4 days. Clones were moved to a bigger dish (section 3.2.2.2) when the confluency reached 70 % (96 to 24 to 6 well plates). The clones that failed to grow were discarded. Finally, the cells were transferred to a 10 cm dish, the knockout of NME6 was tested by Western blot and PCR (sections 3.2.2.7.1 and 3.2.2.7.2) and used for further several experiments. Validated clones were frozen and kept at -80 °C (section 3.2.2.3).

### 3.2.2.7.4 PCR verification of NME6-KO clones

Genomic DNA was isolated from selected clones by using GenElute miniprep kit according to manufacturer's instructions, and eluted in qH<sub>2</sub>O. DNA concentration was measured by nanodrop (3.2.1.1.4). PCR reactions were performed using 3 sets of primers listed in Table 13, to detect NME6-WT (wild type) and NME6-KO DNA sequence (primers LF and RR), but also to verify the left (primers LF and LR) and right (Primers RF and RR) integration of the insert, as described in the result section (Figure 21). PCR reactions were performed using expand long template PCR system kit as described in (Table 21 and Table 22), using Geneamp2700 machine.

Table 21 : PCR reaction mix for the control of NME6-KO

Genomic DNA	20 ng
Primer 1	0.3 $\mu$ M
Primer 2	0.3 $\mu$ M
dATP	350 $\mu$ M
dCTP	350 $\mu$ M
dGTP	350 $\mu$ M
dTTP	350 $\mu$ M
10 $\times$ Buffer1	2.5 $\mu$ L
DMSO 20 %	2.5 $\mu$ L
Enzyme mix	0.2 $\mu$ L
qH <sub>2</sub> O	Up to 25 $\mu$ L
Total volume	25 $\mu$ L

Table 22 : PCR parameters used for the control of NME6-KO

	94 °C	3 min	
<b>Denaturation</b>	<b>95 °C</b>	<b>15 s</b>	<b>30<math>\times</math></b>
<b>Annealing</b>	<b>60 °C</b>	<b>30 s</b>	
<b>Elongation</b>	<b>68 °C</b>	<b>4 min</b> <b>(*1 min 45 s)</b>	
	68 °C	7 min	
	4 °C	$\infty$	

Note: Four minutes of elongation was used for screening NME6-KO and NME6-WT genes with primer LF and RR. \*One minute and forty-five second of elongation was used for screening the left (Primers LF and LR) and right (Primers RF and RR) integration junctions (Table 13).

All PCR product were analyzed in the agarose gel as described in section 3.2.1.1.2 using a mix of 1  $\mu$ L of sample, 2  $\mu$ L of 5 $\times$ LB and 7  $\mu$ L of qH<sub>2</sub>O.

### **3.2.3 Protein analysis**

All procedures were performed on ice to avoid protein degradation.

#### **3.2.3.1 Cell lysate preparation for Western blot analysis**

The cell pellet from section 3.2.2.2 was resuspended in 100  $\mu$ L of PBS supplemented with 1 $\times$  protease inhibitor and subjected to sonication on ice using the Labsonic system with the 1 mm probe, 3  $\times$  10 s, with 1 min cooling period between each burst. Protein concentration was measured as described in section 3.2.3.2.1.

#### **3.2.3.2 Protein concentration measurement**

##### **3.2.3.2.1 Bicinchoninic acid (BCA) method**

Protein concentration assay was performed using the *Pierce BCA* kit according to manufacturer's instruction. In a 96 well plate, blank and standards were loaded as follows: 20  $\mu$ L of blank (qH<sub>2</sub>O) and 20  $\mu$ L of BSA standards of 125, 250, 375, 500, 750, 1000 and 1500  $\mu$ g/mL. Samples were loaded in duplicates as follows: 18  $\mu$ L of qH<sub>2</sub>O + 2  $\mu$ L cell lysate sample. Two hundred microliters of working reagent (A + B in ratio 50:1) from the kit was added to each well. The plate was mixed by gentle shaking for a few seconds and incubated in the dark at 37 °C for 30 min. The plate was allowed to cool down few minutes at room temperature and the absorbance was measured at 570 nm using the multiskan spectrophotometer. The standards' absorbance was used to create a standard curve and calculate the concentration of the protein sample, paying attention to the 10 $\times$  dilution factor between the standard and the samples.

##### **3.2.3.2.2 Bradford method**

The Bradford method was used to measure NME6-His protein concentration after recombinant protein purification (section 3.2.1.3.3). The BCA method could not be used then, due to incompatibility of the kit's chemicals with the storage buffer.

In a 96 well plate, the blank and standards were loaded as follows: 20  $\mu$ L of blank (storage buffer) and 20  $\mu$ L of BSA standards of 125, 250, 375, 500, 750, 1000 and 1500  $\mu$ g/mL. Samples were loaded in triplicates as follows: 18  $\mu$ L of storage buffer + 2  $\mu$ L the purified protein sample. Two hundred microliters of 1 $\times$  Bradford was added to each well. The plate was mixed by gentle shaking for 1 min and the absorbance was measured at 595 nm using the multiskan spectrophotometer. The standards' absorbance was used to create a standard curve and

calculate the concentration of the protein sample, paying attention to the 10× dilution factor between the standard and the samples.

### 3.2.3.3 Standard immunoblotting

#### 3.2.3.3.1 Preparation of standard gel for SDS-PAGE

The gel for electrophoresis was prepared fresh at the desired acrylamide/bis-acrylamide percentage as described in Table 23. First, the running gel solution was prepared, poured in the casting stand system, and covered with 2 mL of isopropanol. After polymerization, the isopropanol was removed, the stacking gel solution was prepared and poured on top of the running layer, followed by the insertion of combs. After polymerization, the gel was immediately used for electrophoresis.

Table 23 : Poly-acrylamide gel composition for SDS-PAGE

	Running gel			Stacking gel
	10 %	12 %		5 %
<b>dH<sub>2</sub>O (mL)</b>	4.000	3.300	<b>dH<sub>2</sub>O (mL)</b>	2.700
<b>30 % AAS (mL)</b>	3.300	4.000	<b>30 % AAS (mL)</b>	0.670
<b>Tris 1.5 M, pH 8.8 (mL)</b>	2.500	2.500	<b>Tris 1 M, pH 6.8 (mL)</b>	0.500
<b>10 % SDS (mL)</b>	0.100	0.100	<b>10 % SDS (mL)</b>	0.040
<b>10 % APS (mL)</b>	0.100	0.100	<b>10 % APS (mL)</b>	0.040
<b>TEMED (mL)</b>	0.004	0.004	<b>TEMED (mL)</b>	0.004

#### 3.2.3.3.2 SDS-PAGE and Western blot

The gel was placed in the mini-protean III apparatus and filled with running buffer (RB). Samples were prepared at the desired protein concentration in 4×LB to reach 1×LB. Samples were boiled 5 min at 95 °C and immediately loaded in the gel, together with Precision Plus protein standard. Proteins were separated by SDS-PAGE first at 90 V for 10 min to allow samples to enter the stacking gel, and then at 110 V for two hours, or until the blue front line exits the gel. After electrophoresis, proteins were transferred from the gel to a 0.2 µm nitrocellulose membrane using transfer buffer (TB) in the mini protean III system. The transfer was allowed for 90 min, 200 mA at room temperature, or overnight, 13 V at 4 °C. The recovered membrane was stained with naphthol blue solution for 1 min and destained for 10 min in

distaining solution to assess visually the correct separation of proteins. An image was captured to perform densitometry when needed. Membrane was washed three times in TBST for 10 min, then blocked for 30 min with blocking milk buffer. Membrane was incubated overnight at 4 °C with the blocking milk buffer supplemented with the primary antibody. The next day the membrane was washed three times in TBST for 10 min. Incubation with the secondary antibody diluted in blocking milk buffer was performed at room temperature for 1 h after which the membrane was washed three times for 10 min with TBST. The detection was performed using first the Western lightning plus ECL chemiluminescent reagents. Other chemiluminescent substrates listed in Table 6 were used upon low signal intensity. Images were acquired using Uvitec alliance 4.7 system.

#### **3.2.3.4 Phospho-Histidine immunoblotting**

##### **3.2.3.4.1 Preparation of a modified pHis-gel**

A modified electrophoresis gel was freshly prepared. The preparation was the same as described in section 3.2.3.3.1, except that 1 M Tris, pH 7.4 was used instead of 1 M Tris, pH 6.8 for the production of the stacking gel, in order to preserve histidine phosphorylation. After polymerization, the gel was cooled down at 4 °C before use.

##### **3.2.3.4.2 SDS-PAGE and Western blot in pHis preserving conditions**

The polyacrylamide gel and buffers RB, TB, TBST and PBS were cooled down at 4 °C. Buffers were adjusted to pH 8.2. The pHis-5×LB was cooled down, adjusted to pH 8.8 and diluted in PBS to pHis-2×LB on the day of the experiment. Cells were grown until 90 % confluency in a 10 cm dish, washed twice in PBS and collected by scrapping in 500 µL of pHis-2×LB. The sample was incubated 10 min on ice before sonication using the Labsonic system (3 × 10 s, 4 °C) and clarified by centrifugation (14 000 g, 10 min, 4 °C). The supernatant was carefully collected and equally divided in two parts, one incubated on ice (4 °C), the other boiled (95 °C) for 10 min just before loading. Samples (10 µL) and precision plus protein standard were loaded onto the pHis-gel placed in the mini-protean III apparatus and run in RB at 110 V for 2 h, 4 °C. The proteins were transferred to a 0.2 µm nitrocellulose membrane in TB at 200 mA for 90 min, 4 °C. After transfer, the membrane was washed three times for 10 min in TBST and immediately blocked for 40 min at 4 °C with Blocking BSA buffer. The membrane was incubated with the primary antibody diluted in Blocking BSA buffer, overnight at 4 °C, the membrane was washed three times for 10 min in TBST. The incubation with the secondary antibody diluted in Blocking BSA buffer was performed for 2 h at 4 °C, after which the

membrane was washed three times for 10 min in TBST. Proteins were visualized with the chemiluminescent reagent listed in Table 6 using Uvitec alliance 4.7 system.

### **3.2.3.5 Immunoprecipitation**

Immunoprecipitation was performed in a forward and reverse manner using MDA-MB-231T wild type cells or transiently transfected MDA-MB-231T cells that express one of the following: NME3-FLAG, NME4-FLAG, NME6-186-FLAG or NME6-194-FLAG.

#### **3.2.3.5.1 Cell lysate preparation**

Cells were transfected (section 3.2.2.5), collected 48 h post transfection (section 3.2.2.2), and resuspended in 100  $\mu$ L of TEEN buffer supplemented with 1 $\times$  protease inhibitor. Cells were sonicated using Labsonic system with a 1 mm probe, 2  $\times$  10 s at 4  $^{\circ}$ C with 1 min cooling period between each burst. Cell lysates were centrifuged at 16 000 g, 20 min at 4  $^{\circ}$ C. Supernatant was saved and named Input (I), while the pellet was discarded. Protein concentration was measured as described in section 3.2.3.2.1.

#### **3.2.3.5.2 Immunoprecipitations using Dynabeads Protein G**

Immunoprecipitations using Dynabeads Protein G were performed according to manufacturer's instructions. Briefly, 50  $\mu$ L of beads were washed two times with 200  $\mu$ L of PBS-TWEEN. Beads were incubated 40 min with 2  $\mu$ g of antibody diluted in 200  $\mu$ L of PBS-TWEEN, on the rotator at room temperature. Anti-NME1 (OP48 Calbiochem), anti-NME6 (HPA017909, Sigma) and anti-RCC1-L (SAB1401860, Sigma) were used to pull down NME1, NME6 and RCC1-L proteins, respectively. Beads-Antibody complexes were washed in PBS-TWEEN, 200  $\mu$ g of Input protein (I) was added in a final volume of 200  $\mu$ L in PBS-TWEEN, and incubated overnight on the rotator at 4  $^{\circ}$ C. The next day, supernatant (Sn) was saved while Beads-Antibody-Antigen complexes were washed in PBS-TWEEN and eluted in 20  $\mu$ L of 2 $\times$ LB by heating the sample at 95  $^{\circ}$ C for 10 min (IP). The whole elution volume (IP) was loaded onto SDS-PAGE, while 30  $\mu$ g of Input (I) and supernatant (Sn) were loaded, and analyzed by Western blot (section 3.2.3.3).

#### **3.2.3.5.3 Immunoprecipitations using FLAG-agarose**

Immunoprecipitations using FLAG-agarose were done according to manufacturer's instructions. Briefly, 40  $\mu$ L of slurry was washed in TEEN buffer and incubated overnight with 200  $\mu$ g of input protein (I) diluted in 200  $\mu$ L of TEEN buffer, on the rotator at 4  $^{\circ}$ C. The next day, supernatant (Sn) was saved while FLAG-agarose-Antigen complexes were washed in

PBS-TWEEN and eluted in 20  $\mu$ L of 2 $\times$ LB by heating up the sample at 70  $^{\circ}$ C for 10 min (IP). The whole elution volume (IP) was loaded onto SDS-PAGE, while 30  $\mu$ g of Input (I) and supernatant (Sn) were loaded and analyzed by Western blot (section 3.2.3.3).

### **3.2.3.6 NME6 expression in human cell lines**

Endogenous NME6 protein expression profile was assayed in a large number of human cell lines with different tissues of origins (Table 10). Cancerous and non-cancerous human cell lines were selected upon their tissue of origin to represent the diversity of human tissues. Cells were thawed (section 3.2.2.3) in the appropriate complete media (Table 10), cultured in 6-well plate and allowed to grow for 15 days (section 3.2.2.2.1). On the day of the experiment, upon cells reaching 80-90% confluency, cells were collected (section 3.2.2.2.2), proteins were extracted (section 3.2.3.1) and 20  $\mu$ g of the cell lysate was analyzed by Western blot (section 3.2.3.3) using anti-NME6 and anti-Actin antibodies.

### **3.2.3.7 NDPK activity**

NDP kinase activity assay of purified NME1-His, NME6-186-His and NME6-194-His recombinant proteins was performed using the pyruvate kinase-lactate dehydrogenase coupled assay, described by Agarwal et al. [130] with minor modifications.

NME6-His proteins were produced according to (section 3.2.1.3), while NME1-His protein was a kind gift from Dr.sc. Helena Četković. All buffers were freshly prepared on the day of the experiment and kept at 4  $^{\circ}$ C in the dark. Experiments were performed at room temperature in a 1 cm quartz cuvette containing 512.5  $\mu$ L of reaction mixture composed of 50 mM Tris-HCl pH 7.5, 75 mM KCl, 5 mM MgCl<sub>2</sub>, 1 mg/mL BSA, 1 mM phosphoenolpyruvate, 0.45 mM NADH, 1 mM ATP, 0.2 mM dTDP, 2 units of pyruvate kinase, 2.5 units of lactate dehydrogenase and 200 ng of the recombinant NME protein. The experiment follows the degradation of NADH by measuring the decrease of its absorbance at 340 nm, which is directly dependent on the NDPK activity of NME proteins according to the following reaction scheme (Figure 17).



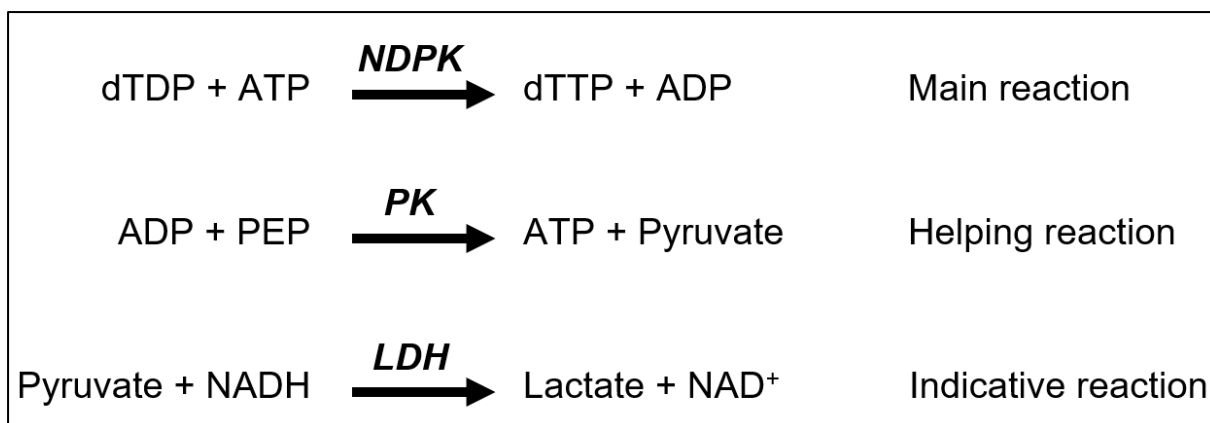


Figure 17 : Pyruvate kinase-lactate dehydrogenase coupled assay. The assay is composed of three enzymatic reactions processed by NME protein (NDPK), pyruvate kinase (PK) and lactate dehydrogenase (LDH). The production of ADP by NDPK activity (main reaction) will trigger the helping and the indicative reaction, eventually leading to the degradation of NADH. The decrease of NADH absorbance, directly proportional to NDPK activity, is followed at 340 nm.

On the day of the experiment, a standard mixture was prepared for each protein tested, in a volume large enough to allow at minima triplicates from the same standard mixture (Table 24).

Table 24 : Preparation of standard mixture used in the NDPK repeated measures

5× TKM	600 $\mu\text{L}$
LDH 12.5 U/mL	1.2 $\mu\text{L}$
NADH 15 mM	30 $\mu\text{L}$
PK 1.54 U/mL	7.8 $\mu\text{L}$
PEP 100 mM	30 $\mu\text{L}$
ATP 100 mM	30 $\mu\text{L}$
NME protein	1.2 $\mu\text{g}$
reH <sub>2</sub> O	Up to 3000 $\mu\text{L}$

Five hundred microliters of the standard mixture (Blank) was loaded in a 1 cm quartz cuvette and inserted in the ultrospec 2100 pro spectrophotometer in the dark. The apparatus absorbance units (AU.) was set to zero, the acquisition was started (every 10 s at 340 nm) and the mixture was allowed to reach room temperature for 5 min. Then 10  $\mu\text{L}$  of 15 mM NADH was added in the cuvette, mixed by pipetting and the absorbance was allowed to stabilize for 2 min. The

reaction was started by addition of 2.5  $\mu\text{L}$  of 40 mM dTDP and the absorbance was measured for the next 7 min. The final volume of the reaction  $V_{\text{tot}}$  was 512.5  $\mu\text{L}$ . NDPK measurements were repeated 6 times over two days.

The maximal speed of the decrease of absorbance at 340 nm after dTDP induction ( $\Delta A_{\text{max}}$ ) was extracted from the data and used in the calculation of enzyme activity defined by unit per milligram of the NDPK enzyme (U/mg), as described in the following calculation:

Calculation method:

$$U/mg = \frac{\Delta A_{\text{max}}}{\epsilon * d} * \frac{V_{\text{tot}}}{m_{\text{prot}}} * 10^6$$

U: Speed of NADH degradation in the experiment (with 200 ng of NME protein) ( $\mu\text{mol}/\text{min}$ )

U/mg: Speed of NADH degradation per milligram of NME protein ( $\mu\text{mol}/\text{min}$ )

$\Delta A_{\text{max}}$ : Maximal speed of absorbance decrease per minute ( $\text{min}^{-1}$ )

$\epsilon$ : NADH molar extinction coefficient at 340 nm ( $6290 \text{ M}^{-1}\text{cm}^{-1}$ )

d : optical path length (cm)

$V_{\text{tot}}$  : Total volume of the reaction (L)

$m_{\text{prot}}$ : Mass of NME protein (mg)

$10^6$  : Correction coefficient, to transform U from mol/min to  $\mu\text{mol}/\text{min}$

### **3.2.3.8 His-Tag removal by thrombin cleavage of NME recombinant proteins**

The removal of the 6 $\times$ His-tag from the purified recombinant NME proteins obtained in section 3.2.1.3 was achieved by incubation with thrombin, an enzyme that is able to cut out a specific amino acid sequence (LVPR\*GS) placed next to the 6 $\times$ His-tag during cloning. His-tag was removed from the NME6-194-His and NME6-186-His recombinant proteins using thrombin sepharose beads according to manufacturers' instruction. In brief, 0.5 mg of purified recombinant proteins were incubated overnight at 4  $^{\circ}\text{C}$  with 7.5  $\mu\text{L}$  of thrombin sepharose beads in the thrombin buffer on the rotator. The sample was centrifuged (2 min, 2 500 g, room temperature) and the supernatant was analyzed by Western blot (section 3.2.3.3) together with the cell lysate from wild type MDA-MB-231T.

### **3.2.3.9 Homo-oligomerization status of NME6 recombinant proteins**

#### **3.2.3.9.1 NME6 oligomerization analysis by crosslinking**

The recombinant protein (section 3.2.1.3) NME6-186-His or NME6-194-His (9.5 µg) was mixed with 0.075 % (v/v) glutaraldehyde in the crosslinking buffer and incubated at 37 °C for 15 min on the thermo-shaker. The reaction products as well as the untreated recombinant proteins (control) were analyzed by SDS-PAGE, transferred to a 0.2 µm nitrocellulose membrane and stained with naphthol blue (section 3.2.3.3).

#### **3.2.3.9.2 NME6 oligomerization analysis by size-exclusion chromatography**

Size-exclusion chromatography was performed at Biocentar d.o.o., Zagreb, Croatia on Akta avant 25 chromatography system (GE Healthcare). The recombinant proteins (NME6-186-His and NME6-194-His) were gel filtrated on Superdex 200 Increase 10/300 GL (GE Healthcare). The column was equilibrated with a mobile phase flow (10 mM NaH<sub>2</sub>PO<sub>4</sub>, 140 mM NaCl, pH 7.4) of one column volume (24 mL) followed by the injection of the sample. The sample was eluted with 1.5 volume of the column (36 mL). Fractions of 1 mL were taken at 2 min intervals. The chromatographic column was calibrated with the following Bio-Rad Gel filtration standards: thyroglobulin (670 kDa), γ-globulin (158 kDa), ovalbumin (44 kDa), myoglobin (17 kDa), and vitamin B12 (1.35 kDa).

#### **3.2.3.10 Multiple reaction monitoring mass spectrometry (MRM-MS)**

The liquid chromatography-mass spectrometry (LC-MS) analysis was performed at Biocentar d.o.o., Zagreb, Croatia on 1290 Infinity LC System (Agilent Technologies, USA) coupled with 6460 Triple Quad Mass Spectrometer (Agilent Technologies, USA). *In silico* digestion of NME6-194 and NME6-186 sequences by trypsin was performed using Skyline software (v. 3.7.0.10940.). The difference in isoforms was obtained within the following sequences: MTQNLGSEMASILR for the NME6-194 isoform and MASILR for the NME6-186 isoform. Total cell lysates from HeLa and MDA-MB-231T cells were digested with trypsin (γ=1 mg/mL) for 18 h at 37 °C and 600 rpm (Digital Shaking drybath, Thermo Scientific, USA). Acquity UPLC BEH separation column C18 1.7 µm, 2.1×150 mm (Waters, USA) was used for chromatographic peptide separation. Mobile phase A (0.1 % (v/v) aqueous formic acid solution) and mobile phase B (acetonitrile) were both degassed in an ultrasonic bath. The separation was performed at 40 °C column temperature, 15 µL of sample was injected with a gradient flow of 0.3 mL/min starting at 95 % A and decreasing to 60 % A over 16 min. Mass

spectra were recorded in a positive resolution mode with the capillary voltage set at 3.5 kV, at a gas temperature of 300 °C, and at a gas pressure of 40 psi. All measurements were performed in duplicate.

### **3.2.3.11 Isolation and purification of mitochondria**

MDA-MB-231T cells were grown to 80 % confluency, and  $350 \times 10^6$  cells were used for the experiment. The whole procedure of mitochondrial isolation and purification was performed on ice as described earlier [94,131] with minor modifications. Cells were scrapped in PBS and centrifuged 5 min at 750 g, 4 °C. The cells were collected, resuspended and combined in 10 mL of Buffer A. Cells were homogenized by 10 passages through a 25G needle. Homogenate (H) was centrifuged 5 min at 2 000 g, 4 °C. The supernatant (S1) was kept on ice and pellet, resuspended again in 10 mL Buffer A, underwent 6 additional passages through a 25G needle and centrifugation (5 min, 2 000 g, 4 °C). Pellet enriched in nuclei (P) was resuspended in 5 mL of Buffer A and kept on ice until analysis. The supernatant was combined with S1 and centrifuged 10 min at 13 000 g, 4 °C. The resulting supernatant enriched in cytosol (C) was kept for analysis. The pellet was resuspended in 1.5 mL of Buffer B and centrifuged 5 min at 500 g, 4 °C. The supernatant was transferred in a clean tube and centrifuged 10 min at 10 000 g, 4 °C. The resulting pellet enriched in crude-mitochondria (MC) was resuspended in 1 mL of Buffer B and purified on 25 % Percoll gradient (section 3.2.3.11.1). Two bands were collected from bottom to top (MP, percoll-pure mitochondria; CON, contaminants) and washed in 10 mL of Buffer B (10 min, 7 000 g, 4 °C). The resulting pellets were resuspended in 0.5 mL Buffer B. Protein concentration was measured using Bradford method (section 3.2.3.2.2) and 2 µg from each fraction was analyzed by Western blot (section 3.2.3.3).

#### **3.2.3.11.1 Percoll gradient purification**

A 25 % Percoll gradient was created in an ultracentrifuge tube by mixing 2 mL of Percoll with 5 mL of Buffer B. The solution was cooled down and 1 mL of crude-mitochondria (MC) sample was gently applied on top of the solution, with great attention to avoid mixing. The tube was ultracentrifuged for 35 min at 100 000 g, 4 °C, using the rotor 60Ti fixed angle. The tube was handled gently to avoid mixing. The tube was kept on ice until collection of the separate bands.

### **3.2.3.12 Mitochondrial subfractionation**

The whole procedure of mitochondrial subfractionation was performed on ice using crude-mitochondria (MC) fraction obtained from MDA-MB-231T cells as described above (section

3.2.3.11), and swelling-shrinking procedure as described earlier [132] with minor modification. After washing in Buffer B (10 000 g, 10 min), MC pellet was resuspended in 200  $\mu$ L of swelling buffer SW1 and incubated 20 min on the rotator. Then 200  $\mu$ L of shrinking buffer SW2 was added and the suspension was incubated for further 1 h on the rotator. The sample was gently sonicated ( $2 \times 15$  s) in a water bath sonicator and centrifuged at 12 000 g for 10 min, 4 °C. The resulting low-speed supernatant (MCss\_ls) was kept on ice while the mitoplast-containing low-speed pellet (MCss\_lp) was washed two times in Buffer A (10 min, 12 000 g) before being resuspended in 400  $\mu$ L of Buffer SW1 and sonicated using the Sonopuls ultrasonic homogenizer with a metal tip,  $3 \times 15$  s, with 60 s cooling interval. Both MCss\_ls and MCss\_lp were centrifuged 1 h at 160 000 g, 4 °C (Beckman ultracentrifuge; 70.1Ti fixed angle rotor). Resulting high-speed pellets (respectively MCss\_ls\_hp and MCss\_lp\_hp) were resuspended in 100  $\mu$ L Buffer B, while resulting high-speed supernatants (respectively MCss\_ls\_hs and MCss\_lp\_hs) were separately concentrated using microconcentrator YM-3 according to manufacturer's instruction. Protein concentration was determined by Bradford method (section 3.2.3.2.2), and 2  $\mu$ g of protein were analyzed by Western blot (3.2.3.3).

### **3.2.3.13 Cell fractionation using a commercial kit**

Cellular fractionation assay was performed using MDA-MB-231T cells and the Cell Fractionation Kit, according to manufacturer's instruction. Crude "Cytosolic", "Mitochondrial" and "Nuclear" enriched fractions were quantified using pierce BCA Kit (section 3.2.3.2.1), and 10  $\mu$ g of proteins from each fraction was analyzed by Western blot (section 3.2.3.3).

### **3.2.4 Confocal microscopy**

Confocal microscopy was performed using Leica TCS SP8 X FLIM confocal microscope equipped with an HC PL APO CS2 63 $\times$ /1.40 oil objective, 405 nm diode laser, argon-gas laser and a supercontinuum excitation laser (Leica Microsystems, Wetzlar, Germany). For confocal imaging of live and fixed cells the excitation wavelengths and detection ranges were as follows: 488 nm and 500–550 nm for EGFP and Alexa488; 644 nm and 655–705 nm for MitoTracker<sup>TM</sup> Deep Red FM; and 458 nm and 470–520 nm for CFP. The hybrid (HyD) detectors were operated in the gated mode in order to suppress parasite reflection from the bottom glass surface of the cell-culture dish. Imaging was performed in a sequential scanning mode.

### **3.2.4.1 Live cell imaging**

MDA-MB-231T cells were seeded in a 4-chamber glass bottom dish and transfected 24 h later with pCFPmito, pNME6-194-GFP or pEGFPN1-NME6-186-GFP using Turbofect transfection reagent (section 3.2.2.5). Forty-eight hours post transfection, cells were washed three times with PBS and stained with DMEMcomp supplemented with 5 nM of MitoTracker™ Deep Red FM for 20 min in incubator. Cells were washed three times in PBS before being cultured in Leibovitz's L-15 medium and immediately imaged using the confocal microscope. The stage-top environmental control system was used for live-cell imaging to maintain the temperature at 37 °C and Leibovitz's L-15 medium was used to support cell growth in the environment without CO<sub>2</sub> equilibration.

### **3.2.4.2 Fluorescent immunocytochemistry**

Cells were seeded in an 8 well chambers slide and transfected 24 h later with pCFPmito (section 3.2.2.5). Twenty-four hours post transfection the cells were washed two times with ice-cold PBS. Cells were fixed by incubation with formaldehyde 2 % for 10 min at room temperature. The cells were washed three times with PBS, and permeabilization was performed with triton X-100 0.1 % solution for 10 min at room temperature. The cells were washed three times with PBS and blocked for 30 min at room temperature with IF blocking buffer. The cells were incubated with primary NME6 antibody diluted in IF blocking buffer overnight at 4 °C. The next day cells were washed three times with PBS and incubated with Alexa-Fluor488-anti-rabbit secondary antibody diluted in IF blocking buffer for 45 min at room temperature in obscurity. After washing in PBS, the mounting medium was applied, the coverslip was mounted and sealed and the slide was analyzed by confocal microscopy.

### **3.2.5 Cellular functions**

To assess the potential influence of NME6 overexpression or downregulation on cellular functions, apoptosis, cell cycle and cellular respiration assays were performed using MDA-MB-231T and RKO cells, upon transient overexpression or silencing, and using MDA-MB-231T clones overexpressing NME6-186-FLAG and NME6-194-FLAG proteins.

#### **3.2.5.1 Apoptosis**

Apoptosis experiments were carried out using RKO cells, due to its p53 wild type status. Cells were either transiently transfected to overexpress NME6-186-FLAG or NME6-194-FLAG

(section 3.2.2.5) and analyzed 48 h post transfection, or silenced for NME6 (section 3.2.2.6) and analyzed 72 h post transfection. Eighteen hours prior to the collection of cells, the positive control for apoptosis was supplemented with Camptothecin (2  $\mu$ M final) directly in the DMEMcomp, without changing the medium, in order to induce apoptosis. On the day of the experiment, cells were collected as described in section 3.2.2.2.2, paying attention to collect both, the attached and the floating cells. The pellet was resuspended in PBS and  $10^5$  cells were stained using the Annexin-V-FLUOS Staining Kit according to the manufacturer's instruction. Analyses were performed using BD FACSCalibur™ Flow Cytometer and the data were analyzed by FlowJo software. Experiments were realized in triplicate.

### **3.2.5.2 Cell cycle**

MDA-MB-231T WT cells, three empty clones (KI-CTRL; Neg 5, 6 and 7), three NME6-186-FLAG KI clones (KI-186; 186-7, 18 and 26) and three NME6-194-FLAG KI clones (KI-194; 194-8, 13 and 17) were seeded in 6-well plates to reach 80 % confluency on the day of the experiment. The cells were either allowed to grow for three days (KI experiment) or were silenced for NME6 expression as described in section 3.2.2.6 and analyzed 72 h after silencing (silencing experiment). On the day of the experiment, cells were collected as described in section 3.2.2.2.2. Pellet was washed in 1 mL PBS, fixed in 70 % ethanol and stored overnight at 4 °C. The next day, cells were resuspended in PBS supplemented with 0.1  $\mu$ g/mL RNase . Cells were stained by adding propidium iodide to a final concentration of 40  $\mu$ g/mL, for 30 min at 37 °C in the dark. Analysis was performed using BD FACSCalibur™ Flow Cytometer and the data were analyzed by FlowJo software. Experiments were realized in triplicate. The data for each related clones were pooled before statistical analysis.

### **3.2.5.3 Cellular respiration**

MDA-MB-321T WT cells, KI clones NME6-186-FLAG and NME6-194-FLAG or NME6-silenced cells (section 3.2.2.6) were used in this experiment. Cells were collected (section 3.2.2.2.2), resuspended at  $100 \times 10^6$  cells/mL in DMEMcomp and kept on ice. The thermostatically controlled Clark electrode oxygraph was prewarmed at 37 °C. A 50  $\mu$ L aliquot ( $5 \times 10^6$  cells) was added in the electrode chamber containing 450  $\mu$ L KET buffer supplemented with inorganic phosphate (5 mM). Digitonin (50  $\mu$ g/mL) was added and the plasma membrane permeabilization was allowed for 2 min. Oxygen consumption was measured after activation of respiratory complex I by addition of glutamate (5 mM) and malate (2.5 mM), or after activation of complex II by addition of succinate (5 mM) and rotenone (1  $\mu$ M) and labelled as

the LEAK state. After LEAK measurement, ADP was added (0.5 mM) and the oxygen consumption measured was labelled as OXPHOS state. At the end, Cytochrome C was added (10  $\mu$ M) and the oxygen consumption was measured to assess the integrity of mitochondrial membranes. Respiration results are expressed as nmol O<sub>2</sub> consumed per minute and per  $5 \times 10^6$  cells. A ratio OXPHOS/LEAK was calculated to help the interpretation of the results. Experiments were realized in triplicate.

### **3.2.6 Statistical analysis**

Statistical analysis was performed using GraphPad Prism (V8.3.0). Experiments supporting statistical analysis were repeated at least three time. The statistical test used is indicated in the description of each figure supporting statistical analysis. Results' significance is represented by stars according to the standards in molecular biology field, as follow: \*  $p < 0.05$ , \*\*  $p < 0.01$ , \*\*\*  $p < 0.001$ , \*\*\*\*  $p < 0.0001$ .



---

## 4 **RESULTS**

### 4.1 **Preparation**

In this study, we aimed to get a clearer picture of human NME6 protein, regarding the cellular localization, quaternary structure, biochemical properties and cellular functions. For that purpose, a major part of the work was to prepare specific material needed for our investigation. This included the cloning and production of specific plasmids (Table 11), used hereafter to produce monoclonal stable MDA-MB-231T cell lines that exhibit overexpressed (KI) or downregulated (KO) NME6 expression, as well as purified recombinant NME6 proteins.

The KI clones were produced by random integration of either pcDNA3.1-NME6-186-FLAG or pcDNA3.1-NME6-194-FLAG plasmids within the nuclear DNA. The KO clones were produced by CRISPR-Cas9 technique, allowing the targeted integration of a specific sequence within the NME6 gene, thus disrupting it and allowing G418 antibiotic resistance.

Worthy to note, the MDA-MB-231T cell line was used as a major model in the study. Preliminary results showed a similar expression pattern in a wide range of human cell line tested (section 4.2.1). Thus we chose to use MDA-MB-231T, a triple negative breast cancer cell line already extensively used and described as a model system in the NME field [97,133–135].

#### 4.1.1 **Production of NME6-KI stable clones**

The production was performed according to the protocol from section 3.2.2.7.1. Viable clones were validated by Western blot using FLAG (Figure 18) and NME6 antibodies (Figure 19). We were able to produce both NME6-186-FLAG and NME6-194-FLAG KI stable clones that we could divide in two categories based on the exogenous NME6-FLAG expression. The “low” clones expressed about 10 time more NME6-FLAG compared to the endogenous NME6 in WT control cells. The “high” clones expressed about 20 time more NME6-FLAG compared to the endogenous NME6 in WT control cells (Figure 19). Note that endogenous NME6 expression is strongly downregulated in NME6-FLAG KI clones, suggesting a possible negative feedback loop inducing repression of the endogenous NME6 gene expression. The production was successful and led to a dozen of usable clones for each isoform of NME6. Clones didn't show morphological differences compared to WT control cells.

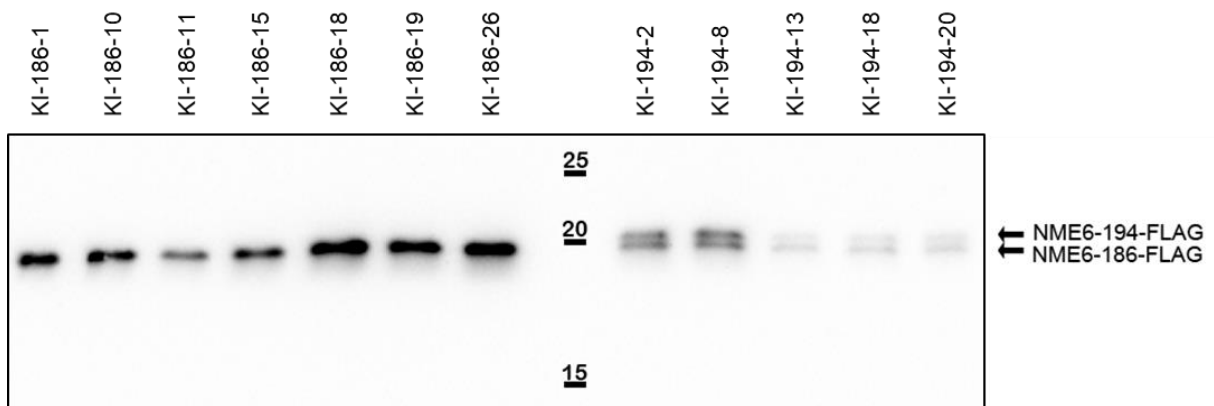


*Figure 18 : Validation of selected stable clone overexpressing NME6-FLAG. Western blot analysis of MDA-MB-231T KI clones overexpressing NME6-186-FLAG (KI-186) or NME6-194-FLAG (KI-194). Cell lysates were evenly loaded and exogenous NME6-FLAG proteins were revealed using anti-FLAG antibody.*

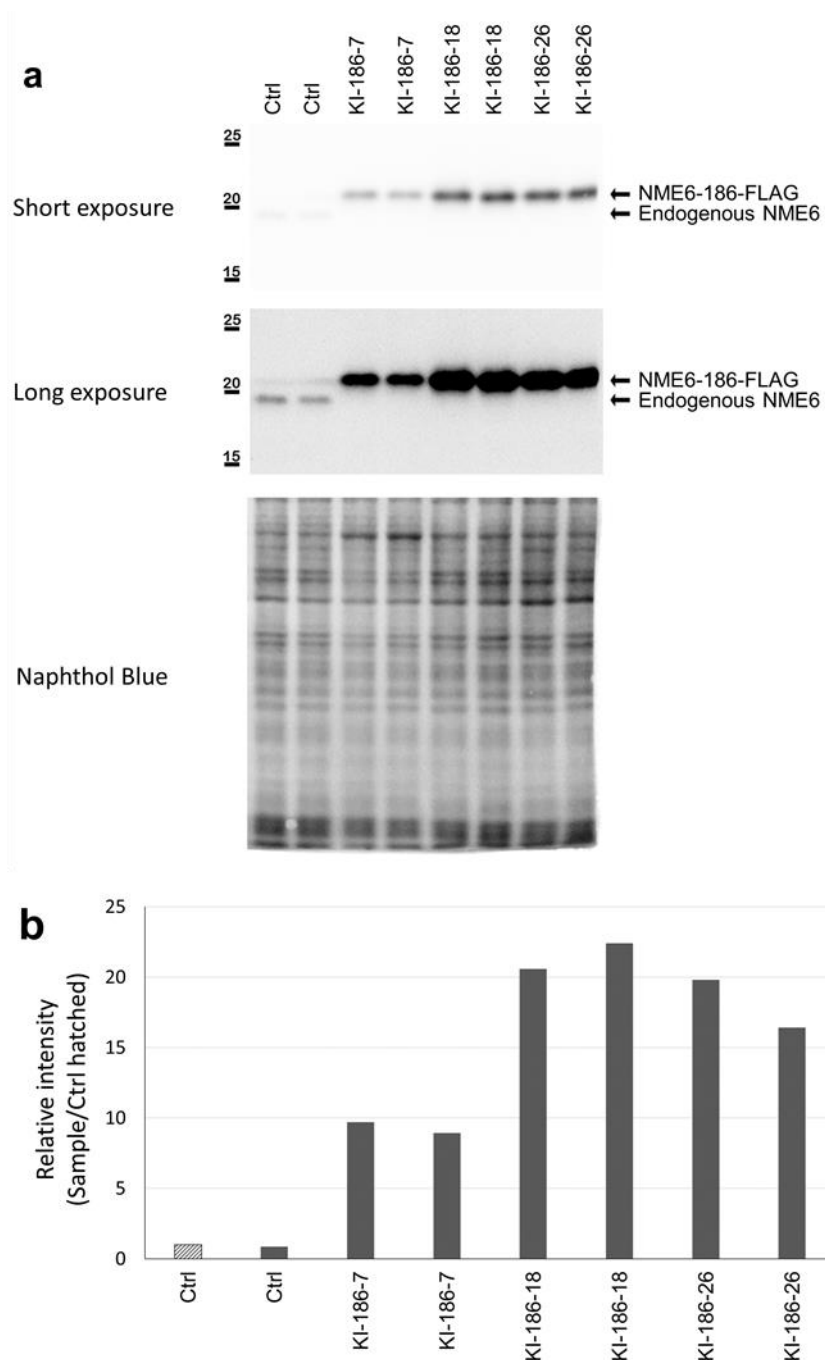


*Figure 19 : KI clones express a high amount of exogenous NME6-186-FLAG. a* Ten micrograms of cell lysate from MDA-MB-231T (Ctrl) and stable clones overexpressing NME6-186-FLAG (KI-186-7, KI-186-18, KI-186-26) were analyzed by Western blot, using anti-NME6 antibody. *b* Quantifications of endogenous NME6 (Ctrl) or exogenous NME6-186-FLAG (KIs) by densitometry were normalized to naphthol blue. Band intensities are displayed as a ratio of the hatched Ctrl sample.

#### 4.1.2 Production of NME6-KO stable clones

The production of NME6-KO stable clones was performed two times separately using the protocol described in section 3.2.2.7.2. After selection based on G418 antibiotic resistance, viable clones were controlled by Western blot using NME6 antibody (Figure 20) and by PCR (Figure 22) using specifically designed primers to assess the NME6 gene disruption and the proper left and right integration of the insert, as described in the scheme (Figure 21). The Western blot analysis of NME6-KO clones revealed no evident downregulation of endogenous NME6 compared to control (Ctrl), at the protein level (Figure 20). Clones were further analyzed by PCR followed by agarose gel separation (Figure 22). Experiment revealed a PCR fragment corresponding to the NME6-KO gene (green), as well as proper left (pink) and right (yellow) integration of the insert within the NME6 gene. Nevertheless, an intense PCR fragment corresponding to wild type NME6 gene (blue) was always observed in NME6-KO clones. The CRISPR-Cas9 experiment led to partial NME6 gene KO, where one allele was successfully disrupted, while the other allele remained intact and able to produce endogenous NME6 protein. Not a single complete KO clone was obtained over the two attempts we made.

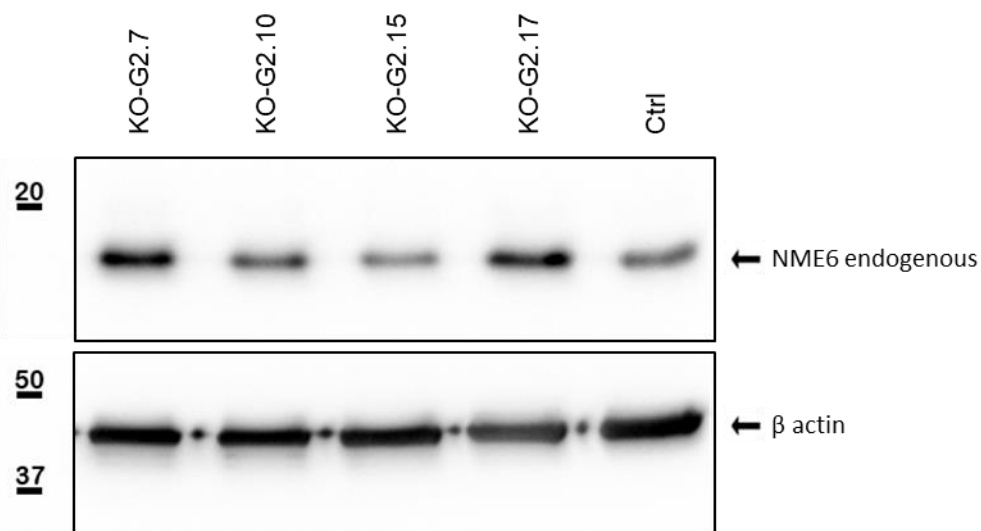


*Figure 20 : Validation of selected NME6-KO clones by Western blot. Western blot analysis of MDA-MB-231T (Ctrl) and four selected NME6-KO clones (KO). Cell lysates were evenly loaded and membrane was stained with anti- $\beta$  actin and anti-NME6 antibodies.*

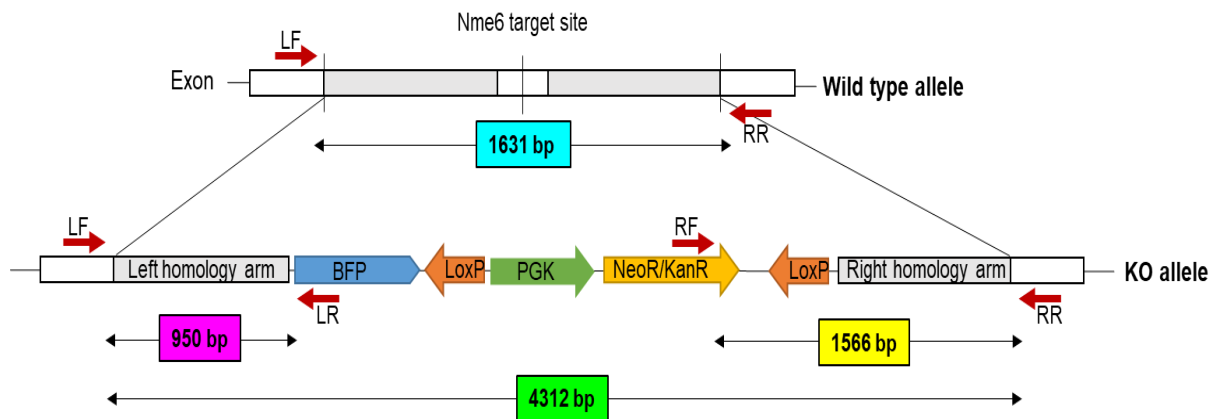


*Figure 21 : Experimental design for the validation of the NME6-KO clones by PCR. NME6 gene was disrupted by targeted insertion of neomycin resistance sequence (NeoR) using CRISPR-Cas9 technique. The correct disruption of NME6 gene was verified by PCR using four specific primers, in pairs (red arrow). LF-RR pair of primers, sitting outside the homology arms, was used to reveal the wild type (1631 bp, blue) and the KO (4312 bp, green) NME6 genes. LF-LR pair, sitting outside the left homology arm and inside the insert, was used to validate the correct left integration (950 bp, pink). RF-RR pair, sitting outside the right homology arm and inside the insert, was used to validate the correct right integration (1566 bp, yellow). PCR fragments were analyzed by gel electrophoresis as displayed in Figure 22.*

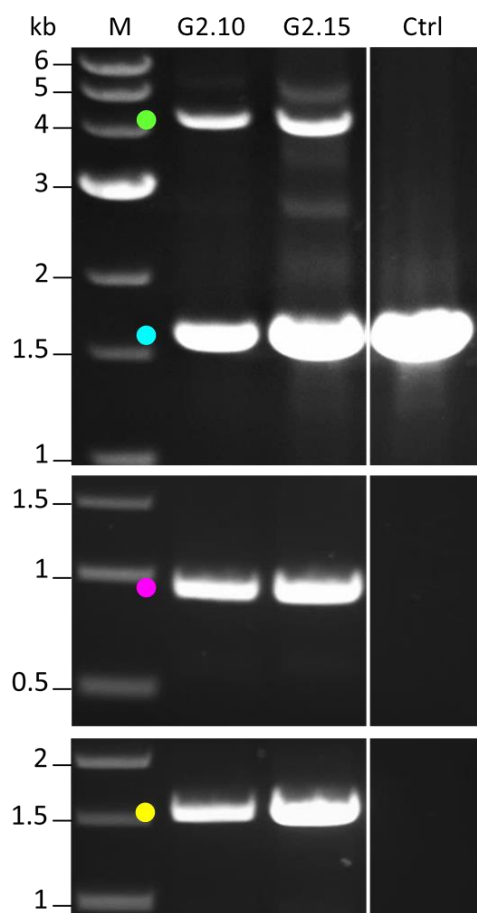
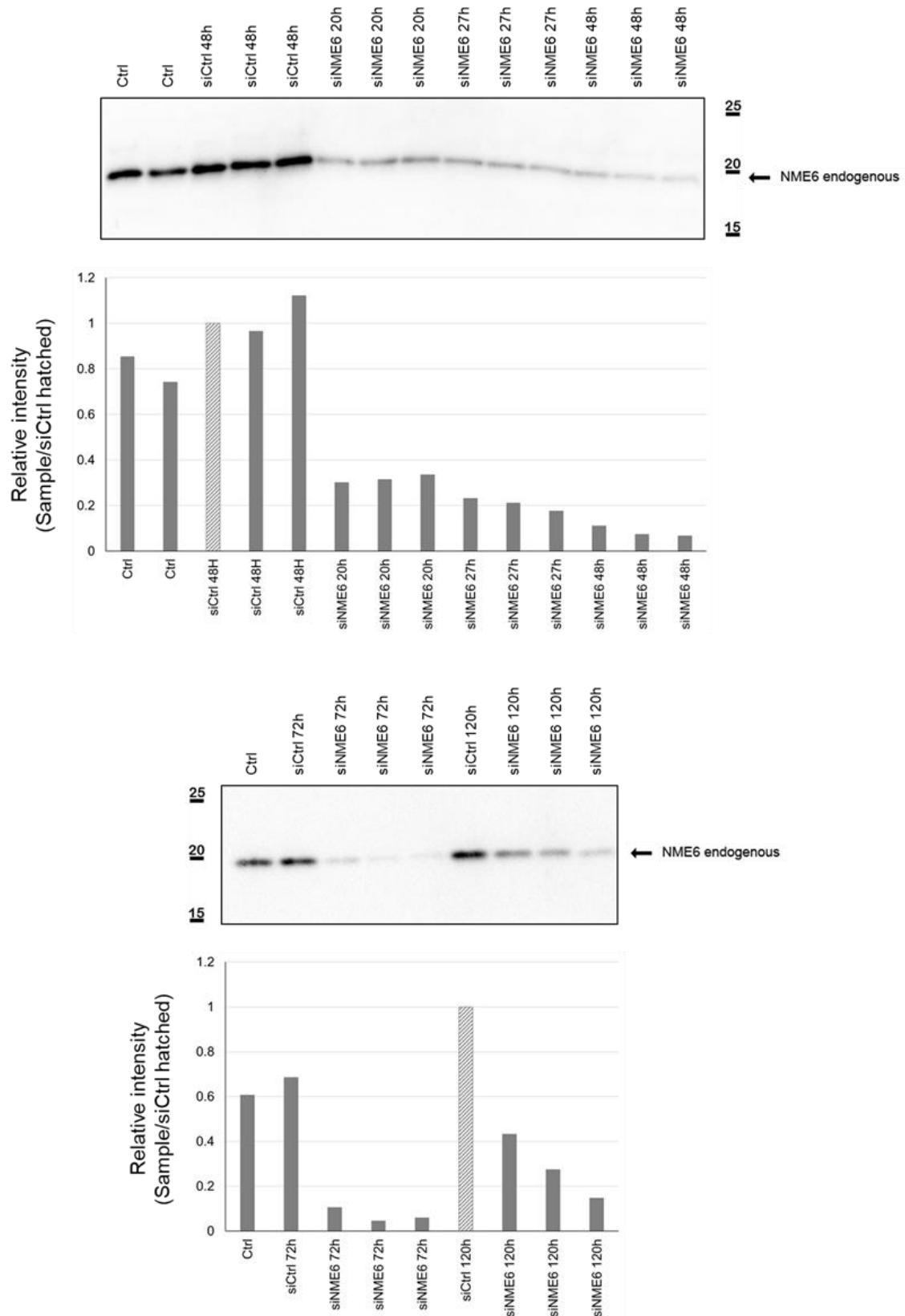


*Figure 22 : Validation of selected NME6-KO clones by PCR. PCR was performed on MDA-MB-231T (Ctrl) and NME6-KO selected clones (G2.10, G2.15) using three pairs of primers presented in Figure 21. PCR fragments were separated by agarose gel electrophoresis. The upper panel used LF and RR primers to amplify both the wild type (1631 bp, blue) and the KO (4312 bp, green) NME6 genes. The middle panel used LF and LR primers to verify the correct left integration of the insert (950 bp, pink). The lower panel used RR and RF primers to verify the correct right integration of the insert (1566 bp, yellow).*

#### **4.1.3 NME6 silencing**

Since we were unable to produce complete NME6-KO clones, we decided to employ silencing methods to suppress the expression of endogenous NME6 (section 3.2.2.6). Silenced cells were collected at different time-points after transfection, and cell lysates were analyzed by Western blot using anti-NME6 antibody (Figure 23). Early testing revealed that NME6 silencing was efficient from 20 h post transfection, indicating a regulation of NME6 protein homeostasis within this timeframe. Silencing was efficient for a period of 120 h post transfection, when the NME6 protein signal started to raise up again (Figure 23). The silencing effectively induced a

strong decrease of the endogenous NME6 abundance of about 70 %, 20 h post transfection to 90 %, 72 h post transfection.



- Figure 23 description is on the next page -

---

*Figure 23 : Silencing of endogenous NME6 protein. Western blot analysis of MDA-MB-231T (Ctrl) cell lysates, silenced with scramble silencers (siCtrl) or silenced with NME6 silencers (siNME6), collected at different time points after transfection. Samples were evenly loaded and the membrane was stained with anti-NME6 antibody. Quantification of endogenous NME6 was performed using densitometry, and normalized to naphthol blue. Band intensities are displayed as a ratio of the hatched siCtrl sample.*

#### **4.1.4 Production of recombinant proteins**

The production of recombinant proteins was essential to study the physical and enzymatic properties of both NME6 isoforms. NME6-186-His and NME6-194-His human proteins were produced in bacteria and purified according to protocol from section 3.2.1.3. Every step of purification was analyzed by SDS-PAGE (Figure 24 and Figure 25), including the filtered sample before purification (Filtrate), the unbound proteins flowing through the column (FT), the column washing steps (W), the column elution steps (E) and the final purified and concentrated recombinant proteins (Conc). Images revealed successful recovery of both NME6 isoforms (Conc), even though some parasite, background proteins were always co-eluted, especially the two between 75 and 50 kDa. However, their amount was negligible compared to the abundance of the recovered NME6-His proteins. About 5 mg of each protein was produced by applying this protocol. The three recombinant proteins were analyzed on SDS-PAGE (Figure 26), and showed a very high level of purification at non-saturating concentration (0.5  $\mu$ g), with almost no other proteins visible. A visible shift can be observed between NME6-186-His and NME6-194-His migration patterns, due molecular weight differences of the two proteins. Note that in the bacterial system, the production of both His-tagged NME6-186 and NME6-194 lead to a single band, i.e., a single protein, in contrast to the two proteins observed after overexpression of NME6-194-FLAG in human cells (Figure 18).



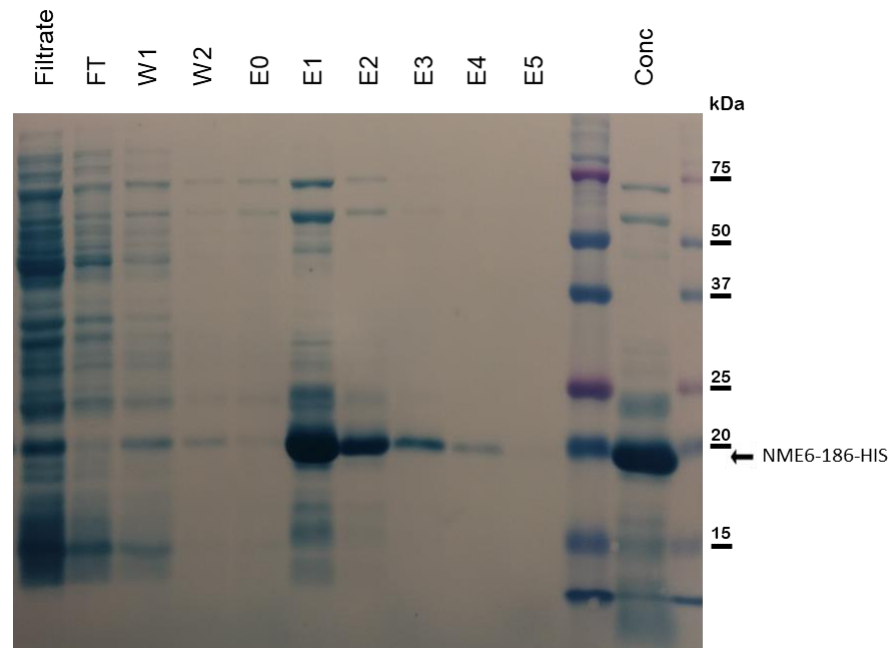
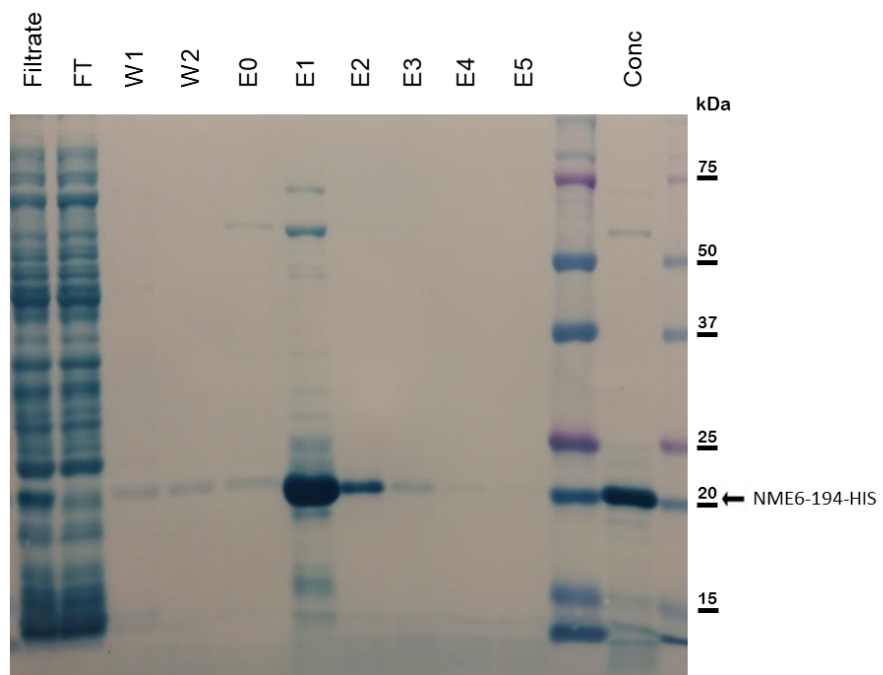


Figure 24 : NME6-186-His recombinant protein production control. The filtered sample before purification (Filtrate), the unbounded proteins flowing through the column (FT), the column washing steps (W), the column elution steps (E) and the final purified and concentrated recombinant proteins (Conc) were analyzed by SDS-PAGE. Proteins were transferred to the membrane and stained with naphthol blue. NME6-186-HIS shows a strong enrichment in the concentrated fraction, below 20 kDa.



- Figure 25 description is on the next page -

Figure 25 : *NME6-194-His recombinant protein production control.* The filtrated sample before purification (Filtrate), the unbounded proteins flowing through the column (FT), the column washing steps (W), the column elution steps (E) and the final purified and concentrated recombinant proteins (Conc) were analyzed by SDS-PAGE. Proteins were transferred to the membrane and stained with naphthol blue. NME6-194-HIS shows a strong enrichment in the concentrated fraction, above 20 kDa.

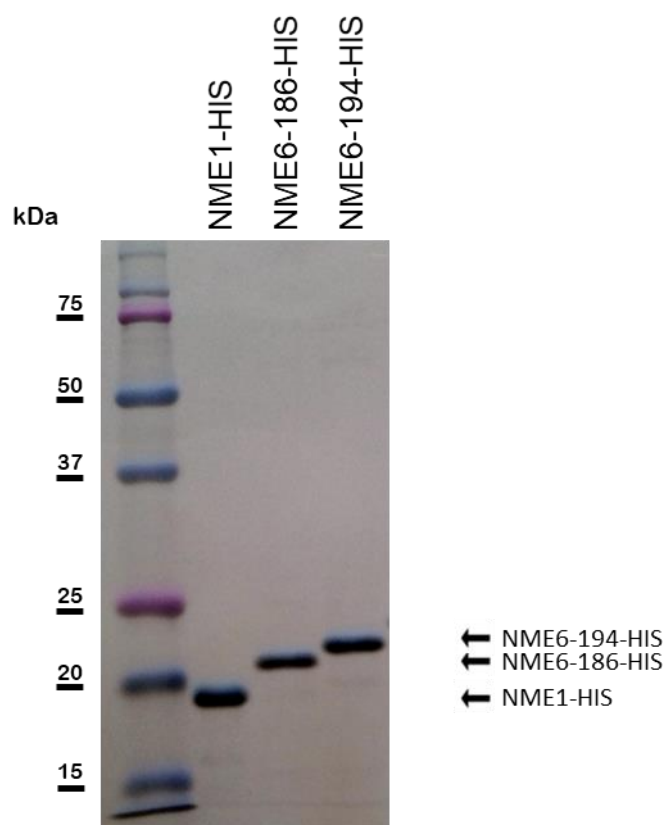


Figure 26 : *Recombinant proteins analysis at non-saturating concentration.* Purified human NME1-His, NME6-186-His and NME6-194-His recombinant proteins were evenly loaded (0.5 $\mu$ g), analyzed by SDS-PAGE, transferred to the membrane and stained with naphthol blue. Proteins display a single band, attesting a high level of purification.

## 4.2 NME6 expression and characterization

We aimed to characterize the expression profile of NME6 in human cell lines, by comparing the protein expression pattern as well as to determine the principal, most abundantly expressed endogenous isoform.

### 4.2.1 NME6 expression in human cell lines

A wide range of cancerous and non-cancerous human cell lines from tissues of different origin (Table 10) were used to determine the expression profile of endogenous NME6 in human. Extracted proteins were analyzed by Western blot using anti-NME6 and anti- $\beta$ -actin (Figure 27). Every cell line exhibited a single band below 20 kDa upon NME6 detection, even though two isoforms have been described in the literature. The expression intensity slightly varied among cell lines, but NME6 signal was always detected. Since all cell lines showed a similar expression pattern, we chose to use MDA-MB-231T, already widely used as a model system in the NME field, as a key model for our further investigations.

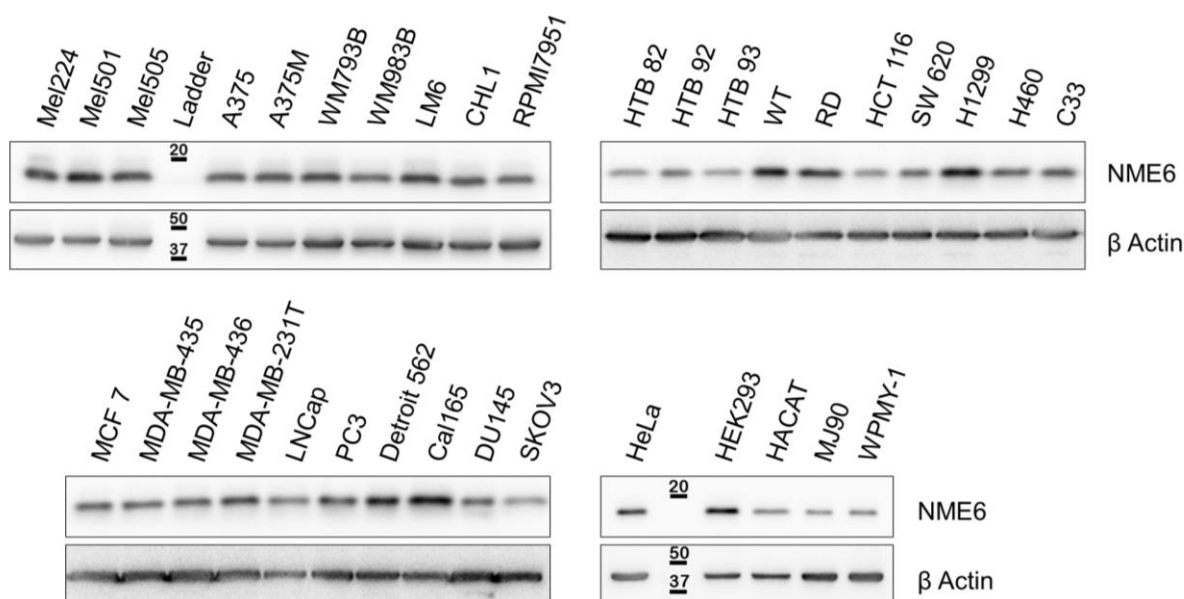
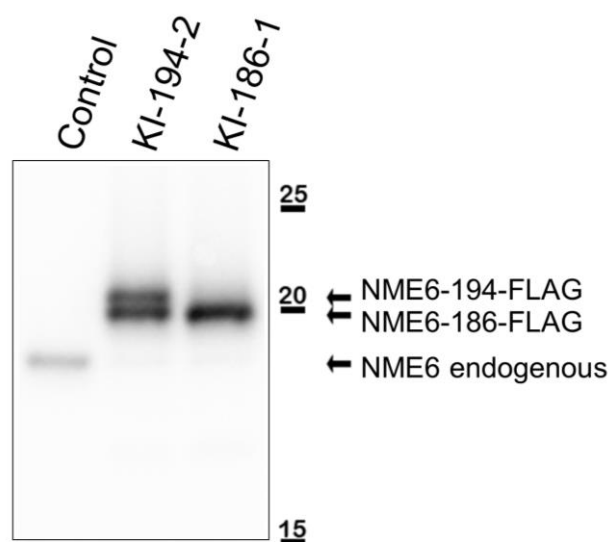


Figure 27 : Endogenous NME6 is ubiquitously expressed as a single protein in cancer and non-cancer human cell lines. The cell lysates were evenly loaded on SDS-PAGE and analyzed by Western blot using NME6 and  $\beta$ -actin antibodies.

#### 4.2.2 Detection of NME6 isoforms by Western blot

A Western blot was conducted using cell lysates from WT MDA-MB-231T (control), KI clones overexpressing NME6-186-FLAG and NME6-194-FLAG (Figure 28), using anti-NME6 antibody. The control displayed a signal for endogenous NME6 way below 20 kDa. The KI of NME6-186-FLAG resulted in a single band at 20 kDa, while the KI of NME6-194-FLAG resulted in two separate bands, corresponding from up to down to NME6-194-FLAG and NME6-186-FLAG. Results showed that the two isoforms could be discriminated by Western blot based on their molecular weight. Interestingly, it can be noticed that when the cells were forced to produce the NME6-194-FLAG protein, they also produced the NME6-186-FLAG protein. As mentioned earlier (section 4.1.1), the expression of the exogenous FLAG-tagged protein somehow leads to a decrease of the endogenous NME6 at the protein level.



*Figure 28 : Discrimination of NME6-186 and NME6-194 by Western blot. Cell lysates from WT MDA-MB-231T (control) and stable clones overexpressing NME6-194-FLAG (KI-194-2) and NME6-186-FLAG (KI-186-1) proteins were evenly loaded and analyzed by Western blot, using anti-NME6 antibody. Overexpression of the exogenous FLAG-tagged NME6 led to downregulation of endogenous NME6 at the protein level.*

#### 4.2.3 NME6-186 isoform predominates in human cells

To confirm which isoform corresponds to the endogenous NME6, we conducted a Western blot analysis of recombinant NME6-His proteins partially digested with thrombin (section 3.2.3.8), together with the cell lysates from WT MDA-MB-231T (control), using anti-NME6 antibody (Figure 29). The aim was to compare the molecular weight of the endogenous and the

recombinant proteins, the latest after removal of the 6×His-tag residues needed for purification, by thrombin digestion. Results showed that the endogenous NME6 and the recombinant NME6-186 migrated similarly, thus displaying the same molecular weight, while a clear shift was observed between the endogenous NME6 and the recombinant NME6-194. Results strongly indicate that NME6-186 is the isoform that is predominantly expressed in human cell lines.

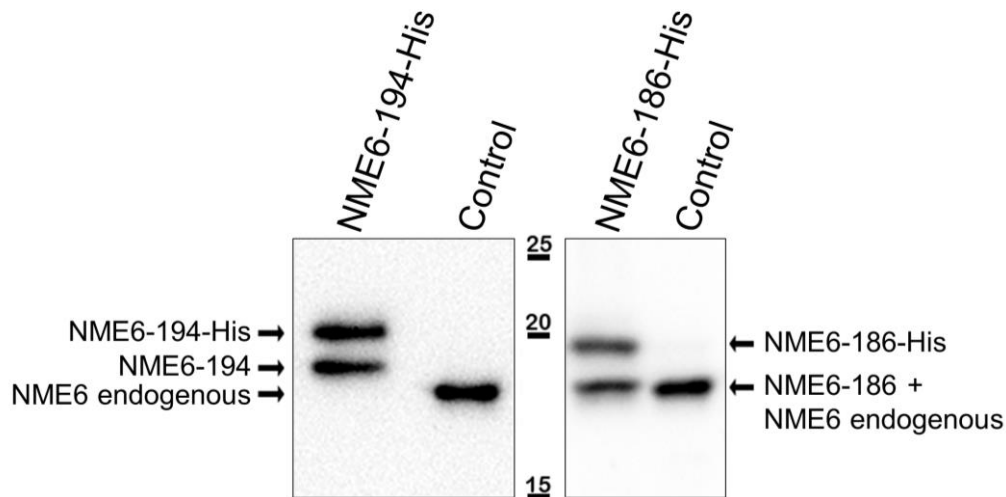


*Figure 29 : Western blot analysis of the recombinant and endogenous NME6 proteins. Human NME6-194-His and NME6-186-His recombinant isoforms were produced in bacteria and purified. The His-tag was partially removed using thrombin and proteins were analyzed by Western blot along with the whole cell lysate from WT MDA-MB-231T (control), using anti-NME6 antibody. The endogenous NME6 and recombinant NME6-186 display similar migration properties.*

#### **4.2.4 Detection of endogenous NME6 isoforms by mass spectrometry**

To investigate the presence of endogenous NME6 isoforms in cell lines with maximum sensitivity, mass spectrometry experiments were designed and conducted on MDA-MB-231T and HeLa cell lysates. A multiple reaction monitoring (section 3.2.3.10) approach allowed the separated detection of endogenous NME6-186 and NME6-194 (Figure 30). Results showed that both isoforms were expressed at a protein level in cell lines analyzed, even though NME6-194 escaped the immunoblotting detection (Figure 27).

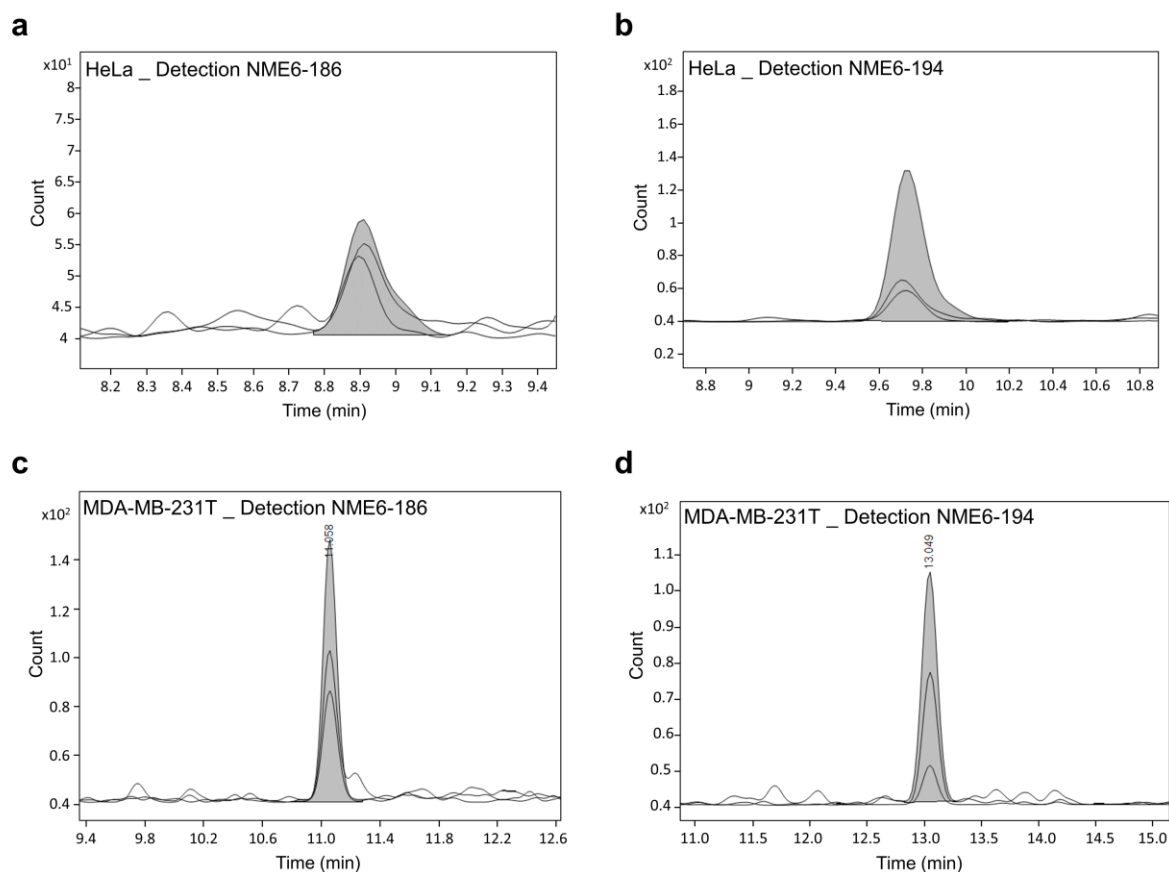


*Figure 30 : Mass spectrometry analysis reveals the presence of both endogenous NME6-186 and NME6-194 isoforms in human cell lines at a protein level. Mass spectrometry analysis of HeLa and MDA-MB-231T cell lysates was designed to detect separately a, c NME6-186 and b, d NME6-194 endogenous isoforms. Experiments were performed in duplicate (n=2). Both NME6-186 and NME6-194 isoforms were detected, without information about their relative abundance.*

### 4.3 NME6 subcellular localization

To begin with the fine description of NME6 protein, we aimed to assign a precise cellular localization of endogenous and exogenous NME6 proteins. This was achieved by both immunofluorescent labeling or live cell imaging followed by confocal microscopy, and by different techniques of cellular fractionation followed by Western blot.

#### 4.3.1 Immunofluorescent labeling of endogenous NME6

To visualize endogenous NME6 subcellular localization the cells were transfected with pCFPmito to produce a cyan fluorescent protein targeted to mitochondria labelling the mitochondria in cyan. Cells were fixed, permeabilized and incubated with anti-NME6 antibodies. Confocal images revealed a smooth overlapping signal between NME6 and CFPmito fluorescence, indicating a mitochondrial localization of endogenous NME6 protein (Figure 31).

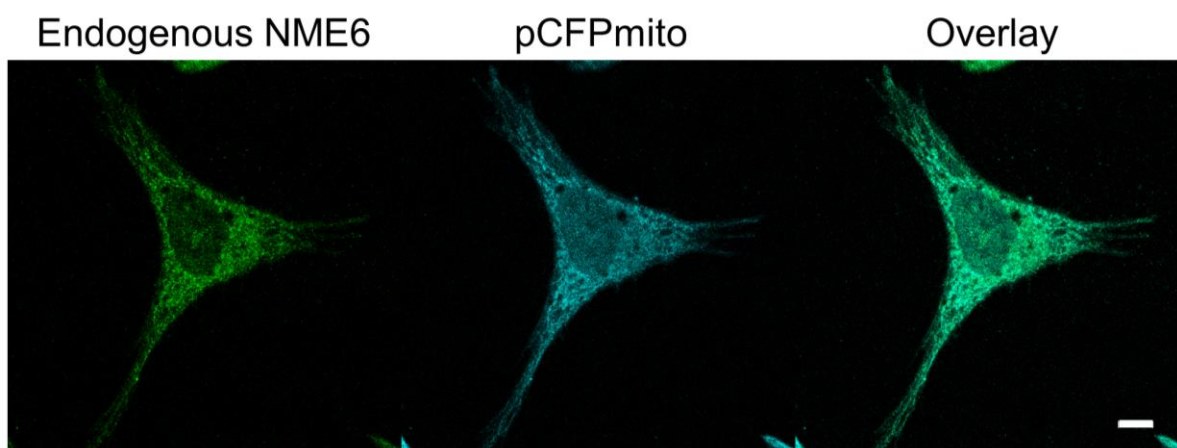


*Figure 31 : Endogenous NME6 colocalize with mitochondria in fixed cells. HeLa cells were transfected with pCFPmito (cyan), fixed and stained with NME6 antibody (green), before acquisition by confocal microscopy (scale bar: 10  $\mu$ m).*

#### 4.3.2 Live cell imaging of exogenous GFP-tagged NME6 isoforms

Visualization of exogenous NME6 in live cells was performed by transfection of MDA-MB-231T cells to express NME6-GFP, either the 186 or 194 isoforms. Mitochondria were labelled either by co-transfection with pCFPmito or by MitoTracker staining. Living cells were analyzed under the confocal microscope (Figure 32), revealing an overlapping signal of both exogenous NME6-GFP isoforms with mitotracker or the CFPmito protein, reinforcing the mitochondrial localization of NME6.

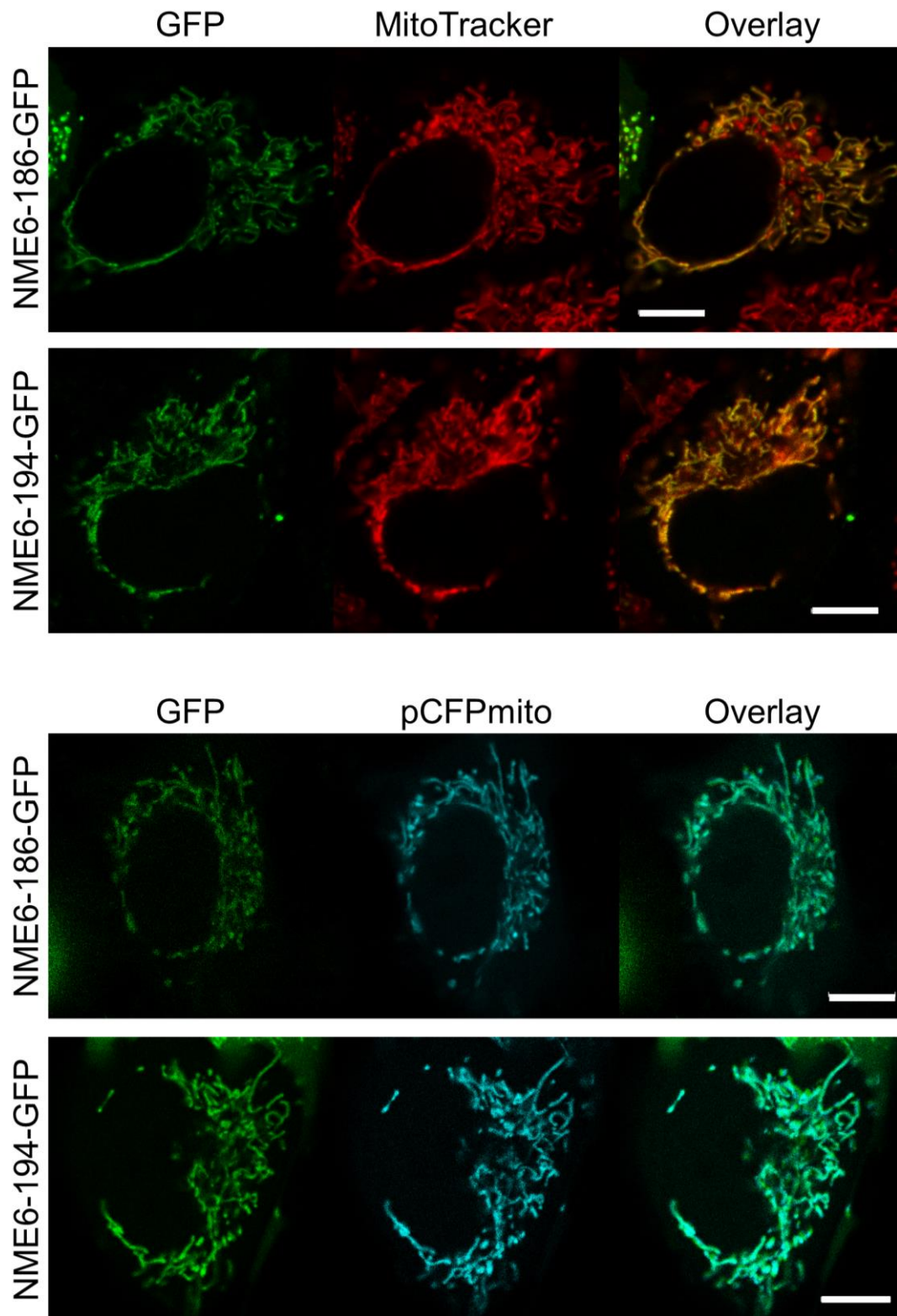
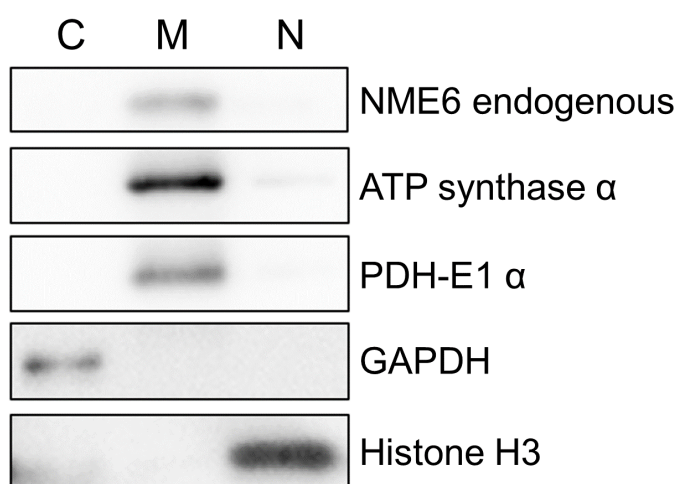


Figure 32 : *The exogenous NME6-GFP colocalizes with mitochondria in living cells.* MDA-MB-231T cells transfected with pEGFPN1-NME6-186-GFP and pNME6-194-GFP were stained with MitoTracker™ (red) or cotransfected with pCFPmito to label mitochondria. Images were acquired 48 h post-transfection by confocal microscopy (scale bar: 10  $\mu$ m).



### 4.3.3 Cellular fractionation

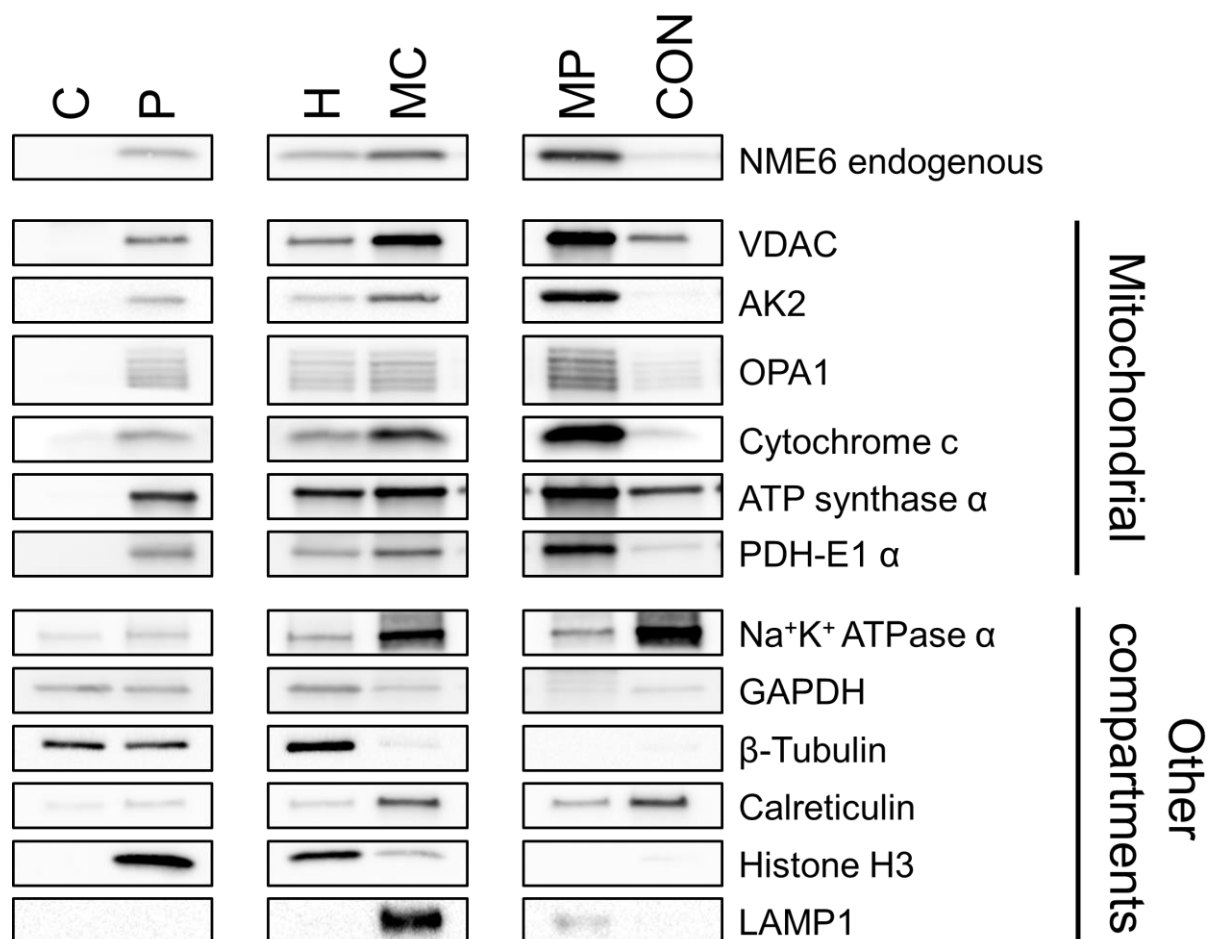
The first attempt to assess NME6 localization by cellular fractionation was realized using a detergent-based commercial kit (ab109719, Abcam) (section 3.2.3.13) (Figure 33). The cytosolic (C), mitochondrial (M) and nuclear-enriched (N) fractions were analyzed by Western blot, using antibodies against NME6 and fractions' markers. Markers efficiently concentrated in their expected fraction: GAPDH with cytosolic-enriched, Histone H3 with nuclear-enriched, ATP synthase  $\alpha$  and PDH-E1  $\alpha$  with mitochondria-enriched. Results clearly showed endogenous NME6 to concentrate in the mitochondrial-enriched fraction, together with mitochondrial markers.



*Figure 33 : Endogenous NME6 localizes in the mitochondria-enriched fraction. MDA-MB-231T cells were fractionated by a commercial, detergent-based method yielding to cytosol-enriched (C), mitochondria-enriched (M) and nuclei-enriched (N) fractions. Ten micrograms of protein were analyzed by Western blot using NME6 and other specific antibodies for different cellular compartments (Mitochondria: ATP synthase  $\alpha$ , PDH-E1  $\alpha$ ; Cytosol: GAPDH; Nucleus: Histone H3).*

To validate the mitochondrial localization of endogenous NME6, another cellular fractionation method based on differential centrifugation was used (section 3.2.3.11) (Figure 34). MDA-MB-231T cell lysate homogenate (H) was divided in fractions enriched with cytosol (C), with nucleus (P), or with crude mitochondria (MC). The latest fraction was further purified on Percoll gradient to obtain pure mitochondria-fraction (MP) and contaminants (CON). Western blot was performed using antibodies against NME6, against mitochondrial proteins or protein markers of other compartments.

The P fraction was the least resolved, with proteins markers from every compartment detected there. Histone H3 (nucleus) was strongly enriched only in this fraction, making it a nuclear-rich fraction. GAPDH (cytosol) and  $\beta$ -tubulin (cytoskeleton) were both enriched in the C fraction, making it the cytosol-rich fraction. Interestingly, membrane-associated proteins  $\text{Na}^+\text{K}^+\text{ATPase}$  (plasma membrane), Calreticulin (endoplasmic reticulum) and LAMP1 (lysosome/endosome membranes) were enriched in the MC fraction, together with mitochondrial proteins. Those contaminants were separated by Percoll purification, and eventually got concentrated in the contaminant fraction CON, leaving the MP fraction highly enriched with mitochondrial proteins and almost free of contaminants from other compartments. Results clearly revealed an enrichment of endogenous NME6 within the MC fraction and further within the MP fraction, together with mitochondrial protein markers, obviously showing mitochondrial localization of endogenous NME6 protein.



- Figure 34 description is on the next page -

---

*Figure 34 : Endogenous NME6 is enriched in Percoll-purified mitochondria. MDA-MB-231T cell fractionation was performed by differential centrifugation of cell homogenate (H) followed by a purification of crude mitochondria (MC) on Percoll gradient (C: cytosol, P: nuclei enriched pellet, MP: Percoll-purified mitochondria, CON: major contaminating band recovered after Percoll gradient). Fractions were evenly loaded on SDS-PAGE and analyzed by Western blot using antibodies against mitochondrial protein markers, markers for other compartments and NME6.*

#### **4.3.4 Mitochondrial sub-fractionation**

Sub-fractionation experiments refined the NME6 localization within mitochondria (section 3.2.3.12). The swelling/shrinking procedure was used to separate the different mitochondrial sub-compartments which were analyzed by Western blot. As described in Figure 35, the swelling-shrinking procedure was applied to break out the MOM and release the IMS content in solution. Low speed centrifugation separated MC<sub>ss</sub>-l<sub>s</sub> supernatant containing IMS and MOM proteins from MC<sub>ss</sub>-l<sub>p</sub> pellet containing the mitoplast, i.e. intact MIM surrounding the matrix space. Both fractions were further ultracentrifuged to separate soluble components from the membrane-bound components. Theoretically, MC<sub>ss</sub>-l<sub>s</sub>-h<sub>s</sub> is enriched with IMS proteins, MC<sub>ss</sub>-l<sub>s</sub>-h<sub>p</sub> is enriched with MOM proteins, MC<sub>ss</sub>-l<sub>p</sub>-h<sub>s</sub> is enriched with matrix proteins and MC<sub>ss</sub>-l<sub>p</sub>-h<sub>p</sub> is enriched with MIM proteins, even though, in practice, the separation is not 100% efficient.

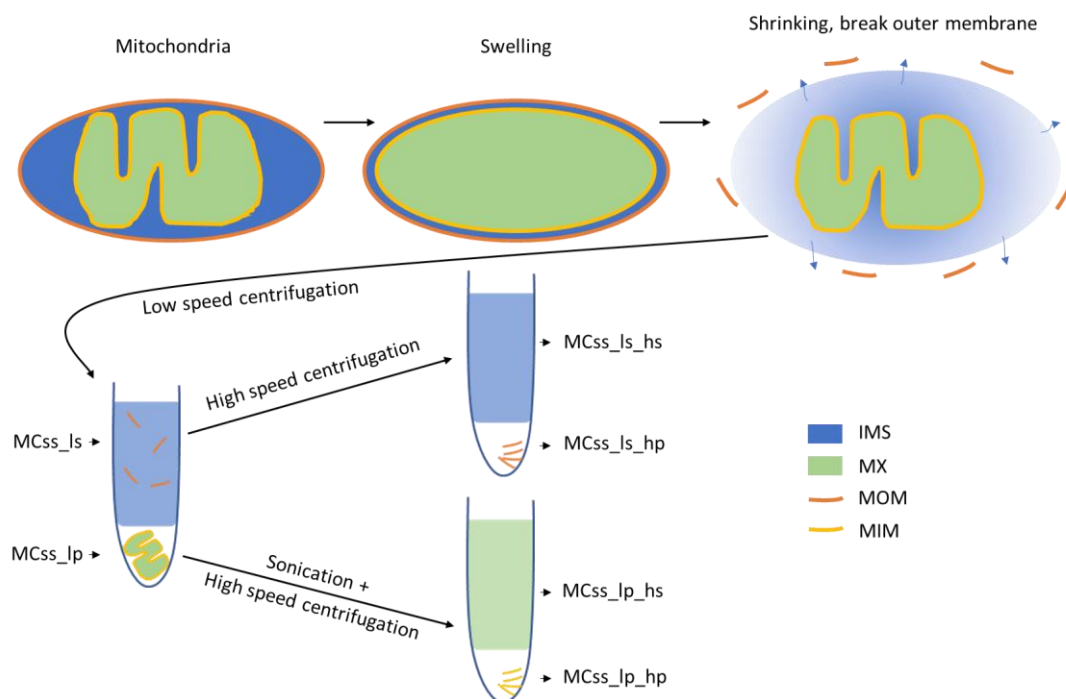


*Figure 35 : Theoretical mitochondrial sub-fractionation by the swelling/shrinking procedure.*

Isolated intact mitochondria were resuspended in a swelling buffer to induce the inflation of the mitoplast (i.e. the intact MIM surrounding the matrix). Mitochondria were resuspended in the shrinking buffer that induce a brutal contraction of the mitoplast, breaking simultaneously the MOM and releasing the IMS in solution. Sample was centrifuged at low speed to separate IMS and solubilized MOM proteins (MCss\_ls) from the mitoplast (MCss\_lp). Each fraction was further centrifuged at high speed to separate the soluble proteins (hs) from the membrane bound proteins (hp).

Each fraction was evenly loaded and analyzed by Western blot, using antibodies against NME6 and protein markers from different mitochondrial compartments (Figure 36). After low-speed centrifugation, the soluble IMS marker AK2 was highly enriched in MCss-ls, indicating a successful breakage of the MOM and release of IMS in solution. PDH-E1  $\alpha$  and ATP synthase  $\alpha$ , two matrix facing proteins peripherally bound to MIM, were highly enriched in MCss-lp, indicating that the MIM was still intact and surrounding the matrix space. Cytochrome C, which is slightly bound to the MIM but also soluble in the IMS, was partitioned between MCss-lp and MCss-ls. The MIM marker OPA1 was expectedly enriched in the MCss-lp fraction. Interestingly, the MOM marker VDAC was enriched in MCss-lp fraction, probably due to MIM-MOM contact sites that forced its retention in the pellet together with the mitoplast.

Results showed an enrichment of the endogenous NME6 in the MCss-lp fraction compared to MCss-ls, indicating a tight link with the mitoplast and an absence of the protein as soluble in

the IMS compartment, contrary to AK2. After ultra-centrifugation of MCss-lp fraction, NME6 was more concentrated in the supernatant (MCss-ls-hs), in a similar pattern as PDH-E1  $\alpha$ , and in a lesser extent ATP synthase  $\alpha$ , two proteins facing the mitochondrial matrix, slightly bound to the MIM. Worthy to note, the NME6 distribution pattern was completely different from the MIM transmembrane protein OPA1, and the MOM transmembrane protein VDAC, both showing an enrichment in the MCss-lp-hp fraction.

Altogether, the NME6 distribution over the fractions resemble the PDH-E1  $\alpha$  and ATP synthase  $\alpha$  distribution, strongly suggesting that NME6 is a matrix facing protein, potentially peripherally bound to the MIM.

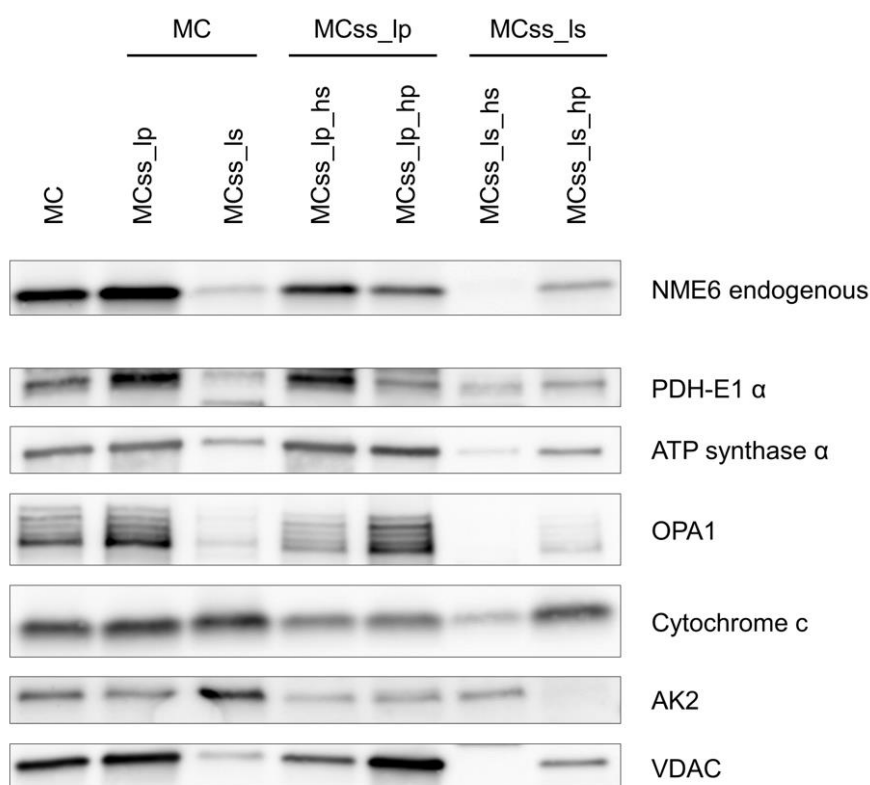


*Figure 36 : Sub-mitochondrial NME6 distribution is typical for proteins associated with the inner membrane and matrix space. Fractions obtained after the swelling/shrinking procedure were evenly loaded and analyzed by Western blot, using antibodies against NME6 and protein markers from the different mitochondrial compartments. These include: pyruvate dehydrogenase E1 component subunit  $\alpha$  (PDH-E1  $\alpha$ ; matrix), ATP synthase subunit  $\alpha$  (a part of the peripheral F1 subcomplex of the MIM ATP synthase, facing matrix space), optic atrophy 1 (OPA1; transmembrane MIM, facing IMS), cytochrome c (peripherally bound to MIM and soluble in IMS), adenylate kinase 2 (AK2; soluble in IMS) and voltage-dependent anion-selective channel (VDAC; MOM and MIM-MOM contact sites).*

## 4.4 NME6 enzymatic properties

NDPK activity is the key enzymatic property of Group I NME proteins, which rely on the phosphorylation of a specific histidine within the catalytic site. The oligomerization of the protein seems to be a prerequisite for measurable enzymatic activity. Here we aimed to study the enzymatic property of NME6 and the related oligomerization status.

### 4.4.1 NDPK activity

The NDPK activity assay was performed as described in section 3.2.3.7. Recombinant NME6-186-His and NME6-194-His were tested while NME1-His was used as a positive control. A reaction mix deprived of NME proteins was used as a negative control. The decrease of absorbance of NADH at 340 nm, directly proportional to NDPK activity, was measured over time. The positive control, NME1-His showed NDPK activity of 155 U/mg, while neither the negative control nor any of the NME6-His isoforms displayed measurable enzymatic activity (Figure 37).

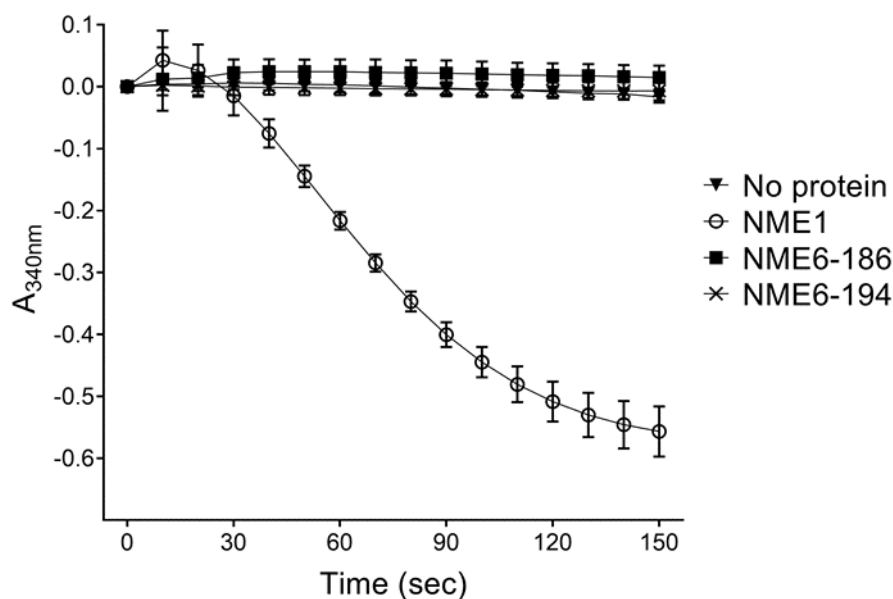


Figure 37 : Recombinant NME6 proteins lack NDPK activity. Purified NME1-His (positive control), NME6-186-His and NME6-194-His recombinant proteins were subjected to enzymatic activity assay where the decrease of NADH absorbance at 340 nm over time is directly proportional to NDPK activity ( $n=6$ ).

#### **4.4.2 Histidine phosphorylation status of endogenous NME6**

While recombinant NME6 isoforms showed no NDPK activity, we attempted to reveal the endogenous NME6 enzymatic property by studying its histidine phosphorylation status (section 3.2.3.4). A Western blot was performed in pHis preserving and non-preserving conditions, using highly specific antibodies against phosphorylated histidine in two conformations (1-pHis and 3-pHis), against NME1 as a positive control, and against NME6 (Figure 38).

pHis detection revealed a single band in the preserving conditions, while no band was observed in the non-preserving condition. NME1 detection revealed two bands under preserving condition, and a single band under non-preserving condition. It is to note that in preserving condition, the higher NME1 band completely superimpose with the pHis signal (turquoise overlay), thus corresponding to histidine-phosphorylated NME1 (pHis-NME1), the positive control. The histidine phosphorylation induced a visible migration shift between NME1 and pHis-NME1. NME6 detection displayed a single band both in preserving and non-preserving conditions. The protein appeared just in between NME1 and pHis-NME1 on the overlay, and did not superimpose with the pHis signal. Contrary to NME1, the endogenous NME6 lacks phosphorylation of any histidine residue, thus including the active site histidine mandatory for NDPK activity.

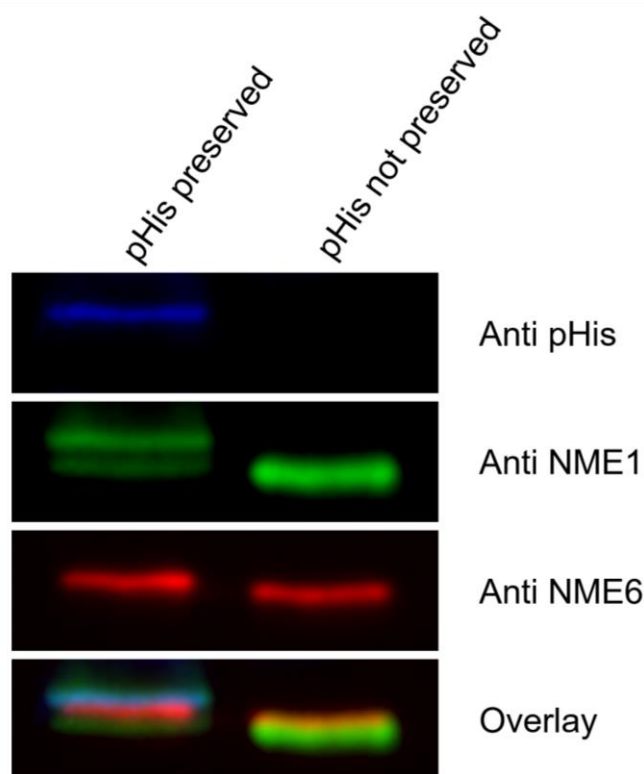
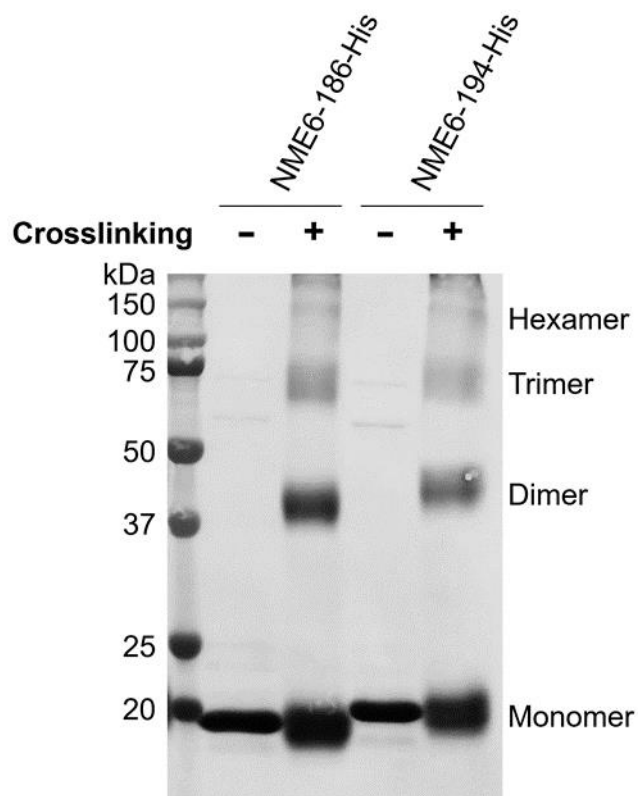


Figure 38 : Endogenous NME6 lacks histidine phosphorylation. MDA-MB-231T cell lysate was immunoblotted with and without preserving histidine phosphorylation, using anti-NME1, a mix of anti-phospho-histidine 1-pHis and 3-pHis and anti-NME6 antibodies. Note: A single overlapping signal is observed only in preserving conditions between NME1 and pHis (turquoise), corresponding to pHis-NME1 (positive control).

#### 4.4.3 Homo-oligomerization status

The homo-oligomerization of human recombinant NME6-His isoforms was first studied by crosslinking, which force the formation of covalent bounds between close-contact peptides (3.2.3.9.1) (Figure 39). Samples were separated by SDS-PAGE, transferred to membrane and stained with naphthol blue. Results showed a predominant monomeric structure for both NME6-186-His and NME6-194-His isoforms. A probable dimeric structure could also be detected, while higher oligomerization species, including hexamers, were practically negligible.





*Figure 39 : NME6 recombinant proteins remain mostly monomeric under crosslinking conditions. Glutaraldehyde crosslinking with pure recombinant NME6-186-His or NME6-194-His proteins were analyzed by SDS-PAGE. Proteins were transferred to the membrane and stained with naphthol blue.*

A size exclusion chromatography experiment (section 3.2.3.9.2) was performed to confirm the results we obtained (Figure 40). The resulting chromatogram of both NME6-186-His and NME6-194-His revealed a similar and almost exclusive monomeric population, indicating that recombinant NME6 proteins are unable to organize in homo-hexamers, which is deemed essential for functional enzymatic activity.

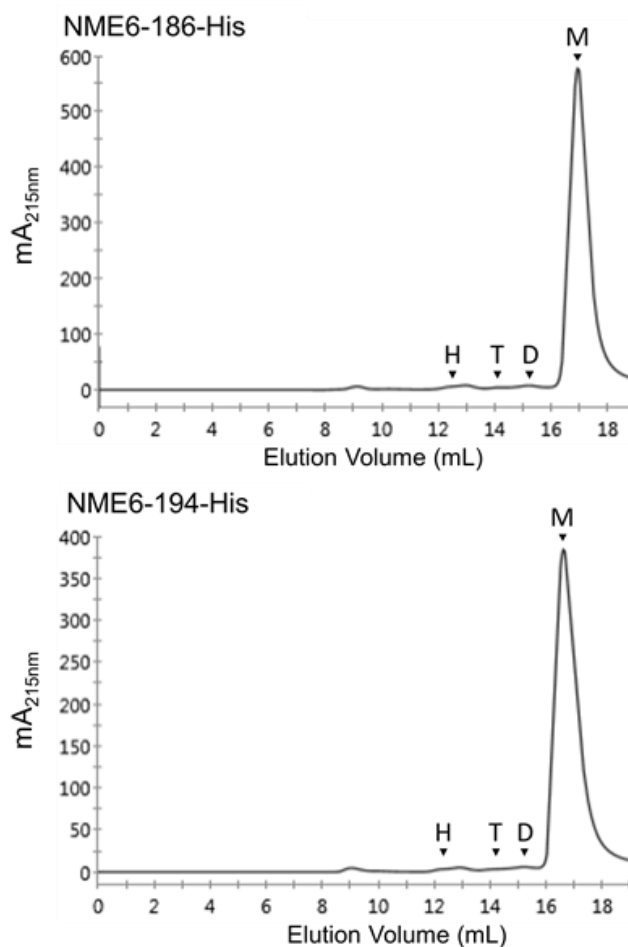


*Figure 40 : NME6 recombinant proteins are mostly monomeric. Size exclusion chromatography was performed by loading purified recombinant proteins NME6-186-His and NME6-194-His onto a Superdex 200 Increase 10/300 GL column, calibrated for molecular mass by a series of standard proteins. The protein elution profile was recorded by absorbance at 215 nm. The elution volume of monomers (M), dimers (D), trimers (T) and hexamers (H) expected from the calibration is indicated by arrows.*

To get insight of the NME6 homo-oligomerization status under the more realistic condition of cellular environment, an immunoprecipitation experiment was performed as described in section 3.2.3.5. MDA-MB-231T cells were transfected to express NME6-186-FLAG or NME6-194-FLAG and proteins were extracted 48 h post transfection. Cell lysates were subjected to immunoprecipitation using FLAG agarose, in order to pull down NME6-FLAG proteins. Western blot was conducted using NME6 antibody to reveal both endogenous and exogenous proteins (Figure 41). Results clearly showed that the pull-down of NME6-FLAG, either 186 or 194, did not co-immunoprecipitate the endogenous NME6 in the IP fraction. This confirmed the lack of homo-oligomerization of NME6 in live cell.

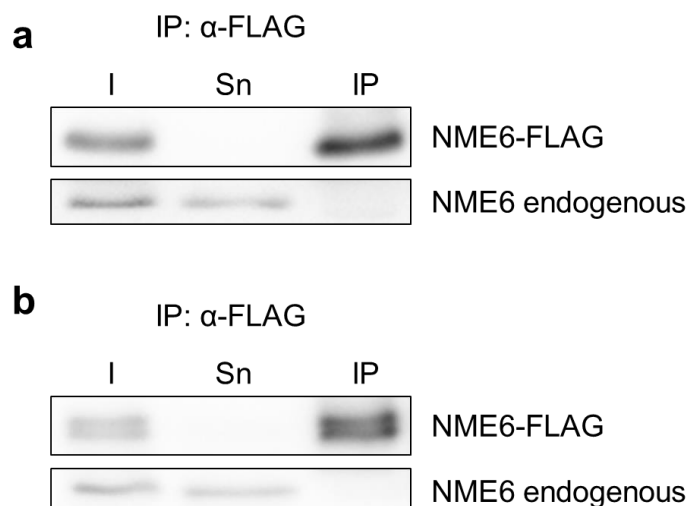


*Figure 41 : Endogenous NME6 and exogenous NME6-FLAG do not interact in the cellular environment.* Cell lysates from MDA-MB-231T cells transiently transfected to express **a** NME6-186-FLAG and **b** NME6-194-FLAG were pulled-down with FLAG-agarose. Input proteins (I), supernatant depleted of pulled-down proteins (Sn) and eluted proteins (IP) were analyzed by immunoblot with anti-NME6 antibody. FLAG-agarose efficiently immunoprecipitated NME6-FLAG, but failed to co-immunoprecipitate the endogenous NME6, revealing a lack of homo-oligomerization.

#### 4.4.4 Hetero-oligomerization status

It has been demonstrated that NME1 and NME2 can assemble as hetero-oligomers to form enzymatically active NME complexes. As NME6 was unable to form homo-oligomers, we studied its ability to form hetero-oligomers with the Group I NME proteins. Immunoprecipitations were performed as described in section 3.2.3.5 in a forward and reverse manner and analyzed by Western blot, using NME6, NME1, NME1/NME2 and FLAG antibodies (Figure 42). First NME1 was immunoprecipitated with a highly specific NME1 antibody that does not recognize NME2. The Western blot was performed using NME6 and NME1/NME2 antibody that recognize both NME1 and NME2. Results show that NME1 is able to co-immunoprecipitate NME2, but not NME6. The reverse experiment confirmed the lack of interaction between endogenous NME1/NME2 and NME6. As endogenous NME3 and NME4 displayed almost undetectable levels by Western blot in our model, MDA-MB-231T cells were transfected to express exogenous NME3-FLAG and NME4-FLAG. Expression of NME4-FLAG generated two detectable bands with the FLAG antibody: a full-length protein and a truncated one after import, due to the cleavage of the mitochondrial targeting sequence.

NME3 and NME4 were efficiently pulled down using FLAG-agarose, but endogenous NME6 was never co-immunoprecipitated. The reverse experiment ended to confirm the lack of interaction between endogenous NME6 and NME3 or NME4. As a result, we can confirm that NME6 is not interacting with any of the Group I NME proteins in the cellular environment, and, therefore, cannot form higher hetero-oligomers.

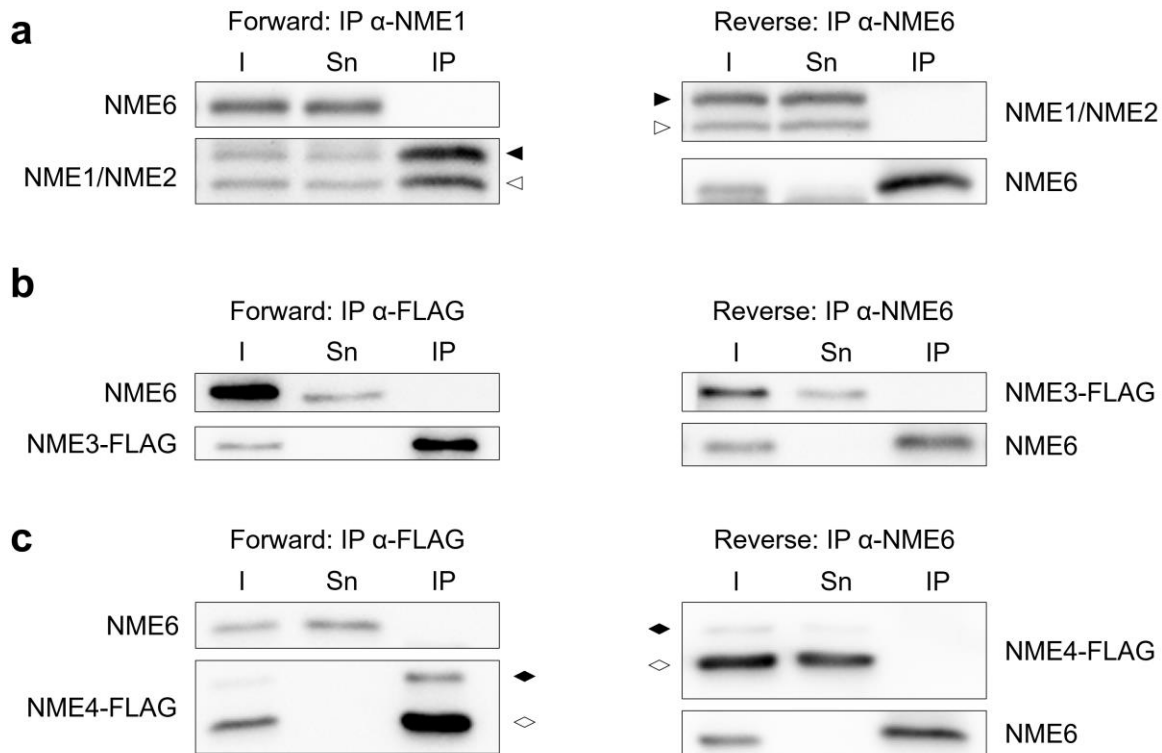


*Figure 42 : Endogenous NME6 does not interact with Group I NME proteins. Co-immunoprecipitations were performed in a forward and reverse manner between Group I NME proteins and endogenous NME6 protein in MDA-MB-231T cells. Input proteins (I), supernatant depleted of immunoprecipitated proteins (Sn) and eluted proteins (IP) were analyzed by Western blot. **a** Endogenous NME proteins were immunoprecipitated using anti-NME1 or anti-NME6 coupled with Dynabeads™ protein G. Western blots were performed using anti-NME1/2 antibody against NME1 ( $\blacktriangleright$ ) and NME2 ( $\blacktriangleright$ ), and anti-NME6. Proteins from cells transiently transfected to express **b** NME3-FLAG or **c** NME4-FLAG were pulled-down using FLAG-agarose or anti-NME6 coupled with Dynabeads™ protein G. Western blots were revealed using anti-FLAG and anti-NME6. NME4-FLAG displays two bands corresponding to NME4-full-length ( $\blacklozenge$ ) and NME4-truncated ( $\blacklozenge$ ) after mitochondrial import. NME6 shows no interaction with Group I NME proteins.*

---

## 4.5 NME6 interacting partners

### 4.5.1 Interactions with other proteins

To foresee the possible NME6 functions, we attempted to find interacting partners. Several potential targets based on available literature were tested by immunoprecipitation (section 3.2.3.5) (Figure 43). Among targets, RCC1L was selected upon its frequent detection as a NME6 interactor in large scale protein-protein interaction mapping studies. OPA1 was selected due to its already described interaction with NME4 and RCC1L. Immunoprecipitations were performed using MDA-MB-231T cells or clones overexpressing NME6-186-FLAG and NME6-194-FLAG, using FLAG, NME6 and RCC1L antibodies to pull down proteins. Irrelevant IgGs were used as a negative control. Results show that OPA1 was not co-immunoprecipitated, either with NME6 or RCC1L protein. RCC1L was successfully co-immunoprecipitated with both endogenous and exogenous NME6. The reverse experiment showed that endogenous NME6 and NME6-FLAG were both co-immunoprecipitated by RCC1L, thus demonstrating the presence of a strong and stable interaction between NME6 and RCC1L. Interestingly, as reported in the section 4.4.3, NME6-FLAG failed to co-immunoprecipitate the endogenous NME6 (IP:  $\alpha$ -FLAG), confirming the absence of an interaction between NME6 monomers, impairing the formation of higher homo-oligomers.

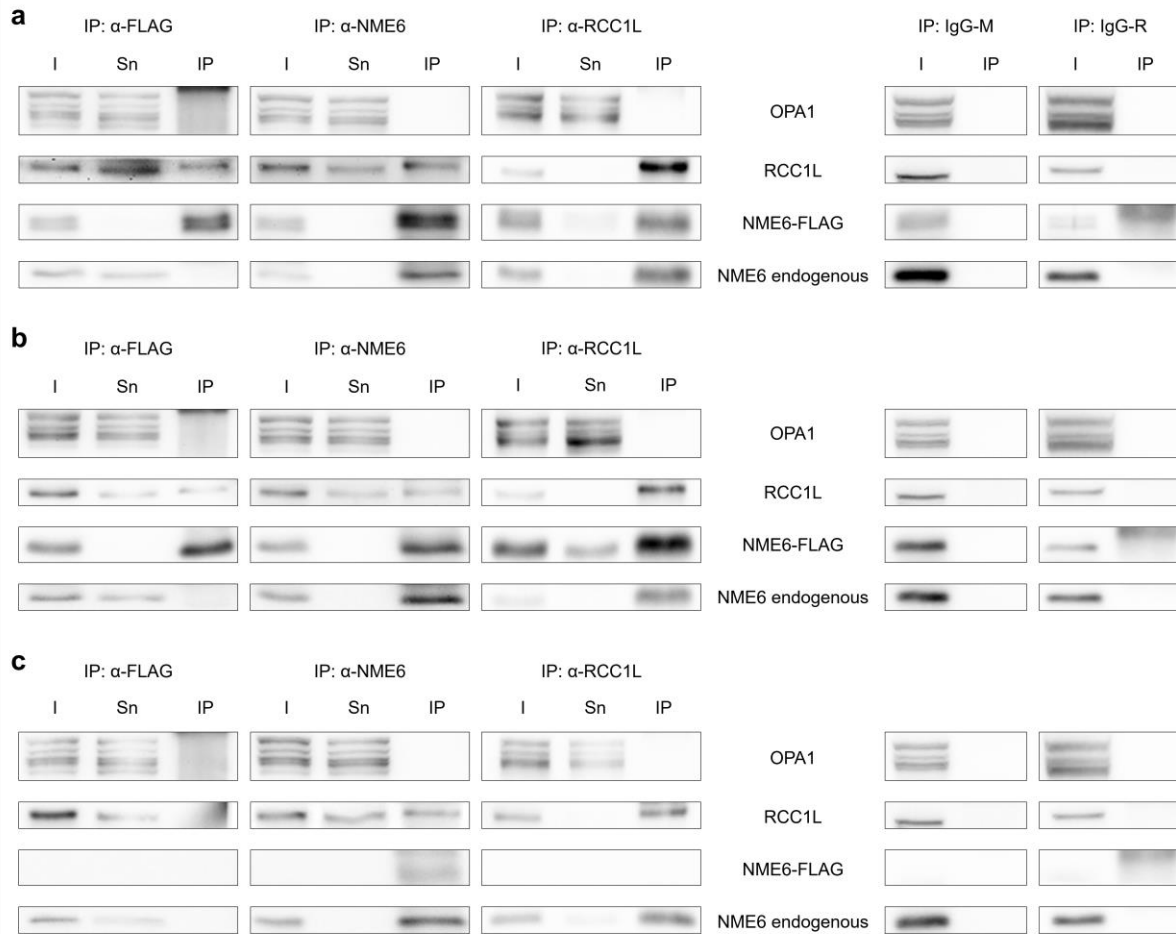


**Figure 43 : Co-immunoprecipitation of RCC1L and NME6 reveal physical interaction.** MDA-MB-231T cells were either transiently transfected to express **a** NME6-194-FLAG or **b** NME6-186-FLAG, or **c** non-transfected control cells were used. Cell lysates were subjected to pull-down with FLAG-agarose, or anti-NME6 and anti-RCC1L antibodies coupled to protein G-Dynabeads™. Immunoprecipitation with irrelevant immunoglobulins from mouse (IgG-M) or from rabbit (IgG-R) were used as a negative control. Input proteins (I), supernatant depleted of pulled-down proteins (Sn) and eluted proteins (IP) were analyzed by immunoblot with anti-OPA1, anti-RCC1L and anti-NME6 antibodies.

## 4.6 NME6 impact on cellular functions

To further understand the role of human NME6 on cellular functions, we aimed to explore the impact of NME6 silencing and overexpression on basic processes such as apoptosis, cell cycle and mitochondrial respiration.

### 4.6.1 Apoptosis

Impact of NME6 overexpression or silencing on apoptosis was studied by flow cytometry (section 3.2.5.1) after annexin V/propidium iodide staining of RKO cells. Those cells were chosen over MDA-MB-231T because of their p53 status. Indeed, p53 is mutated in MDA-MB-231T cells, which can influence apoptosis and the acquired results, while in RKO cells the p53 display a wild type profile. We could not use our stable clones overexpressing NME6-FLAG for this experiment as they were made in MDA-MB-231T cells. We thus performed apoptosis experiments in RKO cells transiently overexpressing NME6-FLAG (KI-186 and KI-194), or silenced for NME6 expression, both after transient transfection, using two different transfection methods as presented in sections 3.2.2.5 and 3.2.2.6. Cells transiently transfected with empty vector served as a knock-in control (KI-CTRL), cells transfected with scramble siRNA represent the silencing control (siCTRL). The apoptosis status was first measured in absence (RKO) and in presence of camptothecin (CAMPTO), a chemical compound triggering apoptosis, and thus used as a positive control. Afterwards, the apoptotic status of negative controls (KI-CTRL and siCTRL) was measured (Figure 44). Results showed that camptothecin was efficiently triggering apoptosis. Compared to RKO, camptothecin treated cells shown a drop of live cells from 90% to 60%, while the fraction of apoptotic cells increased from 10% to 40% and the fraction of dead cells remained unchanged. The transfection method used for silencing (siCTRL) was gentle and resulted in cell distribution highly similar to wild type RKO. On the contrary, the transfection method used for knock-in (KI-CTRL) was stressful for the cells, and led to a drop of live cells (from 90% to 45%) and the accumulation of apoptotic (from 10% to 35%) as well as dead cells (from 2% to 25%) when compared to RKO (Figure 44).

To resume, the transfection method used for KI induced apoptosis and cell death, while transfection method used for silencing did not impact apoptosis.

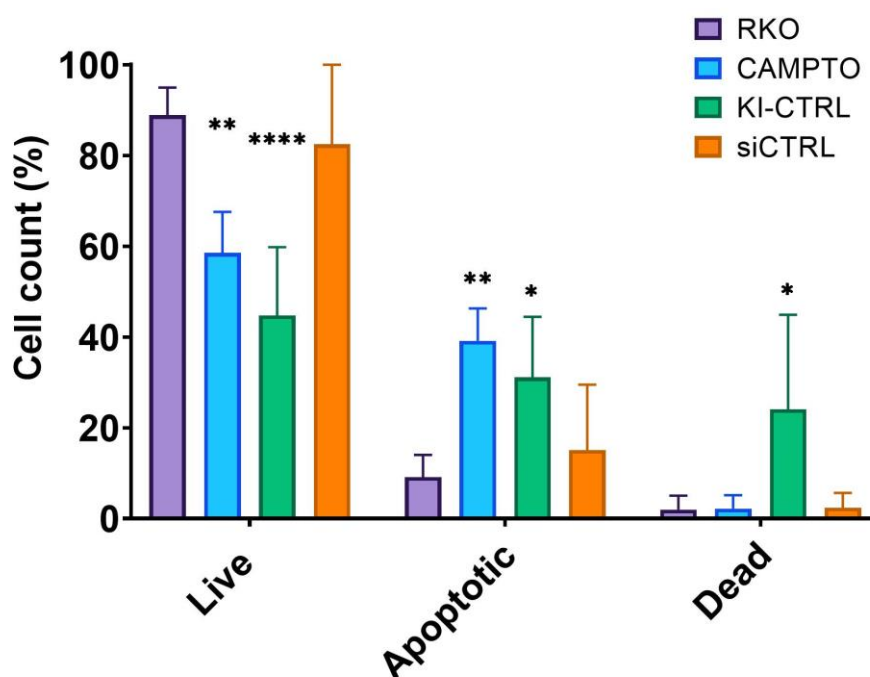


*Figure 44 : Transfection reagents can trigger apoptosis and cell death. RKO cells (RKO), transfected with empty plasmid as a negative control for KI (KI-CTRL), or transfected with scramble siRNA as a negative control for silencing (siCTRL) were assayed by flow cytometry after annexin V/Propidium iodide (AV/PI) staining. RKO cells treated with camptothecin were used as a positive control for apoptosis. Live cells were negative for both markers (AV/PI). Apoptotic category regroups both the early (AV<sup>+</sup>/PI) and late (AV<sup>+</sup>/PI<sup>+</sup>) apoptotic cells. Remaining cells compose the dead category (AV/PI<sup>+</sup>). Data are given as mean  $\pm$  SD (n=4). For comparison between RKO and other conditions, significance is given as \*\*\*\*  $p < 0.0001$ ; \*\*  $p < 0.01$ ; \*  $p < 0.05$  (Two-way ANOVA).*

The analysis of apoptotic status after overexpression of NME6-FLAG, either 186 or 194, did not reveal differences compared to control (Figure 45a). About 35 to 40% of cells were labeled as live, 35-40% were apoptotic and 25-30% were dead. Similarly, the silencing of NME6 did not impact apoptosis (Figure 45b), with a distribution of cells highly similar between siCTRL and siNME6 (80% live, 15% apoptotic, 5% dead). As a result, the overexpression or silencing of NME6 seems to have no impact on apoptosis in RKO cells. However, results should be considered carefully regarding the KI experiment, giving the fact that the transfection itself triggered massive apoptosis and cell death (Figure 44).



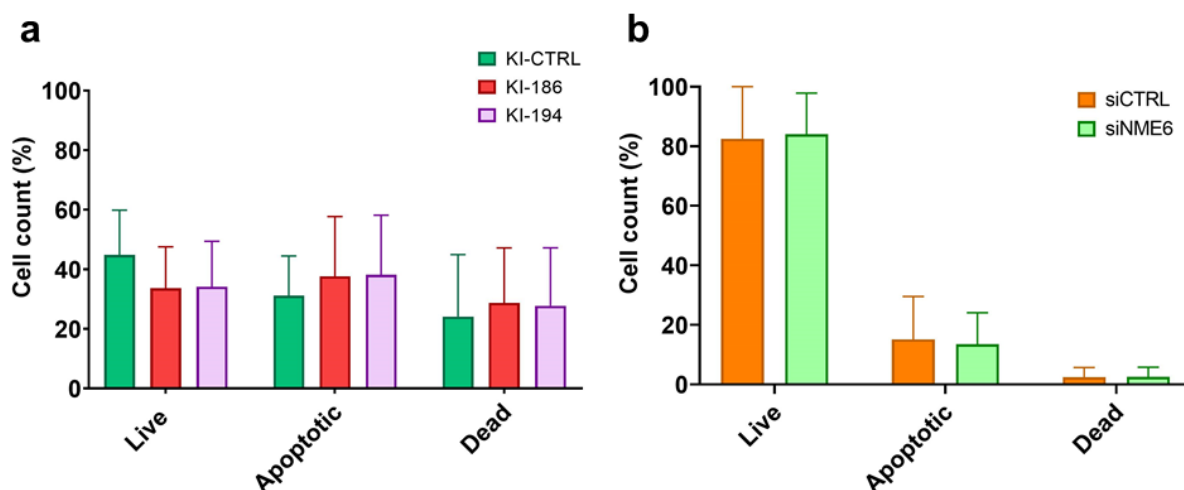


*Figure 45 : NME6 overexpression or silencing does not impact apoptosis. RKO cells (RKO), transfected **a** with empty plasmid as a negative control for KI (KI-CTRL), transfected to overexpress NME6-186-FLAG (KI-186) or NME6-194-FLAG (KI-194) and **b** transfected with scramble siRNA as negative control for silencing (siCTRL) or with NME6 silencers (siNME6) were assayed by flow cytometry after annexin V/Propidium iodide (AV/PI) staining. RKO cells treated with camptothecin were used as a positive control for apoptosis. Live cells were negative for both markers (AV/PI<sup>-</sup>). Apoptotic category regroups both the early (AV<sup>+</sup>/PI<sup>-</sup>) and late (AV<sup>+</sup>/PI<sup>+</sup>) apoptotic cells. Remaining cells compose the dead category (AV<sup>-</sup>/PI<sup>+</sup>). Data are given as mean  $\pm$  SD (n=4).*

#### 4.6.2 Cell cycle

Analysis of the cell cycle was performed by flow cytometry (section 3.2.5.2) on MDA-MB-231T cells after propidium iodide staining. For studying the impact of NME6-FLAG overexpression, the cell cycle status of wild type MDA-MB-231T, three empty clones (KI-CTRL; Neg 5, 6 and 7), three NME6-186-FLAG KI clones (KI-186; 186-7, 18 and 26) and three NME6-194-FLAG KI clones (KI-194; 194-8, 13 and 17) were analyzed. The experiment was repeated three times (n=3), and results from related clones were combined. Wild type MDA-MB-231T cells, empty clones (KI-CTRL) and clones overexpressing NME6-FLAG (KI-186 and KI-194) displayed similar distribution over the different phases of the cell cycle (Figure 46a). About 35-40% of cells were in the G0/G1 phase, 35-40% were in the S phase and 20% were in the G2/M phase. No statistical differences were observed by comparing the groups. In fine, the overexpression of NME6-FLAG did not impact the cell cycle of MDA-MB-231T cells.

We further investigated the impact of NME6 silencing on cell cycle (Figure 46b). Wild type MDA-MB-231T, cells silenced with scramble silencer (siCTRL) and cells silenced for NME6 (siNME6) were analyzed, and experiment was repeated three times (n=3). No statistical differences could be observed between groups. Wild type MDA-MB-231T cells, scramble silenced (siCTRL) or NME6 silenced (siNME6) displayed about 45% of cells in G0/G1 phase, 30% in S phase and 25% in G2/M phase. Results indicate that the transfection itself did not impact cell cycle (MDA-MB-231T vs siCTRL). Furthermore, the silencing of NME6 did not impact cell cycle as well (siCTRL vs siNME6).

Overall, the cell cycle was not affected by the relative changes of NME6 protein abundance within the cell.

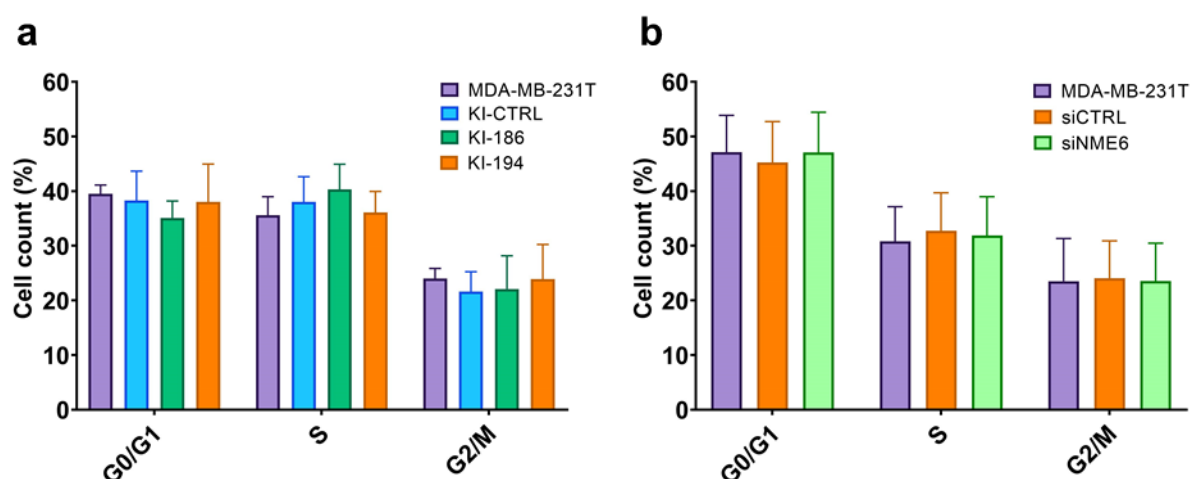


*Figure 46 : NME6 overexpression or silencing does not impact the cell cycle. MDA-MB-231T cells, together with a stable clones carrying empty vector as a negative control for clones (KI-CTRL) and overexpressing NME6-186-FLAG (KI-186) or NME6-194-FLAG (KI-194) and b cells transfected with scramble siRNA as negative control for silencing (siCTRL) or with NME6 silencers (siNME6) were assayed by flow cytometry after propidium iodide staining (n=3).*

#### 4.6.3 Mitochondrial respiration

As we localized NME6 in the mitochondrial matrix, and interacting with RCC1L protein which was shown to negatively impact the abundance of mitochondria-encoded proteins of the respiratory chain [128], we verified mitochondria functional parameters under NME6 overexpression (Figure 47) or silencing (Figure 48). Oxygen consumption rate (OCR) of digitonin-permeabilized cells was measured, using the complex I-linked substrates glutamate/malate or the complex II-linked substrate succinate (section 3.2.5.3).

Upon NME6 overexpression, respiration fueled over complex-I (Figure 47a) or complex-II (Figure 47b) was similar between control and KI-clones (LEAK). Upon addition of ADP (OXPHOS), significant differences occurred. All the NME6 KI clones displayed lower ADP-stimulated respiration compared to control. Accordingly, the ratio OXPHOS/LEAK was significantly reduced in KI clones. A further addition of Cytochrome C did not increase oxygen consumption compared to OXPHOS, indicating in all cases that mitochondria were intact upon measurement. The same set of experiments was realized with NME6 silenced cells (Figure 48). Upon addition of ADP (OXPHOS), silenced cells displayed higher ADP-stimulated respiration compared to control, which is the opposite effect from the one observed for KI clones. However, the difference was lost when calculating the ratio OXPHOS/LEAK. As a result, NME6 overexpression negatively impacts cellular respiration in KI clones, and an inverse tendency can be observed in silenced cells, even though not statistically significant.

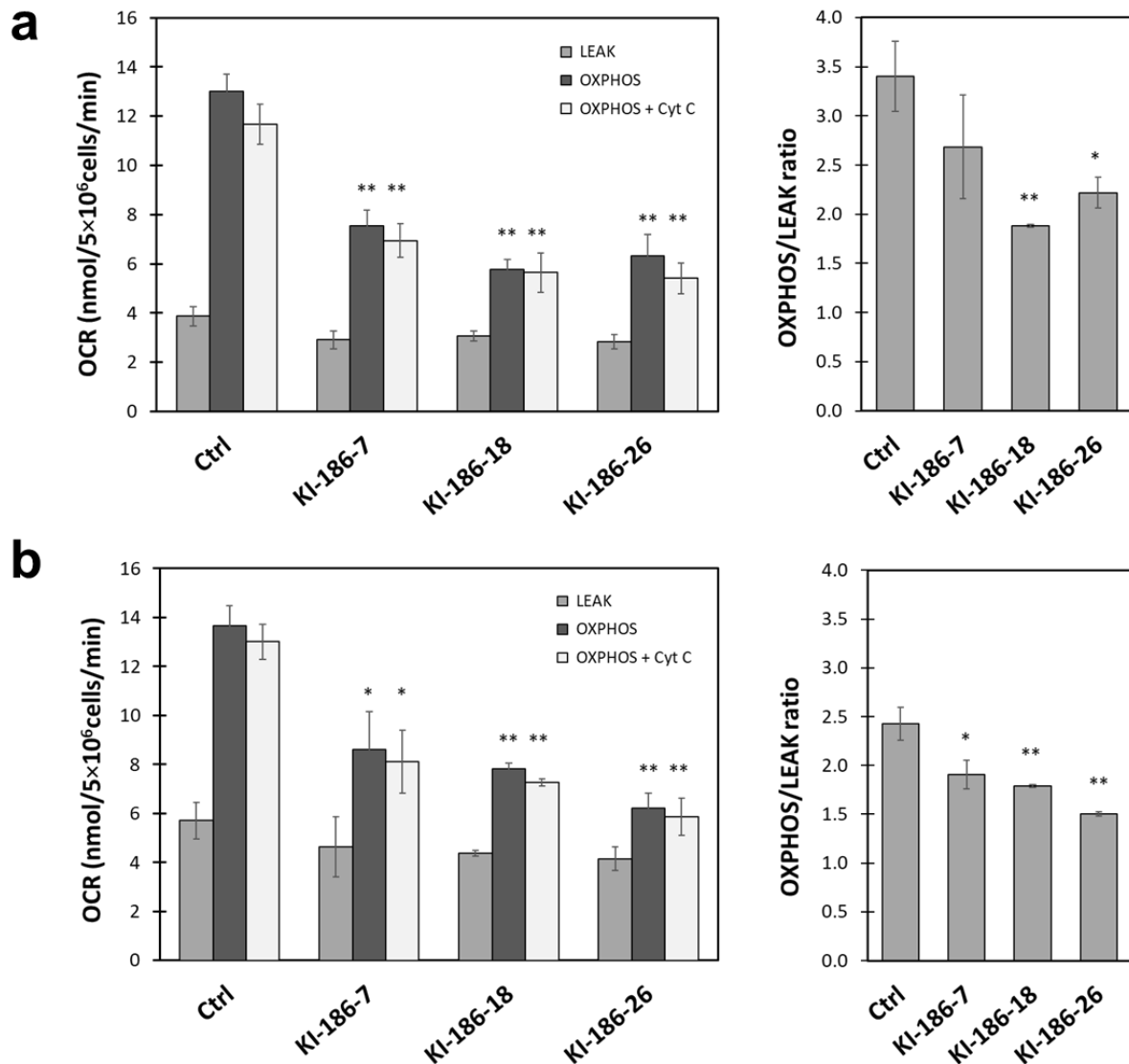
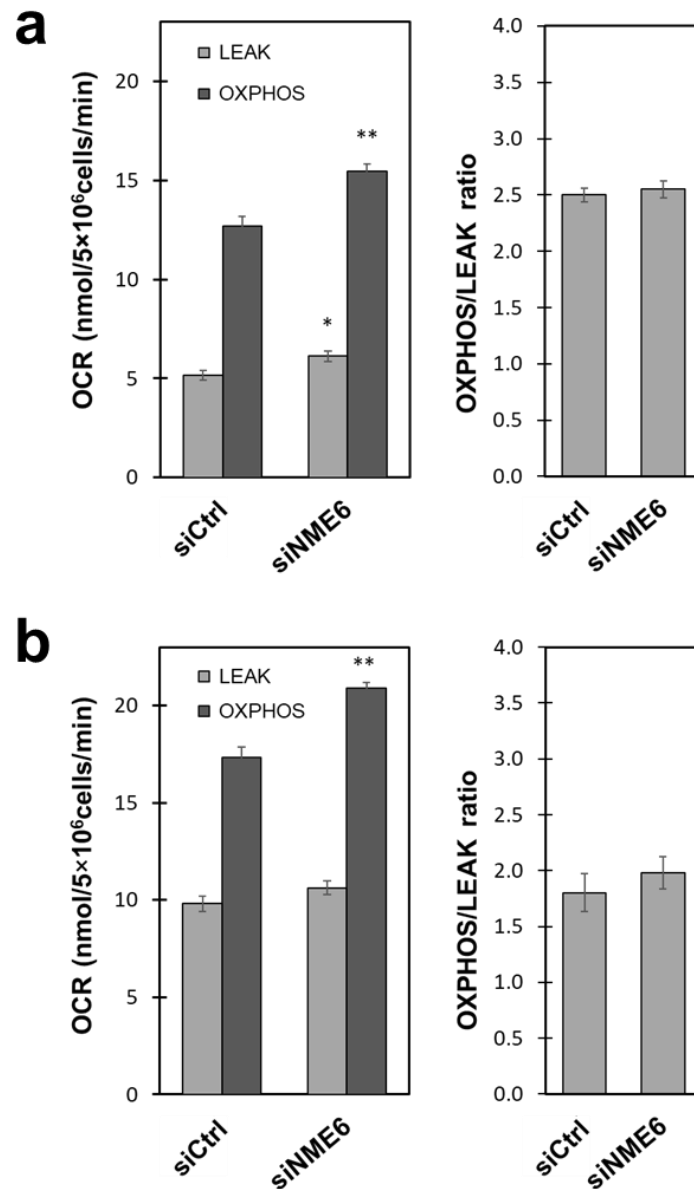


Figure 47 : *NME6* overexpression negatively affects ADP-stimulated respiration of mitochondria. Oxygraphy analysis of respiration in three MDA-MB-231T stable clones overexpressing NME6-186-FLAG (KI-186-7, KI-186-18, KI-186-26), that were digitonin-permeabilized and supplied with substrate (LEAK), stimulated with ADP (OXPPOS), and tested for mitochondrial membrane integrity (addition of cytochrome c). **a** Cellular oxygen consumption with glutamate/malate and associated OXPPOS/LEAK ratios. **b** Cellular oxygen consumption with succinate and associated OXPPOS/LEAK ratios. All data are given as mean  $\pm$  SEM ( $n=3$ ). For comparison between Ctrl and NME6 overexpressing clones, significance is given as \*\*  $p < 0.01$ ; \*  $p < 0.05$  (Student's test).



*Figure 48 : NME6 silencing tend to increase ADP-stimulated respiration of mitochondria. Oxygraphy analysis of respiration in MDA-MB-231T cells transfected with scramble siRNA (siCtrl) or transfected with siRNA against NME6 (siNME6), that were digitonin-permeabilized and supplied with substrate (LEAK) and stimulated with ADP (OXPHOS). **a** Cellular oxygen consumption with glutamate/malate and associated OXPPOS/LEAK ratios. **b** Cellular oxygen consumption with succinate and associated OXPPOS/LEAK ratios. All data are given as mean  $\pm$  SEM (n=3). For comparison between Ctrl and NME6 overexpressing clones, significance is given as \*\*  $p < 0.01$ ; \*  $p < 0.05$  (Student's test).*

#### **4.6.4 Respiratory chain complexes abundance**

The deficiency of ADP-stimulated respiration upon NME6 overexpression raised the question of its impact of respiratory chain complexes abundance. To address this question, a Western blot was conducted on MDA-MB-231T cells lysates (Ctrl), silenced with scramble control (siCtrl), silenced for NME6 (siNME6), and clones overexpressing NME6-186-FLAG (KI-186-7, KI-186-18, KI-186-26). Immunoblotting was performed using an antibody cocktail against OXPHOS complexes C-I to C-V (Figure 49). The experiment was repeated three times, the band intensities were extracted by densitometry and statistical analysis was performed by comparing siCtrl to siNME6 on one hand, and Ctrl to NME6 KI clones on the other hand (Figure 50). Results show that NME6 silencing does not have statistically significant effect on respiratory complexes abundance. However, the overexpression of NME6-186-FLAG strongly decreases the abundance of C-III protein UQCRC2, in all overexpressing clones tested. Similarly, C-I protein NDUFA9 and C-IV protein COX IV tended to be downregulated upon NME6-FLAG overexpression, even though this was not observed for all three NME6 KI clones. C-II protein SDHA and C-V protein ATP5A were unaffected by NME6-FLAG overexpression. The overexpression of NME6 had a direct negative impact on respiratory complexes proteins abundance, which could be responsible for the deficiency of ADP-stimulated respiration (Figure 47).

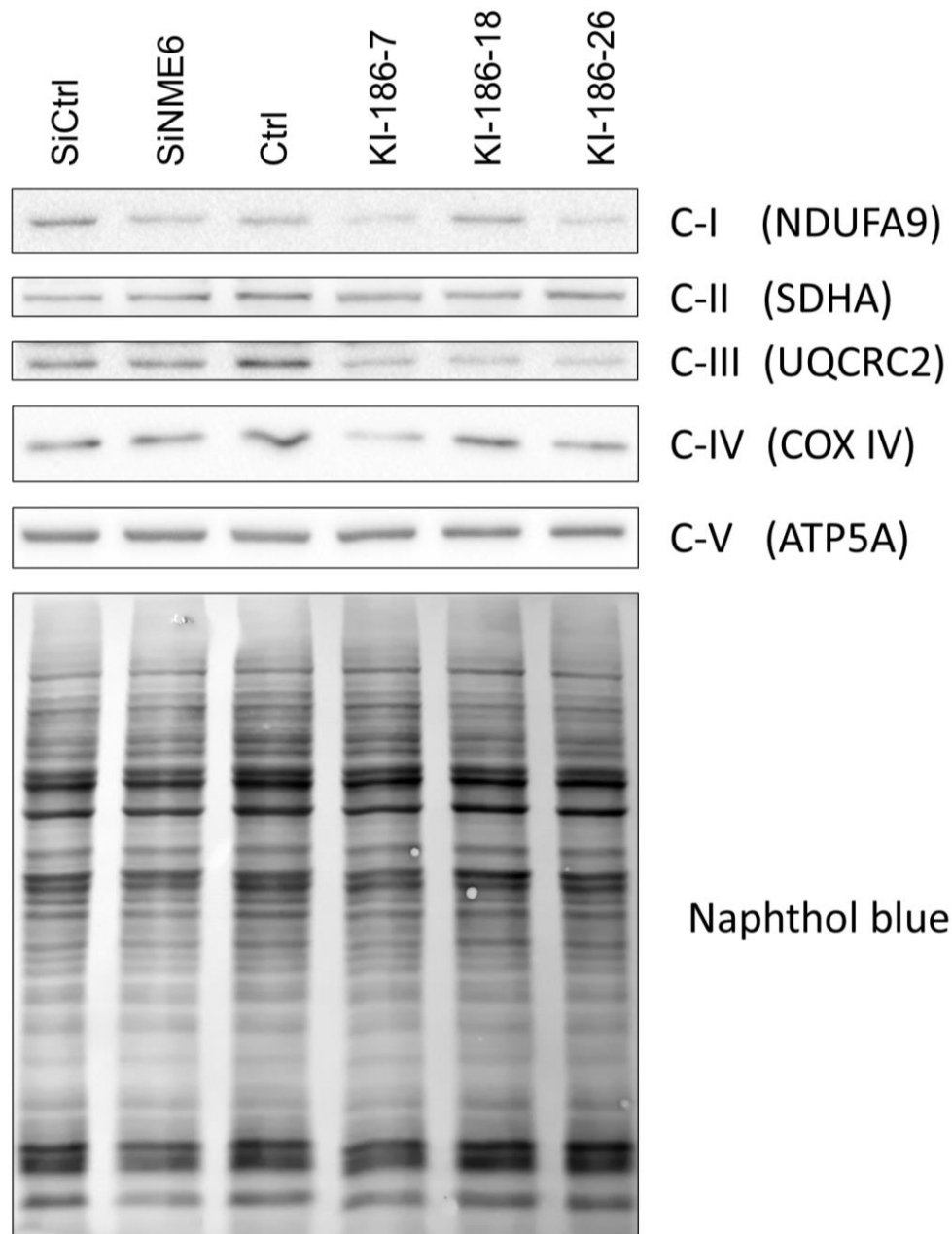


*Figure 49 : Stable overexpression of NME6 reduces Complex-III respiratory chain protein abundance. a Ten micrograms of cell lysate from MDA-MB-231T (Ctrl), silenced with scramble control (siCtrl), silenced for NME6 (siNME6) and stable clones overexpressing NME6-186-FLAG (KI-186-7, KI-186-18, KI-186-26) were analyzed by Western blot, using the antibody cocktail against OXPHOS complexes C-I to C-V.*

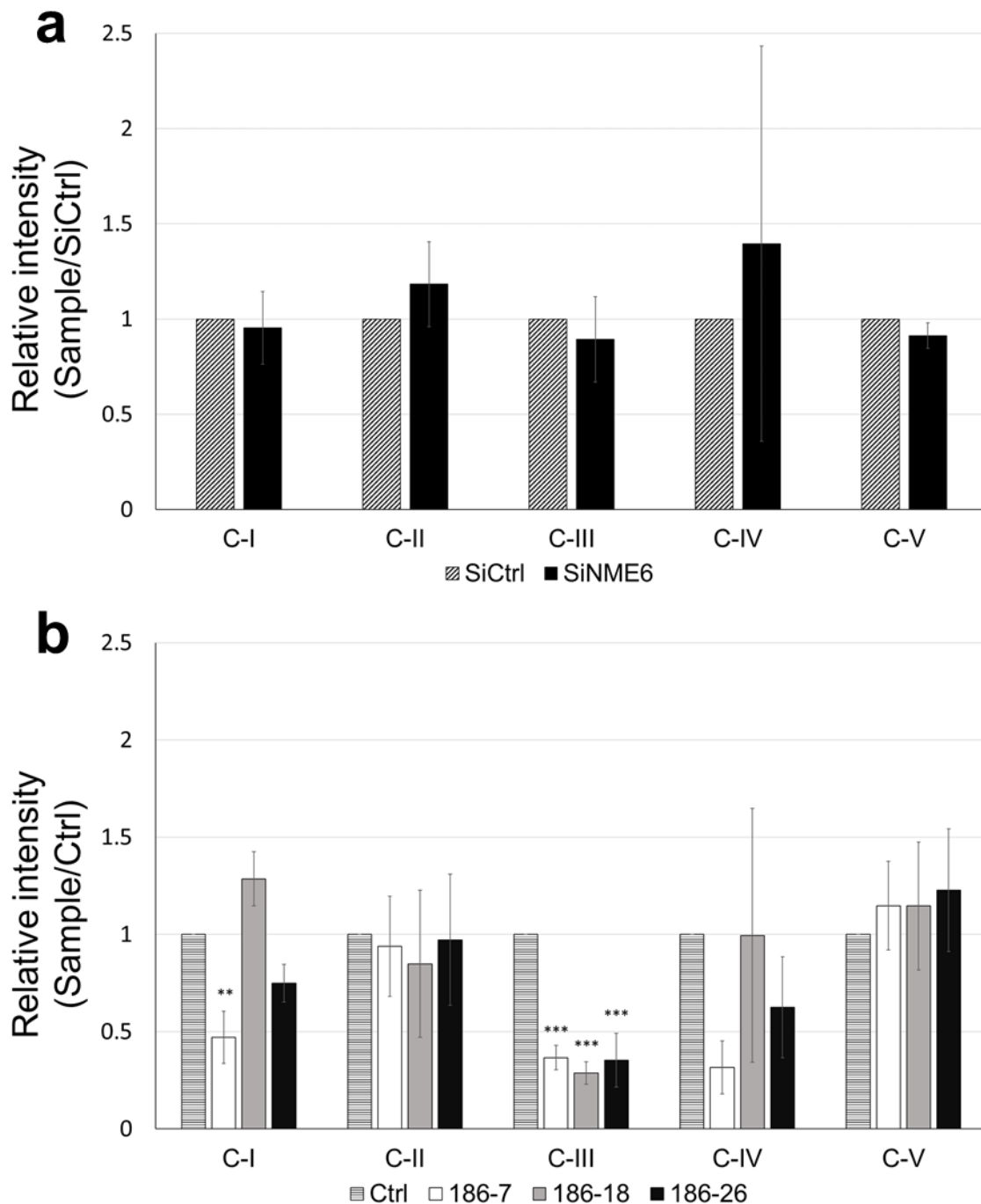


Figure 50 : Statistical analysis of the protein's abundance of respiratory complexes. Experiment described in Figure 49 was realized in triplicate ( $n=3$ ). Band intensity values were extracted by densitometry, normalized to naphthol blue staining, and displayed as a ratio relative to **a** siCtrl or **b** Ctrl. Statistical analysis was performed using **a** Student's test or **b** one-way ANOVA. All data are given as mean  $\pm$  SD. Significances are given as \*\*  $p < 0.01$ ; \*\*\*  $p < 0.001$ .



## 5 DISCUSSION

Human NME genes arose from duplication events of ancient genes that appeared early in the course of evolution [1,136]. In human cells, different members of the NME family are localized to different cellular compartments (cytosol, microtubules, nucleus, mitochondria) [17,19–22]. There, the proteins displaying NDPK activity can locally supply or fuel GTP to GTPases [18,95,137], but can also be involved in other biochemical mechanisms including protein histidine phosphorylation [14], selective intermembrane lipid transfer [95], DNA damage repair [17,20]. While great scientific efforts have been done to describe human NME proteins from the Group I (NME1 to NME4), the Group II NME proteins remained largely unexplored. Accordingly, little is known about the human NME6 protein, for which the main available information dates from its discovery in 1999, and from an article studying the enzymatic activity of NDP kinases in 2005 [6,8,28]. Unfortunately, those results are not consistent and partially contradictory. Two protein isoforms of NME6 have been described, one of 194 aa and the other of 186 aa, shorter in the first eight N-terminal amino acids. The potential NDPK activity of the protein was assayed, but contradictory conclusions were drawn from different teams. While Tsuiki et al. supported a functional NDPK activity for NME6 [8], other teams concluded that the protein is deprived of such activity [6,28]. Similarly, the NME6 expression was either considered to be ubiquitous [28], or tissue-oriented [8].

In this doctoral thesis, we aimed to clarify the information about the human NME6 protein. To this extent, we provided evidence for the existence of two NME6 isoforms in the cellular environment, albeit at different levels, for the ubiquitous expression of the protein and for the absence of NDPK activity. We further detailed that NME6 is unable to homo-oligomerize or form oligomers with Group I NME proteins. Moreover, NME6 lacks phosphorylated histidine, including the one in the catalytic site, thus impairing any kind of phosphotransferase activity such as NDPK activity or protein histidine kinase activity. We confirmed that the protein is mitochondrial and refined its localization to the mitochondrial matrix, partially bound to the MIM. We described a strong and stable interaction with RCC1L, a mitochondrial matrix protein impacting the mitoribosome assembly and the mitochondrial translation. We explored the impact of NME6 on cellular functions, and showed that variations in the protein expression did not impact cell cycle or apoptosis, but overexpression of NME6 strongly reduced the mitochondrial respiration and respiratory complexes abundance.

The production of stable clones overexpressing NME6 and knocked-out clones, as well as the production of recombinant NME6 proteins was of a major importance to further study the structure and function of human NME6 protein. The NME6-KI, overexpressing clones were successfully obtained and their analysis revealed interesting facts. First the overexpression of NME6-186-FLAG resulted in a single band after Western blot analysis, while the overexpression of NME6-194-FLAG revealed two bands, corresponding to both NME6-194-FLAG and NME6-186-FLAG (Figure 18). The expression of both isoforms in the latter condition could be imputed to the presence of two ATG initiation sites in the 5' vicinity of the NME6 mRNA (Figure 14), leading to expression of both isoforms from a single mRNA. However, an alternative splicing producing two mRNA or a post-translational processing of the NME6-194 cannot be excluded to explain this phenomenon. All NME6-KI clones produced were expressing ten to twenty time more of the exogenous NME6-FLAG than the endogenous NME6 in controls (Figure 19). Interestingly, the overexpression of exogenous NME6-FLAG protein always led to the downregulation of endogenous NME6 at the protein level. This strongly suggests the existence of a negative feedback loop repressing the endogenous NME6 gene expression upon overexpression of the exogenous NME6-FLAG.

The NME6-KO clones were envisaged to be produced by CRISPR-Cas9 technology. In our repeated experiments we did not succeed in obtaining a single clone with a visible downregulation of endogenous NME6 at the protein level (Figure 20). The PCR analysis of resistant clones revealed that we successfully knocked-out one allele of the NME6 gene, but another allele remained intact (wild type), (Figure 21 and Figure 22), generating monoallelic NME6-KO clones. We propose that a biallelic NME6-KO could be lethal, which is comforted by the International Mouse Phenotype Consortium database showing that biallelic NME6-KO lead to mice embryonic lethality [138,139]. However, we produced clones in MDA-MB-231T, a cancer cell line displaying chromosomal rearrangements [140]. The absence of complete NME6-KO in our experiments could be the consequence of a possible duplication or multiplication of the NME6 gene, resulting in a multitude of alleles that would represent a challenging task for a complete KO by the CRISPR-Cas9 technique. As we were unsuccessful in producing NME6-KO stable clones, we used a silencing method to transiently downregulate endogenous NME6 expression up to 90% (Figure 23).

Finally, recombinant proteins of the human NME6 (194 and 186) were produced in bacteria. The process required more than a year of tuning, due to low recovery of the NME6 protein in the soluble fraction. After purification, both isoforms were largely enriched, even though not

100% pure (Figure 24 and Figure 25). Nevertheless, the purification level was acceptable, and no other protein could be observed after SDS-PAGE of the recombinant proteins in non-saturating conditions (Figure 26).

Mehus et al. reported the NME6 ubiquitous expression at the mRNA level in 16 human tissues, with slight variations [28]. Similarly, the NME6 ubiquitous expression was described in zebrafish, with the highest mRNA levels found in ovaries [1]. Only Tsuiki et al. described the NME6 mRNA expression to be tissue dependent, mainly in heart, placenta, skeletal muscle and kidney [8]. Our characterization of the endogenous human NME6 protein supports a ubiquitous expression, where NME6 was similarly expressed in cancer and non-cancer cell lines of different tissues of origin (Figure 27). Not a single cell line was found with undetectable levels of NME6, underlining the importance of the protein for the cell. Two NME6 isoforms, 194 aa and 186 aa, have been described in the literature and could be discriminated by Western blot based on their molecular weight (Figure 28). Mass spectrometry analysis revealed that both NME6-186 and NME6-194 protein isoforms were expressed in MDA-MB-231T and HeLa cell lysates, without giving information about their relative abundance (Figure 30). However, the detection of endogenous NME6 protein by Western blot consistently resulted in a single band in a large panel of human cell line tested (Figure 27). Moreover, the comparison with recombinant NME6 isoforms clearly showed that the main endogenous NME6 protein detected by Western blot corresponds to the isoform of 186 aa (Figure 29). Altogether, even though both isoforms are expressed in human cells, the endogenous NME6 is mainly expressed as a single protein isoform of 186 aa, while the scarcely expressed NME6-194 escapes Western blot detection.

The mitochondrial localization of NME6 was first suggested by Tsuiki et al. on the basis of immunofluorescent staining [8], and by large-scale mitochondrial proteomic studies [112,113,116], but without making distinction between NME6 isoforms. We designed a co-localization experiment using confocal microscopy, and stained mitochondria using two methods, to avoid false positive results. First, cells were transfected to express a fluorescent protein targeted to mitochondria (CFPmito). A second approach used the common MitoTracker staining solution that incorporates in mitochondria. We confirmed the mitochondrial localization of endogenous NME6 (Figure 31) and both 194 aa and 186 aa GFP-fused isoforms (Figure 32) by confocal microscopy. The C-terminal tagged NME6-GFP isoforms retained the mitochondrial localization over a 24h time-laps period [81]. Interestingly, the GFP-fused proteins failed to localize with mitochondria when the GFP was placed on the N-terminus of

NME6, highlighting that this portion of NME6 is important for mitochondrial targeting (data not shown). The mitochondrial localization of endogenous NME6 was further confirmed by cellular fractionation techniques (Figure 33 and Figure 34), where NME6 was enriched in the pure mitochondrial fraction together with well-defined mitochondrial markers (Figure 34). The subfractionation of mitochondria helped to refine the localization of NME6 within the mitochondria. We found that NME6 is not a soluble protein of the IMS, but is rather facing the mitochondrial matrix compartment, probably partially interacting with the MIM (Figure 36). This is consistent with large-scale proteomic studies of the mitochondrial compartments, detecting NME6 in the matrix proteome [113] but showing its absence from the IMS [114] or MOM-facing-cytosol [115] proteomes.

NME6 is deprived of the classical cleavable N-terminal mitochondrial targeting sequence (MTS), but still localizes within the mitochondrial matrix. The import pathway of the protein is still unclear, but a possible internal MTS (iMTS) could help the entry of NME6 in the mitochondria [50,51,141]. Indeed, an iMTS predictor service predicted a high iMTS propensity for the middle section of the NME6 protein [51,142], which was confirmed by another approach described by Backes et al., using the TargetP algorithm [141]. Lately, a team working with mitochondrial import of mitoribosome proteins in yeast demonstrated that some iMTS, corresponding to TOM20-binding motifs together with positive charges along the short protein Mrp17, was sufficient to trigger mitochondrial protein import [50]. NME6 displays in its sequence five typical TOM20-binding motifs [143–145], and their *in-silico* mutation drastically reduced the predicted iMTS propensity of NME6 [142]. Whether those mutations can preclude the mitochondrial localization of the protein *in vivo* still need to be demonstrated.

As described in numerous journal articles and reviews of the NME family, the NDPK activity specific for those proteins is detectable under certain conditions. According to the available literature, NME proteins displaying NDPK activity form oligomers [10,13,66], and, therefore, the oligomerization is deemed essential for their enzymatic activity. Homohexamers, an assembly of 6 monomers of the same protein into higher quaternary structure, or heterohexamers, an assembly of 6 monomers from different NME protein (for example NME1 and NME2) were found in eukaryote, archaea and some bacteria [10,68–72]. In some other bacteria, NME proteins fold as tetramers, an assembly of 4 monomers [73–75]. The NDPK activity relies on the phosphorylation of a specific histidine within the catalytic site, bringing the proteins into a high-energy histidine-phosphorylated status. In our hands, both recombinant NME6 isoforms failed to display NDPK activity, while the positive control NME1 nicely

displayed an activity of 155 U/mg (Figure 37). The lack of NDPK activity is consistent with the results published by Mehus et al. and Yoon et al., but are in disagreement with the results of Tsuiki et al. [6,8,28]. Tsuiki et al. followed a radiolabeled phosphate group ( $^{32}\text{P}$ ) along the NDPK enzymatic reaction of recombinant NME1 and NME6. They reported a low level of autophosphorylation (“ping”) of NME6, about 30 time less than NME1, and a measurable transfer to cold CDP (“pong”) [8]. Their data, divergent from other studies, could be explained by the highly sensitive method they used and/or by the presence of bacterial NME protein traces contaminating the recombinant NME6 protein.

Altogether, the pure recombinant NME6 protein is likely deprived of NDPK activity. But some can argue that a pure recombinant protein produced in bacteria is somehow dissimilar from a native protein found in the human cellular environment. After all, NME6 conserved in its sequence the principal amino acids deemed essential for the protein structure and enzymatic activity [1]. To get further details, the histidine phosphorylation status of endogenous NME6 was studied in its cellular environment, using newly-developed antibodies specifically recognizing phosphorylated histidine on Western blot analysis [64]. Results showed that NME6 lacks phosphorylation on histidines, including the main catalytic-site histidine, contrary to NME1 (Figure 38). This critical result pinpoints that in the cellular environment, the high-energy histidine-phosphorylated NME6 does not exist. Similar results were obtained on pure recombinant NME proteins, where phosphorylated histidines were detected for NME1, NME2, NME4, NME5 and NME7, but not for NME6 [64]. Consequently, NME6 would be deprived of any enzymatic activities depending on the phosphorylated histidine in the catalytic site, including NDPK activity but also protein histidine kinase activity.

This lack of enzymatic activity could be the results of a three amino acid insertion in the *Kpn* loop and a C-terminal extension (compared to NME1), as suggested for NME5 [11]. The *Kpn* loop is an important structure of NME proteins. It plays a role in stabilizing the substrate in the catalytic site, and helps to maintain the quaternary structure of oligomers together with the C-terminal part of the protein [13]. Accordingly, the analysis of recombinant NME6 oligomerization showed that the protein remains mostly monomeric (Figure 39 and Figure 40). The crosslinking profile of human NME6 protein was highly similar to the sponge variant of NME6, NME6Sd [27], where the hexameric form was negligible. Moreover, it was strikingly dissimilar to human NME1, and NMEGp1Sd from the sponge, where the hexameric form predominated and the other oligomers were barely detectable [26]. Likewise, in the human cellular environment, the endogenous NME6 and the exogenous NME6-FLAG (194 aa or 186

aa) failed to interact with each other in the immunoprecipitation experiment (Figure 41), confirming once again the lack of interaction between NME6 monomers.

As NME proteins have been shown to form heterohexamers [10,17], we verified the potential interaction of NME6 with Group I NME protein (Figure 42). NME1 and NME2 interacted with each other, but not with NME6. The result was expected considering the mostly cytosolic localization of NME1 and NME2 [85]. More interest was given to the mitochondrial NME3, partially localizing at the outer face of the MOM [19,20], and the mitochondrial NME4, interacting with the MIM and facing either the IMS or the matrix [94]. The immunoprecipitation revealed the absence of stable interactions between NME6 and NME3, a rational result considering their respective localization, where the proteins would be physically separated by two lipidic membranes, the MIM and the MOM. Similarly, we showed the absence of an interaction between NME6 and NME4. Nevertheless, a proximity ligation assay indicated that the two proteins are localized in close vicinity within the mitochondria [81].

To narrow down the potential mitochondrial pathways in which NME6 could be involved, we searched for possible protein interacting partners. *In silico* analysis of large-scale protein-protein interaction studies pinpointed RCC1L as a potential interactor [116–120]. Indeed, those studies using yeast two hybrid or affinity purification followed by mass spectrometry, with NME6 as a bait and/or a prey, consistently detected NME6/RCC1L interaction with high scores. OPA1 protein was also included in our screen, due to its well-known interaction with NME4 [146], and to its described interaction with RCC1L [127]. Co-immunoprecipitation realized in a forward and reverse manner confirmed that endogenous NME6 and exogenous NME6-FLAG (194 aa and 186 aa) both interact with the endogenous RCC1L protein (Figure 43). Interestingly, in a proximity-dependent biotinylating assay using over 100 mitochondrial baits from all compartments of the mitochondria, NME6 was detected in proximity to RCC1L with infinite specificity [116]. In other words, none of the other 100 baits detected NME6 in its neighborhood, indicating a highly specific interaction between NME6 and RCC1L. No interaction was found between NME6 and OPA1 (Figure 43), and interestingly, the OPA1/RCC1L interaction described in the literature [127] could not be confirmed in our hands.

RCC1L (also called WBSCR16) is a mitochondrial matrix protein belonging to the RCC1 superfamily. The most studied protein of the family, RCC1, is localized in the nucleus and acts as a guanine exchange factor (GEF) for the RAN GTPase [121,123]. The mitochondrial RCC1L was described to interact with, and to act as a GEF for OPA1 [127], even though in

our hands we did not detect RCC1L/OPA1 interaction. The recent focus on RCC1L unraveled an important role along the mitochondrial translation processes. RCC1L is a component of the pseudouridylation module and is, therefore, related to the post transcriptional modification of mtRNA, including the pseudouridylation of 16S rRNA, a structural RNA constituent of the large subunit of the mitoribosome [117,125]. Silencing or overexpression of RCC1L was associated with a decreased level of 16S rRNA, thus affecting mitochondrial translation [117,128]. Moreover, RCC1L was shown to interact with both subunits of the mitochondrial ribosome, and silencing or overexpression negatively affected the mitoribosome biogenesis [128]. Consequently, the tuning of RCC1L expression led to a strong decrease of the *de novo* synthesis of mitochondria-encoded proteins, eventually decreasing the abundance of the respiratory chain complexes and leading to a global decrease in oxygen consumption [117,125,128]. Noteworthy, the silencing of any component of the pseudouridylation module leads to a decrease of 16S rRNA abundance, FASTKD2 excluded [117].

In the light of these information, the study of mitochondrial respiration was included in our screen of NME6 impact in basic cellular processes, namely apoptosis and cell cycle. We found that the overexpression or silencing of NME6 had no impact on both apoptosis and cell cycle (Figure 45 and Figure 46). Our cell cycle analysis showed clear-cut results, with no differences observed between wild-type cells, NME6-overexpressing and control clones or NME6-silencing and controls. Interestingly, the overexpression of NME6 was previously described to influence the cell cycle, by blocking the cells in the G2/M phase, and eventually driving the generation of multinucleated cells [8]. These contradictory results could be explained by the different approaches in the experimental design. First, different cell lines were used. While Tsuiki et al. [8] used an osteosarcoma cell line isolated from the primary tumor site (SAOS2), we used a mammary adenocarcinoma cell line isolated from a metastatic pleural effusion (MDA-MB-231T). Second, Tsuiki et al. used an inducible approach to overexpress NME6, driven by the Cre-recombinase delivered by adenovirus 96h prior analysis, while we produced stable clones constantly overexpressing NME6 protein. Hence, as stated by authors in their article, “we cannot completely rule out the possibility that the overexpression of Cre-recombinase by adenovirus may have some effects on cell cycle regulation”[8]. On the other hand, our stable clones that survived a harsh antibiotic selection while overexpressing NME6 protein could have adapted to be more resilient, thus influencing the cell cycle results. An extensive analysis of the cell cycle upon NME6 overexpression or downregulation should be

performed in a large panel of human cell lines in order to conclude on the general effect of NME6 on cell cycle.

Regardless, NME6 localizes completely within the mitochondria, and is absent from the nucleus, where the regulation of the cell cycle occurs. Even though a deregulation of mitochondrial fusion/fission could have potentially affected the cell cycle [52,147], the absence of NME6 impact we observed on MDA-MB-231T was somehow expected.

As NME6 localized within the mitochondria, which represents an important hub along the apoptosis process, a possible involvement of the protein was envisaged to impact apoptosis. Our results showing that NME6 overexpression or silencing does not impact apoptosis, remained open to discussion. Indeed, the apoptosis experiment was conducted on RKO cells due to their wild type p53 status, while p53 is mutated in MDA-MB-231T cells which we used as our major model system. As our stable clones overexpressing NME6 were produced in MDA-MB-231T cell line, they were not usable for this experiment. Thus, a transient transfection approach was chosen to overexpress NME6 proteins in RKO cells. Unfortunately, the transfection method used for KI was itself driving cells into apoptosis and causing cell death, while the transfection reagents used for silencing was not harmful for the cells (Figure 44). Results showed no statistical difference between KI-CTRL and KI-NME6, but this result needs to be considered carefully, giving the fact that the apoptosis driven by the transfection method itself could potentially mask a minor effect of NME6 on apoptosis. Our experiment implies that NME6 overexpression or silencing does not have a drastic impact on apoptosis in RKO cells. However, a thorough study should be performed using NME6-KI stable clones in several cell lines to abrogate the transfection-induced apoptosis, and potentially reveal a minor effect of NME6 on apoptosis.

The impact of NME6 expression on mitochondrial respiration was studied with attention, after the discovery of RCC1L/NME6 interaction within the mitochondrial matrix. The basal respiration (LEAK) of digitonin-permeabilized cells was largely unaffected by the overexpression of NME6 in clones. However, the ADP-stimulated respiration (OXPHOS) was largely decreased in all overexpressing clones, leading to a ratio OXPHOS/LEAK significantly different when compared to control (Figure 47). The NME6 silencing showed a trend for an opposite effect, but the significance was lost when calculating the OXPHOS/LEAK ratio (Figure 48). Even though the silencing was efficient (up to 90% downregulation), it was not



complete and the remaining NME6 protein present in the mitochondria could have been sufficient to maintain respiratory parameters close to the one of the control cells.

We showed that the overexpression of NME6 strongly negatively impacted the mitochondrial respiration in presence of ATP, suggesting a reduced OXPHOS capacity. Consistently, we observed a significant decrease of the respiratory chain complex-III abundance at the protein level upon NME6 overexpression, while a similar trend was observed for complex-I and complex-IV. The complex-II which is entirely encoded by the nuclear DNA was unaffected by the overexpression of NME6. All proteins used as complex markers in this experiment were encoded in the nucleus (Figure 49). Nevertheless, our latest experiments show that NME6 overexpression strongly downregulate some of the components of the respiratory chain complexes encoded within the mitochondria (unpublished data). Thus, experimental data point to a repressing role of NME6 along the mitochondrial translation process, with its overexpression eventually leading to a reduced abundance of respiratory chain complexes and to a decrease of mitochondrial respiration.

Interestingly, the protein we used as a complex-III marker, UQCRC2, assemble at the MIM/matrix interface by forming a dimer with the complex-III protein UQCRC1. Worthy to note, the latest protein is encoded in the nucleus on chromosome 3p21.31, and is in a close vicinity of the NME6 gene, with only 260 kb separating the two genes [104]. An attractive hypothesis would postulate that both genes, clustering in a DNA domain such as topologically associating domain, would display a coordinated expression upon cellular needs [148,149], even though testing this hypothesis is beyond the scope of this work. Nevertheless, this improbable gene proximity reinforces the obvious link between NME6 and the respiratory chain.

Altogether, our work suggests a role of NME6 in mitochondrial translation, in concert with RCC1L. Both proteins arose early in the course of evolution [1,27,121], are localized in the mitochondrial matrix and interact with one another [81,128]. The tuning of either of their expression levels leads to a decrease of respiratory chain complexes abundance, and to a reduction of mitochondrial respiration [81,117,128]. At the level of the organism, the loss of NME6 expression [138] or homozygous mutation of RCC1L [127] both lead to early embryonic lethality in mice. At the cellular level, RCC1L KO increases apoptosis in HeLa cells [127], while we were unable to produce homozygous NME6 KO clones in MDA-MB-231T cells, probably due to cell lethality of the later condition. We propose a joint role of NME6

with RCC1L within the mitochondrial matrix, regulating the mitochondrial translation and consequently the mitochondrial respiration. NME6 could play a role in the maturation of mtRNA, either mRNA, tRNA or rRNA, by influencing their pseudouridylation status via the NME6 interaction with RCC1L. Moreover, NME6 could direct the biogenesis of mitoribosomes through its interaction with RCC1L, and/or help the mitoribosome assembly. The exact roles of NME6 are only emerging and remain unclear, but the extensive description of the protein we produced helped to drastically narrow down the possible pathway(s) in which NME6 is involved.

## **6 CONCLUSION**

To conclude, we produced an extensive description of the human NME6 protein. We argued in favor of the ubiquitous expression of NME6 in human cell lines. We demonstrated the expression of two NME6 isoforms in the cell, even though the shorter 186 amino acid isoform was dominantly expressed at the protein level. We confirmed that both endogenous and exogenous NME6 are localizing in the mitochondria and refined the localization to the matrix compartment, partially interacting with the mitochondrial inner membrane. We described the enzymatic properties of NME6 and showed a lack of NDPK activity associated with the inability of the protein to oligomerize with itself or with Group I NME proteins. We further revealed the NME6 inactive catalytic site, supported by the absence of a high-energy histidine-phosphorylated NME6 in the cellular environment, thus precluding enzymatic activities such as NDPK and protein histidine kinase activities. We described an interaction of NME6 with RCC1L, a mitochondrial matrix protein affecting mitochondrial translation. Apoptosis and cell cycle distribution were not disturbed by changes in NME6 expression levels. However, the mitochondrial respiration was largely downregulated upon overexpression of NME6, concomitant with a global downregulation of respiratory complexes at the protein level. Therefore, we suggest a new role of NME6 independent of its phosphotransfer-activity, and hypothesize a synergistic role of NME6 and RCC1L within the mitochondrial matrix, involved along the mitochondrial translation process, thus affecting mitochondrial respiration.

## **7 ABBREVIATION**

AA: Amino acid

ACETYL COA: Acetyl-Coenzyme A

AK2: Adenylate kinase 2

ANT: Adenine nucleotide translocator

APAF1: Apoptotic peptidase activating factor 1

AU: Absorbance unit

AWD: Abnormal wing discs

BAK: BCL2 homologous antagonist/killer

BAX: BCL2 associated X

BCA: Bicinchoninic acid

BSA: Bovine serum albumin

CJ: Cristae junction

DRP1: Dynamin-related protein 1

ECS: Embryonic stem cell

ER: Endoplasmic reticulum

ETC: Electron transport chain

GEF: Guanine exchange factor

HFIS1: Mitochondrial fission 1

HR: Heptad repeat

IBM: Inner boundary membrane

IMAC: Immobilized metallic affinity chromatography

IMS: Intermembrane space

iMTS: Internal mitochondrial targeting sequence

KI: Knock-in

KO: Knockout

Kpn: Killer of prune

LC: Liquid Chromatography

MFN1: Mitofusin 1

MFN2: Mitofusin 2

MIM/IMM/IM: Mitochondrial inner membrane

MOM/OMM/OM: Mitochondrial outer membrane

MOMP: Mitochondrial outer membrane permeabilization

MRM: Multiple reaction monitoring

MS: Mass spectrometry

mtCK: Mitochondrial creatine kinase

mtDNA: Mitochondrial DNA

MTS: Mitochondrial targeting sequence

NDP: Nucleoside diphosphate

NDPK : Nucleoside diphosphate kinase

NM23: Non-metastatic clone 23

NME: Non-metastatic

NTP: Nucleoside triphosphate

OCR: Oxygen consumption rate

OMI: Serine protease HTRA2

OPA1: Optic atrophy 1

OXPPOS: Oxidative phosphorylation

PBS: Phosphate-buffered saline

PDH-E1  $\alpha$ : Pyruvate dehydrogenase E1 component subunit  $\alpha$

pHis: Phosphorylated histidine

Pi: Inorganic phosphate

RB: Running buffer

RCC1: Regulator of chromosome condensation 1

RCC1L: RCC1-like G exchanging factor-like

RLD: RCC1-like domain

SDS-PAGE: Sodium dodecyl sulfate- Polyacrylamide gel electrophoresis

SMAC: Second mitochondria-derived activator of caspase

TB: Transfer buffer

TCA: Tricarboxylic acid cycle

TIM: Translocase of the inner membrane

TOM: Translocase of the outer membrane

VDAC: Voltage dependent anion channel

WBS: Williams-Beuren syndrome

WBSCR16: Williams-Beuren syndrome chromosomal region 16

WT: Wild type

XIAP: E3 ubiquitin-protein ligase

## 8 LITERATURE

- [1] Desvignes T, Pontarotti P, Fauvel C, Bobe J (2009) Nme protein family evolutionary history, a vertebrate perspective. *BMC Evol. Biol.* 9: 256.
- [2] Berg P, Joklik WK (1953) Transphosphorylation between nucleoside polyphosphates. *Nature.* 172: 1008–1009.
- [3] Krebs HA, Hems R (1953) Some reactions of adenosine and inosine phosphates in animal tissues. *Biochim. Biophys. Acta.* 12: 172–180.
- [4] Dearolf CR, Hersperger E, Shearn A (1988) Developmental consequences of awdb3, a cell-autonomous lethal mutation of *Drosophila* induced by hybrid dysgenesis. *Dev. Biol.* 129: 159–168.
- [5] Lacombe M-L, Tokarska-Schlattner M, Boissan M, Schlattner U (2018) The mitochondrial nucleoside diphosphate kinase (NDPK-D/NME4), a moonlighting protein for cell homeostasis. *Lab. Investig.* 98: 582–588.
- [6] Yoon J-H, Singh P, Lee D-H, Qiu J, Cai S, O'Connor TR, Chen Y, Shen B, Pfeifer GP (2005) Characterization of the 3' → 5' exonuclease activity found in human nucleoside diphosphate kinase 1 (NDK1) and several of its homologues. *Biochemistry.* 44: 15774–15786.
- [7] Boissan M, Schlattner U, Lacombe M-L (2018) The NDPK/NME superfamily: State of the art. *Lab. Investig.* 98: 164–174.
- [8] Tsuiki H, Nitta M, Furuya A, Hanai N, Fujiwara T, Inagaki M, Kochi M, Ushio Y, Saya H, Nakamura H (2000) A novel human nucleoside diphosphate (NDP) kinase, Nm23-H6, localizes in mitochondria and affects cytokinesis. *J. Cell. Biochem.* 76: 254–269.
- [9] Steeg PS, Bevilacqua G, Kopper L, Thorgeirsson UP, Talmadge JE, Liotta LA, Sobel ME (1988) Evidence for a novel gene associated with low tumor metastatic potential. *JNCI J. Natl. Cancer Inst.* 80: 200–204.
- [10] Gilles AM, Presecan E, Vonica A, Lascu I (1991) Nucleoside diphosphate kinase from human erythrocytes. Structural characterization of the two polypeptide chains responsible for heterogeneity of the hexameric enzyme. *J. Biol. Chem.* 266: 8784–9.
- [11] Munier A, Feral C, Milon L, Pinon VP-B, Gyapay G, Capeau J, Guellaen G, Lacombe

- M-L (1998) A new human nm23 homologue ( nm23 -H5) specifically expressed in testis germinal cells. *FEBS Lett.* 434: 289–294.
- [12] Vieira PS, de Giuseppe PO, de Oliveira AHC, Murakami MT (2015) The role of the C-terminus and Kpn loop in the quaternary structure stability of nucleoside diphosphate kinase from *Leishmania* parasites. *J. Struct. Biol.* 192: 336–341.
- [13] Georgescauld F, Song Y, Dautant A (2020) Structure, folding and stability of nucleoside diphosphate kinases. *Int. J. Mol. Sci.* 21: 6779.
- [14] Adam K, Ning J, Reina J, Hunter T (2020) NME/NM23/NDPK and histidine phosphorylation. *Int. J. Mol. Sci.* 21: 5848.
- [15] Postel EH (2003) Multiple biochemical activities of NM23/NDP kinase in gene regulation. *J. Bioenerg. Biomembr.* 35: 31–40.
- [16] Puts GS, Leonard MK, Pamidimukkala N V, Snyder DE, Kaetzel DM (2018) Nuclear functions of NME proteins. *Lab. Investig.* 98: 211–218.
- [17] Radić M, Šoštar M, Weber I, Četković H, Slade N, Herak Bosnar M (2020) The subcellular localization and oligomerization preferences of NME1/NME2 upon radiation-induced DNA damage. *Int. J. Mol. Sci.* 21: 2363.
- [18] Boissan M, Montagnac G, Shen Q, Griparic L, Guitton J, Romao M, Sauvonnnet N, Lagache T, Lascu I, Raposo G, Desbourdes C, Schlattner U, Lacombe M-L, Polo S, van der Blik AM, Roux A, Chavrier P (2014) Nucleoside diphosphate kinases fuel dynamin superfamily proteins with GTP for membrane remodeling. *Science.* 344: 1510–1515.
- [19] Chen C-W, Wang H-L, Huang C-W, Huang C-Y, Lim WK, Tu I-C, Koorapati A, Hsieh S-T, Kan H-W, Tzeng S-R, Liao J-C, Chong WM, Naroditzky I, Kidron D, Eran A, Nijim Y, Sela E, Feldman HB, Kalfon L, Raveh-Barak H, Falik-Zaccai TC, Elpeleg O, Mandel H, Chang Z-F (2019) Two separate functions of NME3 critical for cell survival underlie a neurodegenerative disorder. *Proc. Natl. Acad. Sci.* 116: 566–574.
- [20] Chen C-W, Tsao N, Zhang W, Chang Z-F (2020) NME3 regulates mitochondria to reduce ROS-mediated genome instability. *Int. J. Mol. Sci.* 21: 5048.
- [21] Milon L, Meyer P, Chiadmi M, Munier A, Johansson M, Karlsson A, Lascu I, Capeau J, Janin J, Lacombe M-L (2000) The human nm23-H4 gene product is a mitochondrial nucleoside diphosphate kinase. *J. Biol. Chem.* 275: 14264–14272.



- [22] Gui M, Farley H, Anujan P, Anderson JR, Maxwell DW, Whitchurch JB, Botsch JJ, Qiu T, Meleppattu S, Singh SK, Zhang Q, Thompson J, Lucas JS, Bingle CD, Norris DP, Roy S, Brown A (2021) De novo identification of mammalian ciliary motility proteins using cryo-EM. *Cell*. 184: 5791–5806.
- [23] Bilitou A, Watson J, Gartner A, Ohnuma S (2009) The NM23 family in development. *Mol. Cell. Biochem.* 329: 17–33.
- [24] Herak Bosnar M, Radić M, Četković H (2018) A young researcher's guide to NME/Nm23/NDP Kinase. *Period. Biol.* 120: 3–9.
- [25] Desvignes T, Pontarotti P, Bobe J (2010) Nme gene family evolutionary history reveals pre-metazoan origins and high conservation between humans and the sea anemone, *Nematostella vectensis*. *PLoS One*. 5: e15506.
- [26] Perina D, Herak Bosnar M, Bago R, Mikoč A, Harcet M, Deželjin M, Četković H (2011) Sponge non-metastatic Group I Nme gene/protein - structure and function is conserved from sponges to humans. *BMC Evol. Biol.* 11: 87.
- [27] Perina D, Herak Bosnar M, Mikoč A, Müller WEG, Četković H (2011) Characterization of Nme6-like gene/protein from marine sponge *Suberites domuncula*. *Naunyn. Schmiedebergs. Arch. Pharmacol.* 384: 451–460.
- [28] Mehus JG, Deloukas P, Lambeth DO (1999) NME6: A new member of the nm23 /nucleoside diphosphate kinase gene family located on human chromosome 3p21.3. *Hum. Genet.* 104: 454–459.
- [29] Roger AJ, Muñoz-Gómez SA, Kamikawa R (2017) The origin and diversification of mitochondria. *Curr. Biol.* 27: R1177–R1192.
- [30] Gray MW, Burger G, Lang BF (2001) The origin and early evolution of mitochondria. *Genome Biol.* 2: 1018.1–1018.5.
- [31] Cavalier-Smith T (2006) Origin of mitochondria by intracellular enslavement of a photosynthetic purple bacterium. *Proc. R. Soc. B Biol. Sci.* 273: 1943–1952.
- [32] Lemasters JJ, Holmuhamedov E (2006) Voltage-dependent anion channel (VDAC) as mitochondrial governor—Thinking outside the box. *Biochim. Biophys. Acta - Mol. Basis Dis.* 1762: 181–190.

- 
- [33] Lemasters JJ (2007) Modulation of mitochondrial membrane permeability in pathogenesis, autophagy and control of metabolism. *J. Gastroenterol. Hepatol.* 22: S31–S37.
- [34] Gottschalk B, Madreiter-Sokolowski CT, Graier WF (2022) Cristae junction as a fundamental switchboard for mitochondrial ion signaling and bioenergetics. *Cell Calcium.* 101: 102517.
- [35] Reichert AS, Neupert W (2002) Contact sites between the outer and inner membrane of mitochondria—role in protein transport. *Biochim. Biophys. Acta - Mol. Cell Res.* 1592: 41–49.
- [36] Kühlbrandt W (2015) Structure and function of mitochondrial membrane protein complexes. *BMC Biol.* 13: 89.
- [37] Barchiesi A, Vascotto C (2019) Transcription, processing, and decay of mitochondrial RNA in health and disease. *Int. J. Mol. Sci.* 20: 2221.
- [38] Xavier VJ, Martinou J-C (2021) RNA granules in the mitochondria and their organization under mitochondrial stresses. *Int. J. Mol. Sci.* 22: 9502.
- [39] Itoh Y, Andréll J, Choi A, Richter U, Maiti P, Best RB, Barrientos A, Battersby BJ, Amunts A (2021) Mechanism of membrane-tethered mitochondrial protein synthesis. *Science.* 371: 846–849.
- [40] Protasoni M, Zeviani M (2021) Mitochondrial structure and bioenergetics in normal and disease conditions. *Int. J. Mol. Sci.* 22: 586.
- [41] Tilokani L, Nagashima S, Paupe V, Prudent J (2018) Mitochondrial dynamics: Overview of molecular mechanisms. *Essays Biochem.* 62: 341–360.
- [42] Kyriakoudi S, Drousiotou A, Petrou PP (2021) When the balance tips: Dysregulation of mitochondrial dynamics as a culprit in disease. *Int. J. Mol. Sci.* 22: 4617.
- [43] Ramachandran R (2018) Mitochondrial dynamics: The dynamin superfamily and execution by collusion. *Semin. Cell Dev. Biol.* 76: 201–212.
- [44] Kurland CG, Andersson SGE (2000) Origin and evolution of the mitochondrial proteome. *Microbiol. Mol. Biol. Rev.* 64: 786–820.
- [45] Jedynak-Slyvka M, Jabczynska A, Szczesny RJ (2021) Human mitochondrial RNA

- processing and modifications: Overview. *Int. J. Mol. Sci.* 22: 7999.
- [46] Calvo SE, Mootha VK (2010) The mitochondrial proteome and human disease. *Annu. Rev. Genomics Hum. Genet.* 11: 25–44.
- [47] Quirós PM, Mottis A, Auwerx J (2016) Mitonuclear communication in homeostasis and stress. *Nat. Rev. Mol. Cell Biol.* 17: 213–226.
- [48] Needs HI, Protasoni M, Henley JM, Prudent J, Collinson I, Pereira GC (2021) Interplay between mitochondrial protein import and respiratory complexes assembly in neuronal health and degeneration. *Life.* 11: 432.
- [49] Wiedemann N, Pfanner N (2017) Mitochondrial machineries for protein import and assembly. *Annu. Rev. Biochem.* 86: 685–714.
- [50] Bykov YS, Flohr T, Boos F, Zung N, Herrmann JM, Schuldiner M (2022) Widespread use of unconventional targeting signals in mitochondrial ribosome proteins. *EMBO J.* 41: e109519.
- [51] Schneider K, Zimmer D, Nielsen H, Herrmann JM, Mühlhaus T (2021) iMLP, a predictor for internal matrix targeting-like sequences in mitochondrial proteins. *Biol. Chem.* 402: 937–943.
- [52] Giacomello M, Pyakurel A, Glytsou C, Scorrano L (2020) The cell biology of mitochondrial membrane dynamics. *Nat. Rev. Mol. Cell Biol.* 21: 204–224.
- [53] Vaux DL, Korsmeyer SJ (1999) Cell death in development. *Cell.* 96: 245–254.
- [54] Bock FJ, Tait SWG (2020) Mitochondria as multifaceted regulators of cell death. *Nat. Rev. Mol. Cell Biol.* 21: 85–100.
- [55] Tuzlak S, Kaufmann T, Villunger A (2016) Interrogating the relevance of mitochondrial apoptosis for vertebrate development and postnatal tissue homeostasis. *Genes Dev.* 30: 2133–2151.
- [56] Cooper GM (2000) *The cell: A molecular approach*. 2nd ed. Sunderland (MA): Sinauer Associates.
- [57] Zhao R, Jiang S, Zhang L, Yu Z (2019) Mitochondrial electron transport chain, ROS generation and uncoupling (Review). *Int. J. Mol. Med.* 44: 3.
- [58] Ikon N, Ryan RO (2017) Cardiolipin and mitochondrial cristae organization. *Biochim.*

- Biophys. Acta - Biomembr. 1859: 1156–1163.
- [59] Yusoff AAM, Ahmad F, Idris Z, Jaafar H, Abdullah JM (2015) Understanding mitochondrial DNA in brain tumorigenesis, in: Molecular considerations and evolving surgical management issues in the treatment of patients with a brain tumor, InTech.
- [60] Lascu I, Gonin P (2000) The catalytic mechanism of nucleoside diphosphate kinases. J. Bioenerg. Biomembr. 32: 237–46.
- [61] Schlattner U (2021) The complex functions of the NME family—A matter of location and molecular activity. Int. J. Mol. Sci. 22: 13083.
- [62] Norman AW, Wedding RT, Black MK (1965) Detection of phosphohistidine in nucleoside diphosphokinase isolated from Jerusalem artichoke mitochondria. Biochem. Biophys. Res. Commun. 20: 703–709.
- [63] Cleland WW (1963) The kinetics of enzyme-catalyzed reactions with two or more substrates or products. I. Nomenclature and rate equations. Biochim. Biophys. Acta. 67: 104–137.
- [64] Fuhs SR, Meisenhelder J, Aslanian A, Ma L, Zagorska A, Stankova M, Binnie A, Al-Obeidi F, Mauger J, Lemke G, Yates JR, Hunter T (2015) Monoclonal 1- and 3-phosphohistidine antibodies: New tools to study histidine phosphorylation. Cell. 162: 198–210.
- [65] Yu H, Rao X, Zhang K (2017) Nucleoside diphosphate kinase (Ndk): A pleiotropic effector manipulating bacterial virulence and adaptive responses. Microbiol. Res. 205: 125–134.
- [66] Lascu I, Giartosio S, Ransac A, Erent M (2000) Quaternary structure of nucleoside diphosphate kinases. J. Bioenerg. Biomembr. 32: 227–236.
- [67] Lascu I, Chaffotte A, Limbourg-Bouchon B, Véron M (1992) A Pro/Ser substitution in nucleoside diphosphate kinase of *Drosophila melanogaster* (mutation killer of prune) affects stability but not catalytic efficiency of the enzyme. J. Biol. Chem. 267: 12775–12781.
- [68] Dumas C, Lascu I, Moréra S, Glaser P, Fourme R, Wallet V, Lacombe ML, Véron M, Janin J (1992) X-ray structure of nucleoside diphosphate kinase. EMBO J. 11: 3203–3208.

- [69] Chiadmi M, Moréra S, Lascu I, Dumas C, Bras G Le, Véron M, Janin J (1993) Crystal structure of the Awd nucleotide diphosphate kinase from *Drosophila*. *Structure*. 1: 283–293.
- [70] Lascu I, Deville-Bonne D, Glaser P, Véron M (1993) Equilibrium dissociation and unfolding of nucleoside diphosphate kinase from *Dictyostelium discoideum*. Role of proline 100 in the stability of the hexameric enzyme. *J. Biol. Chem.* 268: 20268–20275.
- [71] Sedmak J, Ramaley R (1971) Purification and properties of *Bacillus subtilis* nucleoside diphosphokinase. *J. Biol. Chem.* 246: 5365–5372.
- [72] Moynié L, Giraud M-F, Georgescauld F, Lascu I, Dautant A (2007) The structure of the *Escherichia coli* nucleoside diphosphate kinase reveals a new quaternary architecture for this enzyme family. *Proteins Struct. Funct. Bioinforma.* 67: 755–765.
- [73] Williams RL, Oren DA, Muñoz-Dorado J, Inouye S, Inouye M, Arnold E (1993) Crystal structure of *Myxococcus xanthus* nucleoside diphosphate kinase and its interaction with a nucleotide substrate at 2.0 Å resolution. *J. Mol. Biol.* 234: 1230–1247.
- [74] Ginther CL, Ingraham JL (1974) Nucleoside diphosphokinase of *Salmonella typhimurium*. *J. Biol. Chem.* 249: 3406–3411.
- [75] Muñoz-Dorado J, Inouye S, Inouye M (1990) Nucleoside diphosphate kinase from *Myxococcus xanthus*. II. Biochemical characterization. *J. Biol. Chem.* 265: 2707–2712.
- [76] Mesnildrey S, Agou F, Karlsson A, Bonne DD, Véron M (1998) Coupling between catalysis and oligomeric structure in nucleoside diphosphate kinase. *J. Biol. Chem.* 273: 4436–4442.
- [77] Sturtevant AH (1956) A highly specific complementary lethal system in *Drosophila melanogaster*. *Genetics*. 41: 118–23.
- [78] Khan I, Steeg PS (2018) The relationship of NM23 (NME) metastasis suppressor histidine phosphorylation to its nucleoside diphosphate kinase, histidine protein kinase and motility suppression activities. *Oncotarget*. 9: 10185–10202.
- [79] Karlsson A, Mesnildrey S, Xu Y, Moréra S, Janin J, Véron M (1996) Nucleoside diphosphate kinase. *J. Biol. Chem.* 271: 19928–19934.
- [80] Boissan M, Dabernat S, Peuchant E, Schlattner U, Lascu I, Lacombe M-L (2009) The

- mammalian Nm23/NDPK family: From metastasis control to cilia movement. *Mol. Cell. Biochem.* 329: 51–62.
- [81] Proust B, Radić M, Vidaček NŠ, Cottet C, Attia S, Lamarche F, Ačkar L, Mikulčić VG, Tokarska-Schlattner M, Četković H, Schlattner U, Bosnar MH (2021) NME6 is a phosphotransfer-inactive, monomeric NME/NDPK family member and functions in complexes at the interface of mitochondrial inner membrane and matrix. *Cell Biosci.* 11: 195.
- [82] Hartsough MT, Steeg PS (2000) Nm23/nucleoside diphosphate kinase in human cancers. *J. Bioenerg. Biomembr.* 32: 301–308.
- [83] Li Y, Tong Y, Wong YH (2015) Regulatory functions of Nm23-H2 in tumorigenesis: Insights from biochemical to clinical perspectives. *Naunyn. Schmiedebergs. Arch. Pharmacol.* 388: 243–256.
- [84] Hippe H-J, Luedde M, Lutz S, Koehler H, Eschenhagen T, Frey N, Katus HA, Wieland T, Niroomand F (2007) Regulation of cardiac cAMP synthesis and contractility by nucleoside diphosphate kinase B/G protein  $\beta\gamma$  dimer complexes. *Circ. Res.* 100: 1191–1199.
- [85] Herak Bosnar M, de Gunzburg J, Bago R, Brečević L, Weber I, Pavelić J (2004) Subcellular localization of A and B Nm23/NDPK subunits. *Exp. Cell Res.* 298: 275–284.
- [86] Choudhuri T, Murakami M, Kaul R, Sahu SK, Mohanty S, Verma SC, Kumar P, Robertson ES (2010) Nm23-H1 can induce cell cycle arrest and apoptosis in B cells. *Cancer Biol. Ther.* 9: 1065–1078.
- [87] Kang Y, Lee D-C, Han J, Yoon S, Won M, Yeom J-H, Seong M-J, Ko J-J, Lee K-A, Lee K, Bae J (2007) NM23-H2 involves in negative regulation of Diva and Bcl2L10 in apoptosis signaling. *Biochem. Biophys. Res. Commun.* 359: 76–82.
- [88] Herak Bosnar M, Dubravčić K, Bago R, Pavelić J (2008) Head and neck tumor cells exhibit altered proliferation upon overexpression of nm23 genes. *Croat. Chem. Acta.* 81: 183–189.
- [89] Lombardi D, Lacombe M-L, Paggi MG (2000) Nm23: Unraveling its biological function in cell differentiation. *J. Cell. Physiol.* 182: 144–149.

- [90] Lakso M, Steeg PS, Westphal H (1992) Embryonic expression of nm23 during mouse organogenesis. *Cell Growth Differ.* 3: 873–879.
- [91] Fournier H-N, Dupé-Manet S, Bouvard D, Lacombe M-L, Marie C, Block MR, Albiges-Rizo C (2002) Integrin cytoplasmic domain-associated protein 1 $\alpha$  (ICAP-1 $\alpha$ ) interacts directly with the metastasis suppressor nm23-H2, and both proteins are targeted to newly formed cell adhesion sites upon integrin engagement. *J. Biol. Chem.* 277: 20895–20902.
- [92] Murakami M, Lan K, Subramanian C, Robertson ES (2005) Epstein-Barr virus nuclear antigen 1 interacts with Nm23-H1 in lymphoblastoid cell lines and inhibits its ability to suppress cell migration. *J. Virol.* 79: 1559–1568.
- [93] Flentie K, Gonzalez C, Kocher B, Wang Y, Zhu H, Marasa J, Piwnicka-Worms D (2018) Nucleoside diphosphate kinase-3 ( NME3 ) enhances TLR5-induced NF  $\kappa$  B activation. *Mol. Cancer Res.* 16: 986–999.
- [94] Tokarska-Schlattner M, Boissan M, Munier A, Borot C, Mailleau C, Speer O, Schlattner U, Lacombe M-L (2008) The nucleoside diphosphate kinase D (NM23-H4) binds the inner mitochondrial membrane with high affinity to cardiolipin and couples nucleotide transfer with respiration. *J. Biol. Chem.* 283: 26198–26207.
- [95] Schlattner U, Tokarska-Schlattner M, Ramirez S, Tyurina YY, Amoscato AA, Mohammadyani D, Huang Z, Jiang J, Yanamala N, Seffouh A, Boissan M, Epand RF, Epand RM, Klein-Seetharaman J, Lacombe M-L, Kagan VE (2013) Dual function of mitochondrial Nm23-H4 protein in phosphotransfer and intermembrane lipid transfer. *J. Biol. Chem.* 288: 111–121.
- [96] Kagan VE, Jiang J, Huang Z, Tyurina YY, Desbourdes C, Cottet-Rousselle C, Dar HH, Verma M, Tyurin VA, Kapralov AA, Cheikhi A, Mao G, Stolz D, St. Croix CM, Watkins S, Shen Z, Li Y, Greenberg ML, Tokarska-Schlattner M, Boissan M, Lacombe M-L, Epand RM, Chu CT, Mallampalli RK, Bayır H, Schlattner U (2016) NDPK-D (NM23-H4)-mediated externalization of cardiolipin enables elimination of depolarized mitochondria by mitophagy. *Cell Death Differ.* 23: 1140–1151.
- [97] Lacombe M-L, Lamarche F, De Wever O, Padilla-Benavides T, Carlson A, Khan I, Huna A, Vacher S, Calmel C, Desbourdes C, Cottet-Rousselle C, Hininger-Favier I, Attia S, Nawrocki-Raby B, Raingeaud J, Machon C, Guitton J, Le Gall M, Clary G, Broussard C, Chafey P, Théron P, Bernard D, Fontaine E, Tokarska-Schlattner M,

- Steeg P, Bièche I, Schlattner U, Boissan M (2021) The mitochondrially-localized nucleoside diphosphate kinase D (NME4) is a novel metastasis suppressor. *BMC Biol.* 19: 228.
- [98] Lacombe ML, Milon L, Munier A, Mehus JG, Lambeth DO (2000) The human Nm23/nucleoside diphosphate kinases. *J. Bioenerg. Biomembr.* 32: 247–58.
- [99] Cho EH, Huh HJ, Jeong I, Lee NY, Koh W, Park H, Ki C (2020) A nonsense variant in NME5 causes human primary ciliary dyskinesia with radial spoke defects. *Clin. Genet.* 98: 64–68.
- [100] Ma M, Stoyanova M, Rademacher G, Dutcher SK, Brown A, Zhang R (2019) Structure of the Decorated Ciliary Doublet Microtubule. *Cell.* 179: 909–922.
- [101] Duriez B, Duquesnoy P, Escudier E, Bridoux A-M, Escalier D, Rayet I, Marcos E, Vojtek A-M, Bercher J-F, Amselem S (2007) A common variant in combination with a nonsense mutation in a member of the thioredoxin family causes primary ciliary dyskinesia. *Proc. Natl. Acad. Sci.* 104: 3336–3341.
- [102] Sadek CM, Jiménez A, Damdimopoulos AE, Kieselbach T, Nord M, Gustafsson J-A, Spyrou G, Davis EC, Oko R, van der Hoorn FA, Miranda-Vizuete A (2003) Characterization of human thioredoxin-like 2: A novel microtubule-binding thioredoxin expressed predominantly in the cilia of lung airway epithelium and spermatid manchette and axoneme. *J. Biol. Chem.* 278: 13133–42.
- [103] Chan MC, Savela J, Ollikainen RK, Teppo H-R, Miinalainen I, Pirinen R, Kari EJM, Kuitunen H, Turpeenniemi-Hujanen T, Kuittinen O, Kuusisto MEL (2021) Testis-specific thioredoxins TXNDC2, TXNDC3, and TXNDC6 are expressed in both testicular and systemic DLBCL and correlate with clinical disease presentation. *Oxid. Med. Cell. Longev.* 2021: 8026941.
- [104] Cunningham F, Allen JE, Allen J, Alvarez-Jarreta J, Amode MR, Armean IM, Austine-Orimoloye O, Azov AG, Barnes I, Bennett R, Berry A, Bhai J, Bignell A, Billis K, Boddu S, Brooks L, Charkhchi M, Cummins C, Da Rin Fioretto L, Davidson C, Dodiya K, Donaldson S, El Houdaigui B, El Naboulsi T, Fatima R, Giron CG, Genez T, Martinez JG, Guijarro-Clarke C, Gymer A, Hardy M, Hollis Z, Hourlier T, Hunt T, Juettemann T, Kaikala V, Kay M, Lavidas I, Le T, Lemos D, Marugán JC, Mohanan S, Mushtaq A, Naven M, Ogeh DN, Parker A, Parton A, Perry M, Piližota I, Prosovetskaia



- I, Sakthivel MP, Salam AIA, Schmitt BM, Schuilenburg H, Sheppard D, Pérez-Silva JG, Stark W, Steed E, Sutinen K, Sukumaran R, Sumathipala D, Suner M-M, Szpak M, Thormann A, Tricomi FF, Urbina-Gómez D, Veidenberg A, Walsh TA, Walts B, Willhoft N, Winterbottom A, Wass E, Chakiachvili M, Flint B, Frankish A, Giorgetti S, Haggerty L, Hunt SE, Iisley GR, Loveland JE, Martin FJ, Moore B, Mudge JM, Muffato M, Perry E, Ruffier M, Tate J, Thybert D, Trevanion SJ, Dyer S, Harrison PW, Howe KL, Yates AD, Zerbino DR, Flicek P (2022) Ensembl 2022. *Nucleic Acids Res.* 50: D988–D995.
- [105] AlphaFold\_Human NME6 protein predicted structure  
<https://alphafold.ebi.ac.uk/entry/O75414> (accessed May 20, 2022).
- [106] Jumper J, Evans R, Pritzel A, Green T, Figurnov M, Ronneberger O, Tunyasuvunakool K, Bates R, Žídek A, Potapenko A, Bridgland A, Meyer C, Kohl SAA, Ballard AJ, Cowie A, Romera-Paredes B, Nikolov S, Jain R, Adler J, Back T, Petersen S, Reiman D, Clancy E, Zielinski M, Steinegger M, Pacholska M, Berghammer T, Bodenstein S, Silver D, Vinyals O, Senior AW, Kavukcuoglu K, Kohli P, Hassabis D (2021) Highly accurate protein structure prediction with AlphaFold. *Nature.* 596: 583–589.
- [107] Varadi M, Anyango S, Deshpande M, Nair S, Natassia C, Yordanova G, Yuan D, Stroe O, Wood G, Laydon A, Žídek A, Green T, Tunyasuvunakool K, Petersen S, Jumper J, Clancy E, Green R, Vora A, Lutfi M, Figurnov M, Cowie A, Hobbs N, Kohli P, Kleywegt G, Birney E, Hassabis D, Velankar S (2022) AlphaFold protein structure database: Massively expanding the structural coverage of protein-sequence space with high-accuracy models. *Nucleic Acids Res.* 50: D439–D444.
- [108] Seifert M, Welter C, Mehraein Y, Seitz G (2005) Expression of the nm23 homologues nm23-H4, nm23-H6, and nm23-H7 in human gastric and colon cancer. *J. Pathol.* 205: 623–632.
- [109] Ke J, Lou J, Zhong R, Chen X, Li J, Liu C, Gong Y, Yang Y, Zhu Y, Zhang Y, Chang J, Gong J (2016) Identification of a potential regulatory variant for colorectal cancer risk mapping to 3p21.31 in chinese population. *Sci. Rep.* 6: 25194.
- [110] Wang C-H, Ma N, Lin Y-T, Wu C-C, Hsiao M, Lu FL, Yu C-C, Chen S-Y, Lu J (2012) A shRNA functional screen reveals Nme6 and Nme7 are crucial for embryonic stem cell renewal. *Stem Cells.* 30: 2199–2211.

- [111] Ernst O, Sun J, Lin B, Banoth B, Dorrington MG, Liang J, Schwarz B, Stromberg KA, Katz S, Vayttaden SJ, Bradfield CJ, Slepishkina N, Rice CM, Buehler E, Khillan JS, McVicar DW, Bosio CM, Bryant CE, Sutterwala FS, Martin SE, Lal-Nag M, Fraser IDC (2021) A genome-wide screen uncovers multiple roles for mitochondrial nucleoside diphosphate kinase D in inflammasome activation. *Sci. Signal.* 14: eabe0387.
- [112] Pagliarini DJ, Calvo SE, Chang B, Sheth SA, Vafai SB, Ong S-E, Walford GA, Sugiana C, Boneh A, Chen WK, Hill DE, Vidal M, Evans JG, Thorburn DR, Carr SA, Mootha VK (2008) A mitochondrial protein compendium elucidates Complex I disease biology. *Cell.* 134: 112–123.
- [113] Rhee H-W, Zou P, Udeshi ND, Martell JD, Mootha VK, Carr SA, Ting AY (2013) Proteomic mapping of mitochondria in living cells via spatially restricted enzymatic tagging. *Science.* 339: 1328–1331.
- [114] Hung V, Zou P, Rhee H-W, Udeshi ND, Cracan V, Svinkina T, Carr SA, Mootha VK, Ting AY (2014) Proteomic mapping of the human mitochondrial intermembrane space in live cells via ratiometric APEX tagging. *Mol. Cell.* 55: 332–341.
- [115] Hung V, Lam SS, Udeshi ND, Svinkina T, Guzman G, Mootha VK, Carr SA, Ting AY (2017) Proteomic mapping of cytosol-facing outer mitochondrial and ER membranes in living human cells by proximity biotinylation. *Elife.* 6: e24463.
- [116] Antonicka H, Lin Z-Y, Janer A, Aaltonen MJ, Weraarpachai W, Gingras A-C, Shoubridge EA (2020) A high-density human mitochondrial proximity interaction network. *Cell Metab.* 32: 479–497.
- [117] Arroyo JD, Jourdain AA, Calvo SE, Ballarano CA, Doench JG, Root DE, Mootha VK (2016) A genome-wide CRISPR death screen identifies genes essential for oxidative phosphorylation. *Cell Metab.* 24: 875–885.
- [118] Floyd BJ, Wilkerson EM, Velting MT, Minogue CE, Xia C, Beebe ET, Wrobel RL, Cho H, Kremer LS, Alston CL, Gromek KA, Dolan BK, Ulbrich A, Stefely JA, Bohl SL, Werner KM, Jochem A, Westphall MS, Rensvold JW, Taylor RW, Prokisch H, Kim J-JP, Coon JJ, Pagliarini DJ (2016) Mitochondrial protein interaction mapping identifies regulators of respiratory chain function. *Mol. Cell.* 63: 621–632.
- [119] Huttlin EL, Bruckner RJ, Navarrete-Perea J, Cannon JR, Baltier K, Gebreab F, Gygi

- MP, Thornock A, Zarraga G, Tam S, Szpyt J, Gassaway BM, Panov A, Parzen H, Fu S, Golbazi A, Maenpaa E, Stricker K, Guha Thakurta S, Zhang T, Rad R, Pan J, Nusinow DP, Paulo JA, Schweppe DK, Vaites LP, Harper JW, Gygi SP (2021) Dual proteome-scale networks reveal cell-specific remodeling of the human interactome. *Cell*. 184: 3022–3040.
- [120] Wang J, Huo K, Ma L, Tang L, Li D, Huang X, Yuan Y, Li C, Wang W, Guan W, Chen H, Jin C, Wei J, Zhang W, Yang Y, Liu Q, Zhou Y, Zhang C, Wu Z, Xu W, Zhang Y, Liu T, Yu D, Zhang Y, Chen L, Zhu D, Zhong X, Kang L, Gan X, Yu X, Ma Q, Yan J, Zhou L, Liu Z, Zhu Y, Zhou T, He F, Yang X (2011) Toward an understanding of the protein interaction network of the human liver. *Mol. Syst. Biol.* 7: 536.
- [121] Hadjebi O, Casas-Terradellas E, Garcia-Gonzalo FR, Rosa JL (2008) The RCC1 superfamily: From genes, to function, to disease. *Biochim. Biophys. Acta - Mol. Cell Res.* 1783: 1467–1479.
- [122] Ohtsubo M, Okazaki H, Nishimoto T (1989) The RCC1 protein, a regulator for the onset of chromosome condensation locates in the nucleus and binds to DNA. *J. Cell Biol.* 109: 1389–1397.
- [123] Renault L, Kuhlmann J, Henkel A, Wittinghofer A (2001) Structural basis for guanine nucleotide exchange on RAN by the regulator of chromosome condensation (RCC1). *Cell*. 105: 245–255.
- [124] Schubert C, Laccone F (2006) Williams-Beuren syndrome: Determination of deletion size using quantitative real-time PCR. *Int. J. Mol. Med.* 18: 799–806.
- [125] Antonicka H, Choquet K, Lin Z, Gingras A, Kleinman CL, Shoubridge EA (2017) A pseudouridine synthase module is essential for mitochondrial protein synthesis and cell viability. *EMBO Rep.* 18: 28–38.
- [126] Koyama M, Sasaki T, Sasaki N, Matsuura Y (2017) Crystal structure of human WBSCR16, an RCC1-like protein in mitochondria. *Protein Sci.* 26: 1870–1877.
- [127] Huang G, Massoudi D, Muir AM, Joshi DC, Zhang C-L, Chiu SY, Greenspan DS (2017) WBSCR16 Is a Guanine Nucleotide Exchange Factor Important for Mitochondrial Fusion. *Cell Rep.* 20: 923–934.
- [128] Reyes A, Favia P, Vidoni S, Petruzzella V, Zeviani M (2020) RCC1L (WBSCR16)

- isoforms coordinate mitochondrial ribosome assembly through their interaction with GTPases. *PLOS Genet.* 16: e1008923.
- [129] Ćetković H, Herak Bosnar M, Perina D, Mikoč A, Deželjin M, Belužić R, Bilandžija H, Ruiz-Trillo I, Harcet M (2018) Characterization of a group I Nme protein of *Capsaspora owczarzaki*—a close unicellular relative of animals. *Lab. Investig.* 98: 304–314.
- [130] Agarwal RP, Robison B, Parks RE (1978) [49] Nucleoside diphosphokinase from human erythrocytes, in: *Methods in Enzymology*, : pp. 376–386.
- [131] Eskes R, Desagher S, Antonsson B, Martinou J-C (2000) Bid induces the oligomerization and insertion of Bax into the outer mitochondrial membrane. *Mol. Cell. Biol.* 20: 929–935.
- [132] Hovius R, Lambrechts H, Nicolay K, de Kruijff B (1990) Improved methods to isolate and subfractionate rat liver mitochondria. Lipid composition of the inner and outer membrane. *Biochim. Biophys. Acta - Biomembr.* 1021: 217–226.
- [133] Palmieri D, Halverson DO, Ouatas T, Horak CE, Salerno M, Johnson J, Figg WD, Hollingshead M, Hursting S, Berrigan D, Steinberg SM, Merino MJ, Steeg PS (2005) Medroxyprogesterone acetate elevation of Nm23-H1 metastasis suppressor expression in hormone receptor–negative breast cancer. *JNCI J. Natl. Cancer Inst.* 97: 632–642.
- [134] Khan I, Gril B, Steeg PS (2019) Metastasis suppressors NME1 and NME2 promote Dynamin 2 oligomerization and regulate tumor cell endocytosis, motility, and metastasis. *Cancer Res.* 79: 4689–4702.
- [135] Marino N, Marshall J-C, Collins JW, Zhou M, Qian Y, Veenstra T, Steeg PS (2013) Nm23-H1 binds to Gelsolin and inactivates its Actin-severing capacity to promote tumor cell motility and metastasis. *Cancer Res.* 73: 5949–5962.
- [136] Perina D, Korolija M, Mikoč A, Halasz M, Herak Bosnar M, Ćetković H (2019) Characterization of Nme5-Like gene/protein from the red alga *Chondrus crispus*. *Mar. Drugs.* 18: 13.
- [137] Abu-Taha IH, Heijman J, Feng Y, Vettel C, Dobrev D, Wieland T (2018) Regulation of heterotrimeric G-protein signaling by NDPK/NME proteins and caveolins: an update. *Lab. Investig.* 98: 190–197.
- [138] International Mouse Phenotyping Consortium (IMPC)\_NME6

- <https://www.mousephenotype.org/data/genes/MGI:1861676> (accessed December 5, 2021).
- [139] Dickinson ME, Flenniken AM, Ji X, Teboul L, Wong MD, White JK, Meehan TF, Weninger WJ, Westerberg H, Adissu H, Baker CN, Bower L, Brown JM, Brianna Caddle L, Chiani F, Clary D, Cleak J, Daly MJ, Denegre JM, Doe B, Dolan ME, Edie SM, Fuchs H, Gailus-Durner V, Galli A, Gambadoro A, Gallegos J, Guo S, Horner NR, Hsu C wei, Johnson SJ, Kalaga S, Keith LC, Lanoue L, Lawson TN, Lek M, Mark M, Marschall S, Mason J, McElwee ML, Newbigging S, Nutter LMJ, Peterson KA, Ramirez-Solis R, Rowland DJ, Ryder E, Samocha KE, Seavitt JR, Selloum M, Szoke-Kovacs Z, Tamura M, Trainor AG, Tudose I, Wakana S, Warren J, Wendling O, West DB, Wong L, Yoshiki A, MacArthur DG, Tocchini-Valentini GP, Gao X, Flicek P, Bradley A, Skarnes WC, Justice MJ, Parkinson HE, Moore M, Wells S, Braun RE, Svenson KL, Hrabe de Angelis M, Herault Y, Mohun T, Mallon AM, Mark Henkelman R, Brown SDM, Adams DJ, Kent Lloyd KC, McKerlie C, Beaudet AL, Bucan M, Murray SA, McKay M, Urban B, Lund C, Froeter E, LaCasse T, Mehalow A, Gordon E, Donahue LR, Taft R, Kutney P, Dion S, Goodwin L, Kales S, Urban R, Palmer K, Pertuy F, Bitz D, Weber B, Goetz-Reiner P, Jacobs H, Le Marchand E, El Amri A, El Fertak L, Ennah H, Ali-Hadji D, Ayadi A, Wattenhofer-Donze M, Jacquot S, André P, Birling MC, Pavlovic G, Sorg T, Morse I, Benso F, Stewart ME, Copley C, Harrison J, Joynson S, Guo R, Qu D, Spring S, Yu L, Ellegood J, Morikawa L, Shang X, Feugas P, Creighton A, Penton PC, Danisment O, Griggs N, Tudor CL, Green AL, Icoresi Mazzeo C, Siragher E, Lillistone C, Tuck E, Gleeson D, Sethi D, Bayzatinova T, Burvill J, Habib B, Weavers L, Maswood R, Miklejewska E, Woods M, Grau E, Newman S, Sinclair C, Brown E, Ayabe S, Iwama M, Murakami A (2016) High-throughput discovery of novel developmental phenotypes. *Nature*. 537: 508–514.
- [140] Satya-Prakash KL, Pathak S, Hsu TC, Olivé M, Cailleau R (1981) Cytogenetic analysis on eight human breast tumor cell lines: High frequencies of 1q, 11q and HeLa-like marker chromosomes. *Cancer Genet. Cytogenet.* 3: 61–73.
- [141] Backes S, Hess S, Boos F, Woellhaf MW, Gödel S, Jung M, Mühlhaus T, Herrmann JM (2018) Tom70 enhances mitochondrial preprotein import efficiency by binding to internal targeting sequences. *J. Cell Biol.* 217: 1369–1382.
- [142] iMLP : iMTS-L Prediction <http://imlp.bio.uni-kl.de/> (accessed July 1, 2022).

- 
- [143] Obita T, Muto T, Endo T, Kohda D (2003) Peptide library approach with a disulfide tether to refine the Tom20 recognition motif in mitochondrial presequences. *J. Mol. Biol.* 328: 495–504.
- [144] Fukasawa Y, Tsuji J, Fu S-C, Tomii K, Horton P, Imai K (2015) MitoFates: Improved prediction of mitochondrial targeting sequences and their cleavage sites. *Mol. Cell. Proteomics.* 14: 1113–1126.
- [145] Baysal C, Pérez-González A, Eseverri Á, Jiang X, Medina V, Caro E, Rubio L, Christou P, Zhu C (2020) Recognition motifs rather than phylogenetic origin influence the ability of targeting peptides to import nuclear-encoded recombinant proteins into rice mitochondria. *Transgenic Res.* 29: 37–52.
- [146] Schlattner U, Tokarska-Schlattner M, Epanand RM, Boissan M, Lacombe M-L, Kagan VE (2018) NME4/nucleoside diphosphate kinase D in cardiolipin signaling and mitophagy. *Lab. Invest.* 98: 228–232.
- [147] Horbay R, Bilyy R (2016) Mitochondrial dynamics during cell cycling. *Apoptosis.* 21: 1327–1335.
- [148] Tena JJ, Santos-Pereira JM (2021) Topologically associating domains and regulatory landscapes in development, evolution and disease. *Front. Cell Dev. Biol.* 9: 1817.
- [149] Szabo Q, Bantignies F, Cavalli G (2019) Principles of genome folding into topologically associating domains. *Sci. Adv.* 5: eaaw1668.

## 9 CURRICULUM VITAE

Bastien Lucien Jean Proust was born October 1993 in Verneuil-sur-Avre (France). In 2016 he obtained his French-Croatian Master's co-diploma in Biochemistry, Molecular Biology and Biotechnology/Molecular Biology from the Collégium Sciences et Techniques, University of Orléans, France, and Faculty of Science, University of Zagreb, Croatia. Since 2018, he has been working as a research assistant in the Laboratory for Protein Dynamics, Division of Molecular Medicine at the Ruđer Bošković Institute under the mentorship of Dr. sc. Maja Herak Bosnar. In parallel, he enrolled a postgraduate doctoral program in Biology at the Department of Biology, Faculty of Science, University of Zagreb.

He was involved in domestic and international collaborations leading to four peer-reviewed scientific publications in international journals, one as the first author. He has been awarded two grants and actively participated in numerous national and international conferences, meetings and workshops. He was a member of the organizing committee of the *5th meeting of the Croatian Association for Cancer Research (HDIR5), "Translating Science to Medicine – Targets and Therapeutics"* (Croatia 2018).

### PUBLICATIONS :

1. Ozretić P, Hanžić N, **Proust B**, Sabol M, Trnski D, Radić M, Musani V, Ciribilli Y, Milas I, Puljiz Z, Bosnar MH, Levanat S, Slade N (2019) Expression profiles of p53/p73, NME and GLI families in metastatic melanoma tissue and cell lines. *Sci. Rep.* 9: 12470.
2. Pinterić M, Podgorski II, Hadžija MP, Filić V, Paradžik M, **Proust BLJ**, Dekanić A, Ciganek I, Pleše D, Marčinko D, Balog T, Sobočanec S (2020) Sirt3 exerts its tumor-suppressive role by increasing p53 and attenuating response to estrogen in MCF-7 Cells. *Antioxidants.* 9: 294.
3. Kesić M, Baković P, Horvatiček M, **Proust BLJ**, Štefulj J, Čičin-Šain L (2020) Constitutionally high serotonin tone favors obesity: Study on rat sublines with altered serotonin homeostasis. *Front. Neurosci.* 14: 219.
4. **Proust B**, Radić M, Vidaček NŠ, Cottet C, Attia S, Lamarche F, Ačkar L, Mikulčić VG, Tokarska-Schlattner M, Četković H, Schlattner U, Bosnar MH (2021) NME6 is a phosphotransfer-inactive, monomeric NME/NDPK family member and functions in complexes at the interface of mitochondrial inner membrane and matrix. *Cell Biosci.* 11: 195.